


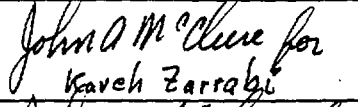

**Calculation Cover Sheet**

Complete only applicable items.

2. Calculation Title  
EQ6 Calculations for Chemical Degradation of Fast Flux Test Facility (FFTF) Waste Packages

3. Document Identifier (including Revision Number) BBA000000-01717-0210-00028 REV 00	4. Total Pages 73
---	----------------------

5. Total Attachments 4	6. Attachment Numbers - Number of pages in each Att.I: 1 page, Att. II: 1 page, Att. III: 8 pages, Att. IV: 4 pages
---------------------------	--

7. Originator	Print Name	Signature	Date
	H. W. Stockman		12-30-98
8. Checker	Kaveh Zarrabi		12/31/98
9. Lead Design Engineer	Peter Gottlieb		12/31/98

10. Remarks

**Revision History**

11. Revision No.	12. Date Approved	13. Description of Revision
Rev 00		Initial Issue

**Table of Contents**

<b><u>Item</u></b>	<b><u>Page</u></b>
1. PURPOSE.....	6
2. METHOD.....	7
3. ASSUMPTIONS.....	8
4. USE OF COMPUTER SOFTWARE.....	13
4.1 EQ3/6 SOFTWARE PACKAGE .....	13
4.2 SOLID-CENTERED FLOW-THROUGH MODE .....	14
4.3 SPREADSHEETS.....	15
4.4 SOFTWARE APPROVED FOR QA WORK.....	15
5. CALCULATION.....	15
5.1 CALCULATION INPUTS.....	15
5.1.1 WP Materials and Performance Parameters.....	15
5.1.1.1 Physical and Chemical Form of FFTF WPs.....	16
5.1.1.2 Chemical Composition of J-13 Well Water .....	21
5.1.1.3 Drip Rate of J-13 Water into a WP .....	21
5.1.1.4 Densities and Molecular Weights of Solids .....	22
5.1.1.5 Atomic Weights .....	22
5.2 DATA CONVERSION .....	23
5.3 EQ6 CALCULATIONS AND SCENARIOS MODELED .....	23
5.3.1 Controls on $GdPO_4 \cdot H_2O$ Solubility.....	23
5.3.2 EQ6 Run Conditions and Nomenclature.....	27
5.3.3 Comparison of Aqueous Gd, Pu, U and pH for Cases 1-12.....	32
5.3.4 Justification for Eliminating Multi-Stage Cases 13 and 14.....	43
5.3.5 Detailed Examination of Cases 2 and 10 .....	46
5.3.6 Compositions, Volumes and Masses of Clay-Like Materials Formed from Degradation of WP Materials.....	57
5.3.7 Effects of Varying Glass Mg Composition.....	59
6. RESULTS.....	67
6.1 SUMMARY OF RESULTS .....	67
6.2 TBV DISCLAIMER.....	68
7. REFERENCES.....	69
8. ATTACHMENTS.....	73

**List of Tables**

<b><u>Item</u></b>	<b><u>Page</u></b>
Table 5-1. Steel Compositions and Degradation Rates.....	17
Table 5-2. Glass Composition and Rates .....	18
Table 5-3. MOX Compositions and Degradation Rates.....	19
Table 5-4. Composition of J-13 Well Water <sup>1</sup> .....	21
Table 5-5. Densities and Molecular Weights of Precipitated Solids.....	22
Table 5-6. Summary of Cases Run, Associated Input File Names, Percent Gd, Pu and U Retained, and Fe Oxide Corrosion Product .....	30
Table 5-7. Volume of Corrosion Products (% of Volume inside CRB) and Moles Elements in Corrosion Products (Normalized to Silicon).....	31
Table 5-8. Case 9: Volumes of Minerals (liters) and Percent of Total Volume inside CRB .....	57
Table 5-9. Case 9: Mass (kg) and Average Density (kg/L) of Minerals Formed within CRB.....	58
Table 5-10. Case 9: Mole Percent of Major Elements in Non-Actinide Corrosion Products .....	58
Table 5-11. Case 10: Volumes of Minerals (liters) and Percent of Total Volume inside CRB .....	58
Table 5-12. Case 10: Mass (kg) and Average Density (kg/L) of Total Minerals Formed within CRB .....	59
Table 5-13. Case 10: Mole Percent of Major Elements in Non-Actinide Corrosion Products.....	59
Table 5-14. Case 9s: Mole Percent of Major Elements in Non-Actinide Corrosion Products.....	60
Table 5-15. Case 10s: Mole Percent of Major Elements in Non-Actinide Corrosion Products.....	60

**Figures**

<b><u>Item</u></b>	<b><u>Page</u></b>
Figure 5–1. Unbroken Lines: Approximate Solubility of $GdPO_4 \cdot H_2O$ , in Terms of Major Species. Dashed Lines: Solubilities Necessary to Achieve 10% Gd Loss in One Million Years at the Specified Drip Rates.....	26
Figure 5–2. Concentrations of Phosphate Species in Equilibrium with $GdPO_4 \cdot 2H_2O$ , for Total Phosphate Concentrations of $10^{-5}$ , $10^{-3}$ and $10^{-2}$ molal. ....	27
Figure 5–3. Aqueous Gd, Pu, U and pH for Case 1 (f00a1111). The pH Low (and Gd Maximum) Correspond to Degradation of A516 in the Outer Web Structure.....	32
Figure 5–4. Aqueous Gd, Pu, U and pH for Case 2 (f00a1112). The pH Low (and Gd Maximum) Correspond to Degradation of A516 in the Outer Web Structure.....	33
Figure 5–5. Aqueous Gd, Pu, U and pH for Case 3 (f00{a,b}1113). The High J-13 Flush Rate Prevents pH from Reaching Extreme Low Values.....	34
Figure 5–6. Aqueous Gd, Pu, U and pH for Case 4 (f00a1211). Because of the High Glass Degradation Rate (Compared to Figure 5–3), Acid from Steel Degradation Is Neutralized, High pH Is Reached, and U and Pu Concentrations Are High.....	35
Figure 5–7. Aqueous Gd, Pu, U and pH for Case 5 (f00a2211). This Case and Case 6 Achieve 100% U Loss. The Gd Peak Is Due to Carbonate Complexes .....	36
Figure 5–8. Aqueous Gd, Pu, U and pH for Case 5 (f00a2221). This Case and Case 5 Achieve 100% U Loss. The Gd Peak Is Due to Carbonate Complexes .....	37
Figure 5–9. Aqueous Gd, Pu, U and pH for Case 7 (f00a2222). Total Pu and U Losses Are 93.8% and 98.8%, Respectively.....	38
Figure 5–10. Aqueous Gd, Pu, U and pH for Case 8 (f00{a,b,c}2122). Compared to Case 7, the Lower Glass Degradation Rate Yields Lower Pu and U Loss (25.5% and 22.0%, Respectively), But Allows 0.7% Gd Loss During pH Low .....	39
Figure 5–11. Aqueous Gd, Pu, U and pH for Case 9 (f01_2204 / f02_2022, Hematite). Initial High U and Pu Concentrations Are from Glass; High Initial Flush Rate Removes Glass Alkalinity. The DOE SNF Canister Is Breached at 3765 Years, Exposing More Pu and U (Fuel) and Gd-Doped Basket; Lower Flush Rate Prevents High Losses.....	40
Figure 5–12. Aqueous Gd, Pu, U and pH for Case 10 (f01g2204 / f00g2022, Goethite). The DOE SNF Canister Is Breached at 3765 Years. Similar to Case 9, But Goethite Allows Slightly Lower pH Minimum.....	41
Figure 5–13. Aqueous Gd, Pu, U and pH for Case 11 (f01g2203 / f00g2021, Goethite). The DOE SNF Canister Is Breached at 3013 Years, Exposing More Pu and U (Fuel) and Gd-Doped Basket. Similar to Case 10, But Lower Flush Rates Throughout.....	42
Figure 5–14. Aqueous Gd, Pu, U and pH for Case 12 (f01g1203 / f00g1021, Goethite). The DOE SNF Canister Is Breached at 5003 Years, Exposing More Pu and U (Fuel) and Gd-Doped Basket. Similar to Case 11, But Lower Steel Degradation Rates.....	43
Figure 5–15. Aqueous Pu, U and pH for Eliminated Case 13 (f00g1103, Pre-Breach of DOE SNF). Despite pH Low, U and Pu Concentrations Remain Modest, and pH Plateaus Near Neutrality.....	44
Figure 5–16. Package Materials Remaining (Per liter Initial Void Space), and pH, for Eliminated Case 13 (f00g1103, Pre-Breach of DOE SNF). The pH Low Is Due to A516 Degradation.....	45
Figure 5–17. Aqueous Pu, U and pH for Eliminated Case 14 (f00g1104, Pre-Breach of DOE SNF). The High Flush Rate Prevents Extreme pH Variation .....	46
Figure 5–18. Case 2: pH and Moles Package Materials Remaining (Per liter Initial Void Space). The pH Minimum Is Associated with Degradation of Steels, Particularly A516.....	47

Figure 5–19. Case 2: Major Minerals and pH. In pH Minimum, Nontronite-H (Hydrogen Nontronite, Open Squares) Replaces Smectite (Solid Squares). Molar Amounts Are Per liter Initial Void Space .....	48
Figure 5–20. Case 2: pH and Solubility-Controlling Minerals for Gd (Rhabdophane), Pu, and U (Soddyite, U-Phosphate). Rhabdophane Completely Dissolves During pH Minimum, But Reprecipitates. Molar Amounts Are Per liter Initial Void Space .....	49
Figure 5–21. Case 2: Predicted Major Pu Species and pH .....	50
Figure 5–22. Case 2: Predicted Major Gd Species and pH. Gd-Carbonate Complexes Dominate Only at Early and Late Time. At Intermediate Time and Lower pH, $Gd^{3+}$ (and Gd-Phosphate Complexes) Dominate .....	52
Figure 5–23. Case 10: pH and Moles Package Materials Remaining (Per liter Initial Void Space). The pH Minimum Is Associated with Degradation of Steels .....	53
Figure 5–24. Case 10: pH and Amounts of Major and Minor Minerals Formed from Corrosion of WP (Per liter Initial Void Space). Parsonsite= $Pb_2UO_2(PO_4)_2 \cdot 2H_2O$ ; Soddyite= $(UO_2)_2SiO_4 \cdot 2H_2O$ .....	54
Figure 5–25. Case 10: pH and Predicted Pu Speciation. Following the pH Minimum, Pu-Phosphate Complexes Dominate as the Gd-Rich Basket Degrades. At Long Times, Pu-Carbonate Complexes Dominate .....	55
Figure 5–26. Case 10: pH and Predicted Gd Speciation. $Gd^{3+}$ Dominates in the pH Minimum, and Gd-Carbonate Complexes Dominate at Long Times .....	56
Figure 5–27. Moles Package Materials and pH for the First Stage (f00g2204 and fs0g2204) of Cases 10 and 10s. The Dashed pH Line Corresponds to Case 10s (with Added Mg) and the Unbroken pH Line Corresponds to Case 10 .....	61
Figure 5–28. Comparison of Case 10 (Solid Lines) and Case 10s Results (Dashed Lines). Case 10s Has a Higher Mg Content, Generates More Calcite Solid Solution ( $(Mg,Ca)CO_3$ ), and Buffers pH Longer than Case 10. This Figure Is for Time before Breach of the DOE SNF Canister .....	62
Figure 5–29. Comparison of Aqueous U, Pu and pH for Case 10 (Solid Lines) and Case 10s (Dashed). This Figure Is for Time before Breach of the DOE SNF Canister .....	63
Figure 5–30. Comparison of Aqueous Gd and pH for Case 10 (Solid Lines and Symbols) and Case 10s (Dashed Lines and Open Symbols). This Figure Is for Time after Breach of the DOE SNF Canister .....	64
Figure 5–31. Comparison of Aqueous Pu and pH for Case 10 (Solid Lines and Symbols) and Case 10s (Dashed Lines and Open Symbols). This Figure Is for Time after Breach of the DOE SNF Canister .....	65
Figure 5–32. Comparison of Aqueous U and pH for Case 10 (Solid Lines and Symbols) and Case 10s (Dashed Lines and Open Symbols). This Figure Is for Time after Breach of the DOE SNF Canister .....	66

## 1. PURPOSE

Fuel from the Fast Flux Test Facility<sup>1,2</sup> (FFTF) has been considered for disposal at the proposed Yucca Mountain site. Because of the high content of fissile material in the fuel, the waste package (WP) design requires special consideration of the amount and placement of neutron absorbers, and the possible loss of absorbers and fuel materials over geologic time. For some WPs, the outer corrosion-allowance barrier and corrosion-resistant barrier (CRB) may breach<sup>3</sup>, allowing the influx of water. Water in the package may moderate neutrons, increasing likelihood of a criticality within the package; and the water may, in time, gradually leach the fissile components and neutron absorbers from the WP, further affecting the neutronics of the system.

This study presents calculations of the long-term geochemical behavior of WPs containing FFTF driver fuel assemblies, an "Ident 69" fuel rod container, and high-level waste (HLW) glass canisters arranged according to the codisposal concept<sup>4</sup>. The specific study objectives were to determine:

- 1) the extent to which criticality control material, suggested for this WP design, will remain in the WP after corrosion/dissolution of the initial package configuration (such that it can be effective in preventing criticality),
- 2) the extent to which fissile plutonium and uranium will be carried out of the degraded WP by infiltrating water (such that internal criticality is no longer possible, but the possibility of external criticality may be enhanced), and
- 3) the nominal chemical composition for the criticality evaluations of the WP design, and to suggest the range of parametric variations for additional evaluations.

For this purpose, the chemical compositions (and consequent criticality evaluations) are modeled for time periods up to  $10^6$  years. This longer time frame is consistent with the one million years time horizon recently recommended by the National Academy of Sciences to the Environmental Protection Agency for performance assessment related to a nuclear repository<sup>5</sup>.

The calculation included elements with high neutron-absorption cross-sections, notably Gd, as well as the fissile materials. The results of this analysis will be used to ensure that the type and amount of criticality control material used in the WP design will prevent criticality.

## 2. METHOD

The method used for this analysis involves the following steps:

- Use of basic EQ3/6 (software package, Section 4.1) capability for tracing the progress of reactions with evolution of the chemistry, including the estimation of the concentrations remaining in solution and the composition of the precipitated solids. (EQ3 is used to determine a starting fluid composition for EQ6 calculations; it does not simulate reaction progress.)
- Evaluation of available data on the range of dissolution rates for the materials involved, to be used as material/species input for each time step.
- Use of “solid-centered flow-through” mode (SCFT) in EQ6; in this mode, an increment of aqueous “feed” solution is added continuously to the WP system, and a like volume of the existing solution is removed, simulating a continuously-stirred tank reactor. This mode is discussed in Section 4.2.
- Determination of fissile concentrations in solution as a function of time (from the output of EQ6 simulated reaction times up to  $10^6$  years).
- Calculation of the amount of fissile material released from the WP as a function of time (which thereby reduces the chance of criticality within the WP).
- Determination of concentrations of neutron absorbers, such as Gd and B, in solution as a function of time (from the output of EQ6 over times up to or somewhat greater than  $10^6$  years).
- Calculation of the amount of neutron absorbers retained within the WP as a function of time.
- Composition and amounts of solids (precipitated minerals or corrosion products, and unreacted package materials).

Further detail on the specific methods employed for each step is available in Section 5 of this set of calculations.

### 3. ASSUMPTIONS

All assumptions are for preliminary design; these assumptions will require verification before this analysis can be used to support procurement, fabrication, or construction activities. All assumptions are used throughout the calculations.

- 3.1 It is assumed that an aqueous solution fills all voids within WPs, and that the solutions that drip into the package will have the composition of J-13 well water (as given in Ref. 6; this composition is given in Table 5-4) for  $\sim 10^6$  years. The basis for the first part of this assumption is that it provides the maximum degradation rate with the potential for the fastest flushing of the neutron absorber from the WP, and is thereby conservative. The basis for the second part of the assumption is that the groundwater composition is controlled largely by transport through the host rock, over pathways of hundreds of meters, and the host rock composition is not expected to change substantially over  $10^6$  years. For a few thousand years after waste emplacement the composition may differ because of perturbations resulting from reactions with engineered materials and from the thermal pulse. These are not taken into account in this calculation because the corrosion allowance barrier and CRB are not expected to breach until after that perturbed period. Therefore, the early perturbation is not relevant to the calculations reported in this document. See Assumption 3.3.
- 3.2 It is assumed that the density of J-13 well water is  $1.0 \text{ g/cm}^3$ . The basis is that for dilute solutions, the density differs extremely little from that for pure water and that any differences are insignificant in respect to other uncertainties in the data and calculations. Moreover, this number is used only initially in EQ3/6 to convert concentrations of dissolved substances from parts per million to molalities.
- 3.3 It is assumed that (1) water infiltrating the WP will have only a minimal contact, if any at all, with undegraded metal in the corrosion allowance barrier, and (2) that any effects of contact with the drift liner will be minimal after a few thousand years. The basis for the first part of this assumption is that the water should move rapidly enough through openings in the WP barriers that its residence time in the corroded barrier will be too small for significant reaction to occur. Furthermore, the water flowing through the barriers will be in contact with the corrosion products left from the barrier corrosion that created the holes in the first place, but these corrosion products will closely resemble iron oxides and hydroxides in the overlying rock. Consequently, the water should already be close to equilibrium with these compounds and would be unaffected by further contact with them, even if it flowed slowly enough to permit significant reaction. The second part of this assumption is justified by the following: (1) the drift liner at the top of the drift is expected to collapse with the roof support well before 1000 years, and (2) the travel time of water through the liner will be much less than the travel time through the rock above the repository, and the liner will likely have pre-equilibrated with the ambient atmosphere, forming calcite in the exposed cement.



- 3.4 It is assumed water may circulate freely enough in the partially degraded WP that all degraded solid products may react with each other through the aqueous solution medium. The basis is that this provides one bound for the extent of chemical interactions within the WP and conservatively simulates potential preferential loss of neutron absorbers from the WP by facilitating contact of any acid that may result from corrosion of steel with neutron absorbers in spent fuel. Such circulation is expected, driven by buoyancy and thermal gradient (Assumption 3.11).
- 3.5 It is assumed that the database supplied with the EQ3/6 computer package is sufficiently accurate for the purposes of this calculation. The basis is that the data have been carefully scrutinized by many experts over the course of several decades and carefully selected by Lawrence Livermore National Laboratory (LLNL) for incorporation into the data base<sup>7,8,9,10</sup>. These databases are periodically updated and/or new databases added, such as one including extensive data on the lanthanides<sup>11</sup>. Every run of either EQ3 or EQ6 documents automatically which database is used. The databases include references internally for the sources of the data. The reader is referred to this documentation, included in electronic files labeled data0 that accompany this calculation, for details<sup>12</sup>. Nevertheless, this review and documentation do not absolutely guarantee that all the data are adequate.
- 3.6 It is assumed that the calculations can be modeled with the 25 °C thermodynamic database. The initial breach may occur when the package contents are at temperatures  $\geq 50$  °C<sup>13</sup>, though at times  $> 25,000$  years, the package temperatures are likely to be closer to 25 °C. Since the solubility of  $GdPO_4$  is retrograde<sup>14</sup> (i.e., decreases with increasing temperature), use of the lower-temperature database is likely to be conservative.
- 3.7 In general it is assumed that chromium and molybdenum will oxidize fully to chromate (or dichromate) and molybdate, respectively. This assumption is based on the available thermodynamic data, which indicate that in the presence of air the chromium and molybdenum would both oxidize to the VI valence state. Laboratory observation of the corrosion of Cr and Mo containing steels and alloys, however, indicates that any such oxidation would be extremely slow. In fact, oxidation to the VI state may not occur at a significant rate in respect to the time frame of interest, or there may exist stable  $Cr^{(III)}$  solids (not present in the EQ3/6 thermodynamic database) that substantially lower aqueous Cr concentration. For the present analyses, the assumption is made that over the times of concern the oxidation will occur. This is conservative for times of several thousand years after WP breach, when the high pH solution from any drift liner effects, has been flushed out of the WP. Acidification of the water will enhance solubility and transport of neutron absorber out of the WP thereby separating it preferentially from fissile material.

- 3.8 It is assumed that the inner CRB of the WP will react so slowly with the infiltrating water (and water ponded in the WP) as to have negligible effect on the chemistry. The bases consist of the facts that the CRB is fabricated from Alloy 22 (see nomenclature in Section 5.1.1), which corrodes very slowly compared (1) to other reactions in the WP and (2) to the rate at which soluble corrosion products will likely be flushed from the package.
- 3.9 It is assumed that gases in the solution in the WP will remain in equilibrium with the ambient atmosphere outside the WP. In other words, it is assumed that there is sufficient contact with the gas phase in the repository to maintain equilibrium with the CO<sub>2</sub> and O<sub>2</sub> present, whether or not this be the normal atmosphere in open air or rock gas that seeps out of the adjacent tuff. Under these conditions the partial pressure of CO<sub>2</sub> exerts important controls on the pH and carbonate concentration in the solution and hence on the solubility of uranium, gadolinium and other elements. As discussed in Ref. 15, the measured composition of J-13 water is not in equilibrium with the partial pressure of CO<sub>2</sub> in the atmosphere. By adjusting the average measured composition of the water slightly, well within the standard deviation of the measurements, it is possible to determine a partial pressure of CO<sub>2</sub> nearly ten times atmospheric (Ref. 15, Table 8; and Ref. 16, p. F-210), with which this water was apparently in equilibrium at depth in the well. This high partial pressure is close to the maximum found by measurement of the rock gas composition (Ref. 15, Table 8). Therefore this high partial pressure was chosen for most of the computer runs used in this analysis. Two runs with normal atmospheric CO<sub>2</sub> levels was used to determine the sensitivity of the calculations to this parameter. The high CO<sub>2</sub> tends to increase the concentration of free carbonate ion and its complexation with the dissolved U<sup>(VI)</sup>, thereby tending to increase the solubility of U, but this is moderated by the reduction of the pH. There is little overall net effect on actinide solubility for otherwise comparable conditions. The effect on Gd solubility is somewhat more complex; higher CO<sub>2</sub> pressures decrease pH, thereby increasing the chance that solid GdOHCO<sub>3</sub> will be dissolved; however, higher CO<sub>2</sub> pressures also increase the capacity of the system to buffer toward intermediate pH (~7.7).
- 3.10 It is assumed that precipitated solids that are deposited remain in place, and are not mechanically eroded or entrained as colloids in the advected water. The basis for this assumption is that it conservatively maximizes the size of potential deposits of fissile material inside the WP.
- 3.11 It is assumed that the corrosion rates will not be significantly enhanced by biologically mediated corrosion. The bases for this assumption are that even at the time that the repository is closed there will be little organic material present to serve as raw materials for growth of living organisms, and that by the time the corrosion barriers are breached essentially all of such material will most likely have decayed to carbon dioxide and dissipated.

- 3.12 It is assumed that sufficient decay heat is retained within the WP over times of interest to cause convective circulation and mixing of the water inside the package. The analysis that serves as the basis for this assumption is discussed in Ref. 17 (Attachment VI).
- 3.13 It is assumed that the alkalinity reported in analyses of J-13 water corresponds to bicarbonate ( $\text{HCO}_3^-$ ) alkalinity. Contributors to alkalinity in J-13 water, in addition to bicarbonate, potentially include borate, phosphate and silicate. However, at pH less than 9 the contribution of silicate will be small, and in any case the concentrations of all three of these components in J-13 water is small. Fluoride ion will not contribute to a typical measured alkalinity because the titration will not be carried out to a sufficiently low pH for its influence to be detectable. Nitrate will likewise not contribute. The validity of this assumption is justified by the observation that the calculated electrical neutrality, using the assumption, is zero within the analytical uncertainty, as it should be. The same assumption is implicitly made in Ref. 6 (Table 4.1, p. 4.2).
- 3.14 It is assumed that the rate of entry of water into, as well as the rate of egress from, a WP is equal to the rate at which water drips onto the package. For most of the time frame of interest, i.e., long after the corrosion barriers become largely degraded, it is more reasonable to assume that all or most of the drip will enter the degraded package than to assume that a significant portion will instead be diverted around the remains. Diversion of the water with a consequent lower entry rate has not been incorporated into the present calculations.
- 3.15 It is assumed that the most insoluble solids for a fissile radionuclide will form, i.e., that equilibrium will be reached. This is conservative for internal criticality because the assumption will lead to simulation for maximal retention of fissile material within the WP.
- 3.16 It is assumed that the decay of  $^{239}\text{Pu}$  to  $^{235}\text{U}$  can be conservatively modeled by a simple exponential correction to the reported amounts of solids in the EQ6 runs, after completion of each run. EQ6 currently has no built-in capability to handle radioactive decay. For internal criticality, this assumption is conservative, since Pu solids are generally less soluble than U solids; the assumption causes an overestimate of the amount of  $^{235}\text{U}$  remaining in the package with time.
- 3.17 Numerous minor assumptions have been made about the geometry of the FFTF codisposal package. These assumptions are outlined and referenced in the spreadsheet `fftf_fuel_hws.xls`<sup>12</sup>, and are also discussed in Section 5.1 below. The assumptions about package geometry are always intended to obtain the greatest accuracy in the representation, and where inadequate information is available to choose between competing models of package geometry, the choice that appears to lead to greatest conservatism is always chosen.

- 3.18 For any package components that were described as “316” stainless steel, without indication of the carbon grade, the alloy was assumed to be the low-carbon equivalent (see Section 5.1.1 for nomenclature). In general, the carbon in the steel is totally insignificant compared to the carbon supplied by the fixed CO<sub>2</sub> fugacity of the EQ3/6 calculation, and to the constant influx of carbonate via J-13 water. An underestimation of carbon in steel leads to a slight overestimation of metals in the steel, which increases acid production very slightly and is therefore conservative.

#### 4. USE OF COMPUTER SOFTWARE

This Section describes the computer software used to carry out the analysis.

##### 4.1 EQ3/6 SOFTWARE PACKAGE

The EQ3/6 software package originated in the mid-1970s at Northwestern University<sup>7</sup>. Since 1978 Lawrence Livermore National Laboratory has been responsible for maintenance of EQ3/6. The software has most recently been maintained under the sponsorship of the Civilian Radioactive Waste Management Program of the U.S. Department of Energy. The major components of the EQ3/6 package include: EQ3NR, a speciation-solubility code; EQ6, a reaction path code which models water/rock interaction or fluid mixing in either a pure reaction progress mode or a time mode; EQPT, a data file preprocessor; EQLIB, a supporting software library; and several (>5) supporting thermodynamic data files. The software deals with the concepts of the thermodynamic equilibrium, thermodynamic disequilibrium and reaction kinetics. The supporting data files contain both standard state and activity coefficient-related data. Most of the data files support the use of the Davies or B-dot equations for the activity coefficients; two others support the use of Pitzer's equations. The temperature range of the thermodynamic data on the data files varies from 25 °C only for some species to a full range of 0-300 °C for others. EQPT takes a formatted data file (a data0 file) and writes an unformatted near-equivalent called a data1 file, which is actually the form read by EQ3NR and EQ6. EQ3NR is useful for analyzing groundwater chemistry data, calculating solubility limits and determining whether certain reactions are in states of partial equilibrium or disequilibrium. EQ3NR is also required to initialize an EQ6 calculation.

EQ6 models the consequences of reacting an aqueous solution with a set of reactants which react irreversibly. It can also model fluid mixing and the consequences of changes in temperature. This code operates both in a pure reaction progress frame and in a time frame. In a time frame calculation, the user specifies rate laws for the progress of the irreversible reactions. Otherwise, only relative rates are specified. EQ3NR and EQ6 use a hybrid Newton-Raphson technique to make thermodynamic calculations. This is supported by a set of algorithms which create and optimize starting values. EQ6 uses an ordinary differential equation (ODE) integration algorithm to solve rate equations in time mode. The codes in the EQ3/6 package are written in FORTRAN 77 and have been developed to run under the UNIX operating system on computers ranging from workstations to supercomputers. Further information on the codes of the EQ3/6 package is provided in Refs. 7, 8, 9 and 10.

In this study EQ3/6 was used to provide:

- 1) a general overview of the nature of chemical reactions to be expected,
- 2) the degradation products likely to result from corrosion of the waste forms and canisters, and
- 3) an indication of the minerals, and their amounts, likely to precipitate within the WP.

The programs have not been used outside the range of parameters for which they have been verified. The EQ3/6 calculations reported in this document used version 7.2b of the code, which is appropriate for the application, and were executed on Pentium series (including "Pentium II") personal computers (PCs).

The EQ3/6 package has been verified by its present custodian, Lawrence Livermore National Laboratory. The source codes were obtained from Software Configuration Management in accordance with M&O QAP-SI-3. The code was installed on the Pentium PCs according to an M&O-approved Installation and Test procedure<sup>18</sup>.

#### **4.2 SOLID-CENTERED FLOW-THROUGH MODE**

EQ6 version 7.2b, as distributed by LLNL, does not contain an SCFT mode. To add this mode, it is necessary to change the eq6.for source code, and recompile the source. However, by using a variant of the "special reactant" type built into EQ6, it is possible to add the functionality of SCFT mode in a very simple and straightforward manner. This mode was added to EQ6 per Software Change Request (SCR) LSCR198, and the Software Qualification Report (SQR) for Media Number 30084-M04-001.

The new mode is induced with a "special-special" reactant. The EQ6 input file nomenclature for this new mode is jcode=5; in the Daveler format, it is indicated by the reactant type DISPLACER). The jcode=5 is immediately trapped and converted to jcode=2, and a flag is set to indicate the existence of the DISPLACER reactant. Apart from the input trapping, the distinction between the DISPLACER and SPECIAL reactants is seen only in one 9-line block of the of the EQ6 FORTRAN source code (in the reacts subroutine), where the total moles of elements in the rock plus water system (mte array) is adjusted by adding in the DISPLACER reactant, and subtracting out a commensurate amount of the total aqueous elements (mtea array).

This new EQ6 mode acts as a substitute for the allpost/nxtinput method described in Ref. 19 and Ref. 20. Early in this study, the allpost/nxtinput method was used to estimate average mineral compositions for neutronics calculations. The codes used for that analysis were identical to those listed in Ref. 19, Attachment III. The tables produced by the older allpost/nxtinput method are given in Section 5.3.6, to provide traceability for other documents, and the input and output files for these calculations are included in the electronic media accompanying this calculation<sup>12</sup>.

### 4.3 SPREADSHEETS

Spreadsheet analyses were performed with Microsoft Excel version 97, installed on a PC. The specific spreadsheets used for results reported in this document are included with the electronic media<sup>12</sup>.

### 4.4 SOFTWARE APPROVED FOR QA WORK

The software package, EQ3/6, Version 7.2b, was approved for QA work by LLNL (Memorandum to File from Royce E. Monks, dated March 28, 1997, QA designator 97/026). An installation and test report<sup>18</sup> was written and submitted to Software Configuration Management (SCM), and the proper installation was verified, before the runs described in this calculation were made. The implementation of the SCFT mode is covered by Software Change Request (SCR) LSCR198, and the Software Qualification Report (SQR) for Media Number 30084-M04-001. The SCFT addendum was installed on three of the Central Processing Units (CPUs) identified in block 16 of the SCR, and the installation and test reports were filed and returned to SCM before the calculations were run.

## 5. CALCULATION

The calculations begin with selection of data for compositions, amounts, surface areas, and reaction rates of the various components of FFTF WPs. These quantities are recalculated to the form required for entry into EQ6. For example, weight percentages of elements or component oxides are converted to mole fractions of elements; degradation rates in micrometers/year are converted into moles per square centimeter per second, etc. Spreadsheets<sup>12</sup> provide details of these calculations, and the general procedure is also described in detail in Ref. 20. The final part of the input to EQ6 consists of the composition of J-13 well water together with a rate of influx to the WP that corresponds to suitably chosen percolation rates into a drift and drip rate into a WP (Section 5.1.1.3). The EQ6 output provides the results of modeling of the chemical degradation of the WP, or components thereof. Sometimes the degradation of the WP is divided into phases, e.g., degradation of HLW glass before breach and exposure of the fuel assemblies and basket materials to the water. The results include the compositions and amounts of solid products and of substances in solution. Details of the results are presented below.

### 5.1 CALCULATION INPUTS

#### 5.1.1 WP Materials and Performance Parameters

This section provides a brief overview of the physical and chemical characteristics of FFTF WPs, and describes how the package is represented in the EQ6 inputs. The conversion of the package physical description, into parameters suitable for the EQ6 input files, is performed by the spreadsheet `fftf_fuel_hws.xls`. Additional details of the description may be found in References 1 and 2 and the references cited therein.

Material nomenclature used throughout this document includes: SB-575 N06022 (hereafter referred to as Alloy 22), SA-240 S31603 (hereafter referred to as 316L), UNS N06625 (hereafter referred to as Alloy 625) and SA-240 S30403 (hereafter referred to as 304L), and SA-516 (hereafter referred to as A516).

#### **5.1.1.1 Physical and Chemical Form of FFTF WPs**

It is convenient to consider the FFTF package as several structural components, specifically: (1) the outer shell, consisting of the corrosion-allowance barrier and the CRB; (2) the “outer web”, a carbon steel (A516) structure designed to hold the high-level waste (HLW) glass-pour canisters (GPCs) in place; (3) the GPCs themselves, including the 304L containers and the solidified HLW glass; (4) the Department of Energy (DOE) spent nuclear fuel (SNF) canister (sometimes called the “18 inch canister”) and its basket structure; (5) the FFTF fuel assemblies, particularly the stainless steel hexagonal duct and the structures inside the driver fuel assemblies, exclusive of the fuel pins; and (6) the individual fuel pins. Each of these components corresponds to a sheet in the spreadsheet `fftf_fuel_hws.xls`.

Table 5–1 provides a summary of the compositions of the principal alloys used in the calculations, along with reasonable maxima and minima for the degradation rates. For a comparable specific surface area, the carbon steel is expected to degrade much more rapidly than the stainless steels (316L and 304L). In addition, the stainless steels contain significant amounts of Cr and Mo, and under the assumption of complete oxidation (Assumption 3.7), should produce more acid, per volume, than the carbon steel. In Table 5–1 and all tables from this document, the number of digits reported does not necessarily reflect the accuracy or precision of the calculation. In most tables, three to four digits after the decimal place have been retained, to prevent round-off errors in subsequent calculations.



**Table 5-1. Steel Compositions and Degradation Rates**

A516 Carbon Steel			304L Stainless Steel		316L Stainless Steel		316L with 3 wt% GdPO4	
Element	wt%	Atom Frac.	wt%	Atom Frac.	wt%	Atom Frac.	wt%	Atom Frac.
C	0.300	1.375E-02	0.030	1.365E-03	0.030	1.383E-03	0.029	1.329E-03
Mn	1.025	1.027E-02	2.000	1.990E-02	2.000	2.016E-02	1.940	1.937E-02
P	0.035	6.221E-04	0.045	7.942E-04	0.045	8.044E-04	0.412	7.297E-03
S	0.035	6.027E-04	0.030	5.129E-04	0.030	5.195E-04	0.029	4.992E-04
Si	0.275	5.391E-03	0.750	1.460E-02	0.750	1.478E-02	0.728	1.421E-02
Cr	0.000	0.000E+00	19.00	1.998E-01	17.000	1.810E-01	16.490	1.739E-01
Ni	0.000	0.000E+00	10.000	9.311E-02	12.000	1.132E-01	11.640	1.087E-01
Mo	0.000	0.000E+00	0.000	0.000E+00	2.500	1.443E-02	2.425	1.386E-02
N	0.000	0.000E+00	0.100	3.904E-03	0.100	3.954E-03	0.097	3.799E-03
Fe	98.330	9.694E-01	68.045	6.661E-01	65.545	6.498E-01	63.579	6.244E-01
Gd	0.000	0.000E+00	0.000	0.000E+00	0.000	0.000E+00	1.871	6.524E-03
O	0.000	0.000E+00	0.000	0.000E+00	0.000	0.000E+00	0.761	2.609E-02
<b>Total</b>	<b>100.00</b>	<b>1.000E+00</b>	<b>100.000</b>	<b>1.000E+00</b>	<b>100.00</b>	<b>1.000E+00</b>	<b>100.00</b>	<b>1.000E+00</b>
<b>Molecular Weight</b>	55.055		54.666		55.365		54.843	
<b>Density (g/cm<sup>3</sup>)</b>	7.832		7.900		7.950		7.811	
<b>Average Rate (μm/year)</b>	35		0.1		0.1		0.1	
<b>Average Rate (moles/cm<sup>2</sup>/sec)</b>	1.58E-11		4.58E-14		4.55E-14		4.55E-14	
<b>High Rate (μm/year)</b>	1.0E+02		1.0		1.0		1.0	
<b>High Rate (moles/cm<sup>2</sup>/sec)</b>	4.51E-11		4.58E-13		4.55E-13		4.55E-13	
References spreadsheet: fff_fuel_hws.xls, sheets one_pin, Steels, Rates.								

Table 5-2 gives the molar composition of the glass used in the calculations (Ref. 21, Attachment V, p. 3.; see note in Section 5.3.7 regarding C and Mg compositions). The actual glass composition used in the GPCs may vary significantly from these values, since the sources of the glass and melting processes are not currently fixed. For example, compositions proposed for Savannah River glass vary by a factor of ~6 in U<sub>3</sub>O<sub>8</sub> content, from 0.53 to 3.16 wt%<sup>22</sup>. The silica and alkali contents (Na, Li and K) of the glass have perhaps the most significant bearing on EQ6 calculations. The amount of silica in the glass strongly controls the amount of clay that forms in the WP, and the silica activity controls the presence of insoluble uranium phases such as soddyite ((UO<sub>2</sub>)<sub>2</sub>SiO<sub>4</sub>·2H<sub>2</sub>O). The alkali content can induce pH to rise in the early stages of the EQ6 run, as glass degrades. The Si and alkali contents in Table 5-2 are typical for proposed DOE glasses, but alkaline earth content is low, and the U content in Table 5-2 is high compared to

compositions recently produced at Savannah River<sup>23</sup>. However, this high U content is conservative, since it enhances the precipitation of U solids, and ultimately the retention of fissile

**Table 5-2. Glass Composition and Rates**

Glass Composition <sup>1</sup>			Transmuted Composition <sup>2</sup>	
Element / Isotope	wt%	Moles	Element	Moles
<sup>6</sup> Li	1.080E-01	1.8000E-02	Li	2.0834E-01
<sup>7</sup> Li	1.332+00	1.9034E-01	B	2.9090E-01
<sup>10</sup> B	6.234E-01	6.2418E-02	C	6.7158E-02
<sup>11</sup> B	2.509E+00	2.2848E-01	O	2.7643E+00
C	8.046E-01	6.7158E-02	F	1.6401E-03
O	4.4102E+01	2.7643E+00	Na	3.5903E-01
F	3.108E-02	1.6401E-03	Al	7.6432E-02
Na	8.233E+00	3.5903E-01	Si	7.8413E-01
Al	2.057E+00	7.6432E-02	P	4.4408E-04
Si	2.1967E+01	7.8413E-01	S	3.9604E-03
P	1.372E-02	4.4408E-04	Cl	3.1984E-03
S	1.263E-01	3.9604E-03	K	7.4764E-02
Cl	1.131E-01	3.1984E-03	Ca	1.6154E-02
K	2.916E+00	7.4764E-02	Ti	1.2188E-02
Ca	6.458E-01	1.6154E-02	Cr	1.5531E-03
Ti	5.823E-01	1.2188E-02	Mn	2.7738E-02
Cr	8.055E-02	1.5531E-03	Fe	1.2945E-01
Mn	1.520E+00	2.7738E-02	Ni	1.2244E-02
Fe	7.211E+00	1.2945E-01	Cu	2.3494E-03
Ni	7.170E-01	1.2244E-02	Ag	4.5163E-04
Cu	1.489E-01	2.3494E-03	Ba	5.9004E-04
Ag	4.906E-02	4.5163E-04	Sm	2.9696E-06
Ba	8.083E-02	5.9004E-04	Pb	2.8781E-04
<sup>149</sup> Sm	4.411E-04	2.9696E-06	U	1.5584E-02
Pb	5.948E-02	2.8781E-04	Np	7.1813E-06
<sup>233</sup> U	9.727E-09	4.1846E-11	Pu	5.2541E-05
<sup>234</sup> U	3.261E-04	1.3969E-06	Sum:	4.8529E+00
<sup>235</sup> U	1.734E-02	7.3961E-05		
<sup>236</sup> U	1.036E-03	4.4002E-06	Density (g/cm <sup>3</sup> )	2.85
<sup>238</sup> U	3.674E+00	1.5473E-02		
<sup>237</sup> Np	7.509E-04	3.1758E-06	Low Rate (g/m <sup>2</sup> /day)	1E-04
<sup>238</sup> Pu	5.153E-03	2.1702E-05	Low Rate (moles/cm <sup>2</sup> /sec)	1.1574E-15
<sup>239</sup> Pu	1.234E-02	5.1752E-05	High Rate (g/m <sup>2</sup> /day)	3E-02
<sup>240</sup> Pu	2.265E-03	9.4594E-06	High Rate (moles/cm <sup>2</sup> /sec)	3.4722E-13
<sup>241</sup> Pu	9.631E-04	4.0055E-06		
<sup>242</sup> Pu	1.906E-04	7.8942E-07		
Sum	9.9746+01	4.8529E+00		

1. Ref. 21 (Attachment V, p. 3); see Section 5.3.7 regarding C, Mg, and U composition.

2. Actinides with half-lives < 7000 years were converted to appropriate daughters.

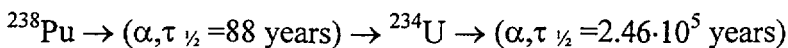
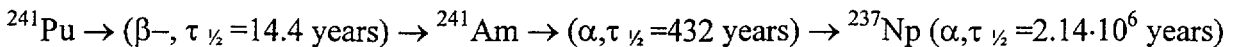
Reference spreadsheet: fftf\_fuel\_hws.xls, sheets Glass&Fuel and Rates.

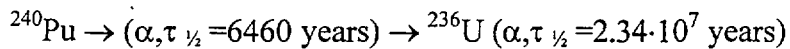
materials within the package. Rates for glass degradation were taken from Ref. 24 (Figure 6.2-5), and normalized in spreadsheet *fftf\_fuel\_hws.xls*<sup>12</sup>, sheet Rates. The high rate corresponds approximately to pH 9 at 70 °C, and the low rate to pH 8 at 25 °C.

**Table 5-3. MOX Compositions and Degradation Rates**

Time=0:		Transmuted:	
	Mole Frac.		Mole Frac.
<sup>239</sup> Pu	2.5419E-01	<sup>239</sup> Pu	2.5437E-01
<sup>240</sup> Pu	3.3937E-02	<sup>240</sup> Pu	0.0000E+00
<sup>241</sup> Pu	2.9764E-03	<sup>241</sup> Pu	0.0000E+00
<sup>235</sup> U	1.4164E-03	<sup>235</sup> U	1.4174E-03
<sup>238</sup> U	7.0678E-01	<sup>238</sup> U	7.0727E-01
<sup>236</sup> U	0.0000E+00	<sup>236</sup> U	3.3961E-02
<sup>237</sup> Np	0.0000E+00	<sup>237</sup> Np	2.9785E-03
SUM	9.9930E-01	SUM	1.0000E+00
Average Molecular Weight (U,Pu,Np)O <sub>2</sub>		270.37	
Density Fuel Pellets (g/cm <sup>3</sup> )		10.02	
Average Fuel Degradation Rate (mg/m <sup>2</sup> /day)		2.8234	
Average Fuel Degradation Rate (moles/cm <sup>2</sup> /sec)		1.2087E-14	
Fast Fuel Degradation Rate (mg/m <sup>2</sup> /day)		13.837	
Fast Fuel Degradation Rate (moles/cm <sup>2</sup> /sec)		5.9235E-14	
References: Reference Spreadsheet: <i>fftf_fuel_hws.xls</i> , sheets <i>one_pin</i> , <i>Glass&amp;Fuel</i> , <i>Rates</i>			

Table 5-3 summarizes the assumed characteristics of the mixed oxide (MOX, or (U,Pu)O<sub>1.96</sub>) fuel. No fission product inventory was available, so the calculations used the composition of fresh fuel. Use of fresh fuel is conservative, since most fission products have significant neutron absorption cross sections, and the unirradiated fuel has a higher fissile content than partially spent fuel. However, it is expected that the breach of the package will not occur until at least 3000 years after emplacement (Ref. 25, p 3-65), and most of the calculation will involve times greater than 10,000 years post-emplacment. Thus the “fresh fuel” composition used in EQ6 has been altered to pre-decay some of the shorter-lived isotopes. In particular, the isotopes on the left side of the following chains were converted completely to the isotopes on the right side, as inputs to the EQ3/6 calculations:





where  $\tau_{1/2}$  is the decay half life for the specified decay mode.

The outer web (Attachment I) is composed of A516 carbon steel, and serves two purposes: it centers and holds in place the DOE SNF canister; and it separates the GPCs and prevents them from transmitting undue stress to the SNF canister in the event of a fall (tip-over) of the entire WP. At the center of the outer web is a thick (3.175 cm) cylindrical support tube, also constructed of A516. In a breach scenario, the outer web will be exposed to water and corrosion before the rest of the package, and is expected to degrade within a few hundred to a few thousand years. The transformation of the web into hematite ( $\text{Fe}_2\text{O}_3$ ) can decrease the void space in the package by ~13%, and the transformation to goethite ( $\text{FeOOH}$ ) can decrease to void space by ~22% (spreadsheet `fftf_fuel_hws.xls`, sheet `Void_calc`, variables `VOW_TO_HEM_DELTA` and `VOW_TO_GOE_DELTA`). Thus the void space can be significantly reduced, soon after breach of the package, by the alteration of the outer web.

The DOE SNF canister fits inside the central support tube of the outer web. The canister is composed primarily of 316L, with two internal, thick impact plates of carbon steel (approximated as A516 in the calculations). Within the DOE SNF canister is a 316L "basket", consisting of a central tube and five radial fins (Attachment II). The central tube of the basket contains one "Ident 69"<sup>1</sup>, which consists of de-rodged fuel pins in a 304L container. The spaces between pairs of fins are partly filled with fuel assemblies (conservatively assumed to be driver fuel assemblies). The assemblies are composed of 316 stainless steel, and are hexagonal in cross section<sup>1</sup>.

Current plans call for addition of  $\text{GdPO}_4$  to the package, to decrease chances of internal criticality. The likely location for the  $\text{GdPO}_4$  is near the basket structure inside the DOE canister, but the method of inclusion is not yet determined. For this study,  $\text{GdPO}_4$  was added as solid inclusions to hypothetical 316L steel. Two compositions were used: steel containing 1.87 % Gd by weight (3%  $\text{GdPO}_4$  by weight); and steel containing 5% Gd by weight. The rate of exposure of the  $\text{GdPO}_4$ -steel mix was then taken to be the corrosion rate of 316L steel (Table 5-1).

Each fuel pin contains ~150 sintered pellets of MOX, and 4 pellets of sintered natural uranium oxide. The pellets are clad in 316 stainless steel, and are helically wrapped with 316 steel wires to provide lateral spacing. Each pin also contains two Inconel reflectors. Based on corrosion rates listed in Ref. 26, this high-Ni alloy appears to have general corrosion properties similar to Alloy 22, and is considered inert per Assumption 3.8.

While the unirradiated MOX composition has been assumed in Table 5-3, the characteristics of irradiated fuel must be considered in the estimation of reaction rates. In particular, irradiated FFTF fuels can have numerous cracks and large central voids. The rates in Table 5-3 were taken

from commercial fuel degradation rates listed in Ref. 24 (p. 6-2, equation 6.2-1) and a multiplication factor (also from Ref. 24, p. 6-5) was used to account for surface area enhancement from fractures and porosity development during irradiation. The heavy metal/oxygen ratio for the MOX was taken as 1/2, since fuels generally become more oxidized with burn-up, and since the oxygen-buffering properties of the MOX are swamped by the assumption of fixed oxygen fugacity.

**5.1.1.2 Chemical Composition of J-13 Well Water**

It was assumed that the water composition entering the WP would be the same as for water from well J-13 (Assumptions 3.1 and 3.3). This water has been analyzed repeatedly over a span of at least two decades (Ref. 6). This composition is reproduced in Table 5-4.

**Table 5-4. Composition of J-13 Well Water<sup>1</sup>**

Component	Units <sup>2</sup>
Na <sup>+</sup>	45.8
K <sup>+</sup>	5.04
Ca <sup>++</sup>	13.0
Mg <sup>++</sup>	2.01
NO <sub>3</sub> <sup>-</sup>	8.78
Cl <sup>-</sup>	7.14
F	2.18
SO <sub>4</sub> <sup>2-</sup>	18.4
Si	28.5
PO <sub>4</sub> <sup>3-</sup>	0.12
Alkalinity <sup>3</sup>	128.9
pH	7.41
1. Ref. 6. 2. mg/L, except for pH. 3. Assumed to be HCO <sub>3</sub> <sup>-</sup> .	

**5.1.1.3 Drip Rate of J-13 Water into a WP**

It is assumed (Assumption 3.14) that the drip rate onto a WP is the same as the rate at which water flows through the WP. The drip rate is taken from a correlation between percolation rate and drip rate (Ref. 27). Specifically percolation rates of 40 mm/yr and 8 mm/yr correlate with drip rates onto the WP of 0.15 m<sup>3</sup>/yr and 0.015 m<sup>3</sup>/yr, respectively. The choice of these particular percolation and drip rates is discussed in detail in Ref. 20.

For the present study, the range of allowed drip rates was extended to include an upper value of 0.5 m<sup>3</sup>/yr and a lower value of 0.0015 m<sup>3</sup>/yr. The upper value corresponds to the 95 percentile

upper limit for a percolation rate of 40 mm/yr (as determined in Ref. 27, and Ref. 25, pp. 10-19 to 10-24), and the lower value is simply 1/10<sup>th</sup> the mean value for the 8 mm/yr percolation rate. These extreme values were used, because prior studies (Ref. 28; Ref. 29) suggested that when ceramic waste forms are codisposed with glass, the greatest chance of Gd removal occurs when: (1) initial high drip rates cause glass leaching and removal of alkali; and (2) subsequent low drip rates allow acid to build from steel degradation.

**5.1.1.4 Densities and Molecular Weights of Solids**

For input to criticality calculations, one must convert moles of solids to solid volumes. A few solid phases contribute the overwhelming bulk of the total volume; the Table 5-5 provides some the densities and molar volumes for these phases. The new SCFT version of EQ6 (Section 4.2) performs the volume calculations automatically.

**Table 5-5. Densities and Molecular Weights of Precipitated Solids**

Solid	Density (kg/m <sup>3</sup> )	Molecular Weight <sup>c</sup>	Mol. Vol. (cm <sup>3</sup> /mol) <sup>c</sup>	Calc. Density (g/cm <sup>3</sup> )
Diaspore (AlOOH)	3400 <sup>a</sup>	59.988	17.760	3.378
Hematite (Fe <sub>2</sub> O <sub>3</sub> )	5240 <sup>b</sup>	159.692	30.274	5.275
Pyrolusite (MnO <sub>2</sub> )	5060 <sup>a</sup>	86.937	17.181	5.060 <sup>a</sup>
Goethite (FeOOH)		88.854	20.820	4.268
Ni <sub>2</sub> SiO <sub>4</sub>		209.463	42.610	4.916
Trevorite (NiFe <sub>2</sub> O <sub>4</sub> )		234.382	44.524	
Nontronite-Ca		424.293	131.100	3.236
Nontronite-K		430.583	135.270	3.183
Nontronite-Mg		421.691	129.760	3.250
Nontronite-Na		425.267	132.110	3.219
References:				
<sup>a</sup> Ref. 30, 172.				
<sup>b</sup> Ref. 16, p. B-121				
<sup>c</sup> Ref. 12 (EQ3/6 Data base, data0.nuc.R8a), g/mole, except for pyrolusite, which is calculated from the density and molecular weight. Trevorite given same molar volume as magnetite in EQ3/6 database.				

**5.1.1.5 Atomic Weights**

Atomic weights were taken from Ref. 31 and Ref. 32, and are listed in Ref. 12 (spreadsheet fftf\_fuel\_hws.xls, sheet AtomicWts).

## 5.2 DATA CONVERSION

The data presented in Section 5.1 are largely not in a form suitable for entry into EQ3/6. The transformation to EQ3/6 format consists largely in converting mass fractions to mole fractions, normalizing surface areas, volumes and moles to 1 liter reactive water in the system, and converting rates to moles/(cm<sup>2</sup> sec). Most of these conversions are straightforward and are performed in the spreadsheets, which are included in the electronic media for this document (Ref. 12). Ref. 20 describes the conversion process in detail.

## 5.3 EQ6 CALCULATIONS AND SCENARIOS MODELED

An internal criticality is possible, if the fissile material remains behind in the WP and the Gd and other neutron absorbers are flushed from the system. Uranium and plutonium are quite soluble in the alkaline, carbonate-rich solutions produced when the HLW glass degrades. The proposed criticality control material, GdPO<sub>4</sub>, will hydrate slightly when exposed to water, to form GdPO<sub>4</sub>·H<sub>2</sub>O. The latter is very sparingly soluble in neutral solutions<sup>14</sup>, though its solubility does increase at low and high pH; complexation at high pH is particularly enhanced by dissolved carbonate<sup>33</sup>. Conditions of low pH could be achieved when steel degrades separately from the HLW glass. One general scenario that maximizes the chance of internal criticality involves early breach of the 304L stainless steel canisters holding the HLW, followed by fast degradation of the HLW glass and removal of the alkaline components during a period of relatively high drip rate. Then the 316L stainless steel DOE canister is allowed to breach, exposing some portion of the MOX fuel; in this second stage, the pH of the ambient solutions is controlled to low values (~5 to ~6), in part by the degradation of the steel.

The scenarios chosen for this study build upon three previous analyses of U, Pu, Gd and B loss from WPs containing fissile waste forms codisposed with HLW glass (Ref. 28; Ref. 29; Ref. 19). These prior studies suggested that the greatest removal of Gd would occur at low drip rates in the second stage described above. However, most previous work was performed on the assumption that GdOHCO<sub>3</sub> would be the solubility-limiting phase; it must be expected that when GdPO<sub>4</sub>·H<sub>2</sub>O is allowed to form, the overall solubility and Gd loss will be lower. But as the solubility product of GdOHCO<sub>3</sub> includes both hydroxyl and carbonate, it must be also be expected that GdPO<sub>4</sub>·H<sub>2</sub>O solubility will be more greatly affected by high pH and high CO<sub>2</sub> pressures.

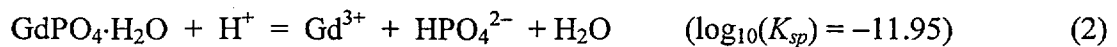
### 5.3.1 Controls on GdPO<sub>4</sub>·H<sub>2</sub>O Solubility

Before discussing the EQ6 calculations, it useful to approximate the concentrations of Gd expected in solution, particularly at "long" times, when the chemistry of the package is dominated by J-13 water influx. These approximations can then be compared against the minimum aqueous Gd concentration needed to cause significant loss of Gd from the co-dipsosal package. Once such a comparison is made, it is easier to understand the results of the EQ6

calculations, and to develop a set of run conditions that will span the conditions likely to maximize loss of Gd.

Two simplified systems can be used to bound the maximum Gd solubility. For the first system (herein called system **A**), it is assumed that the only source of aqueous Gd and phosphorus is the dissolution of solid  $GdPO_4 \cdot H_2O$ . That is, no phosphorus is supplied by steel or glass. These assumptions are reasonable if the system has been flushed for some time, removing the dissolved phosphate contributions from fast-reacting components; however, it could be speculated that such a system would underestimate Gd solubility via aqueous Gd-phosphate complexes. Therefore a second system is considered, in which aqueous Gd concentration is still controlled by  $GdPO_4 \cdot H_2O$ , but aqueous phosphate is varied independently. The second system (herein called system **B**) is used to estimate the maximum contribution of aqueous phosphate complexes, when other phosphate sources (such as glass and steel) exist. For example, the glass composition used the current FFTF calculations contains ~6% as much phosphorus as a steel doped with 3 wt%  $GdPO_4$ ; however, the amount of glass is so large, the glass contains ~3 times as much phosphorus as the Gd-doped steel (this comparison should be kept in mind when discussing the "biological impact" of adding phosphate in the form of  $GdPO_4$ ). For these simplified calculations, all stability constants were obtained from the EQ3/6 database data0.nuc.R8a<sup>12</sup>, and the plots created via spreadsheet Gd\_conc\_needed\_for\_loss.xls. Given the approximate nature of the calculations and the generally dilute solutions, it was assumed concentrations and activities were the same. In these simplified systems, the effect of minor complexants, such as fluoride and sulfate, is not considered.

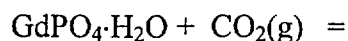
In system **A**, at  $4 \leq pH \leq 6.5$ , the aqueous Gd concentration is dominated by  $Gd^{3+}$  (Ref. 33, p. 1135), and can be estimated from:



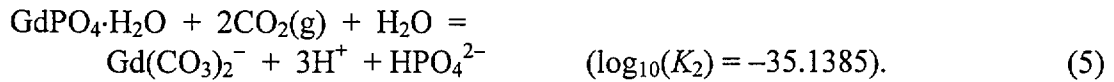
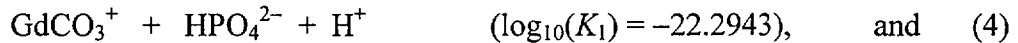
with the approximation  $[Gd^{3+}] \sim [HPO_4^{2-} + H_2PO_4^-] \sim [HPO_4^{2-}]\{1 + [H^+]/K_a\}$  (that is,  $GdPO_4 \cdot H_2O$  dissolution is the only source of phosphorus, and  $PO_4^{3-}$  concentrations are negligible in this pH range). Thus:

$$[Gd^{3+}] \approx \sqrt{[H^+] \cdot K_{sp} \cdot (1 + [H^+]/K_a)}. \quad (3)$$

At higher pH, and at moderate  $CO_2$  pressures, the complexes  $GdCO_3^+$  and  $Gd(CO_3)_2^-$  are expected to dominate; for the heavier rare earths, the carbonate complexes begin to dominate between 6.5 and 7, with complexes like  $Gd(CO_3)_2^-$  becoming most important at  $pH > 8$  (Ref. 33, p. 1135). The concentrations of these species can be determined by the equilibria:







As above, we assume congruent  $\text{GdPO}_4 \cdot \text{H}_2\text{O}$  dissolution, so that the concentration of each Gd-carbonate species is  $\sim [\text{HPO}_4^{2-} + \text{H}_2\text{PO}_4^-] \sim [\text{HPO}_4^{2-}] \{1 + [\text{H}^+]/K_a\}$  in its region of dominance. From simple algebraic substitution into the formulae for equilibrium constants  $K_1$  and  $K_2$ , the concentrations of the Gd-carbonate species, plotted in Figure 5-1, are determined by  $[\text{GdCO}_3^+] \sim \{K_1 \cdot (1 + [\text{H}^+]/K_a) \cdot f\text{CO}_2 / [\text{H}^+]\}^{1/2}$  and  $[\text{Gd}(\text{CO}_3)_2^-] \sim \{[1 + [\text{H}^+]/K_a] \cdot K_2 \cdot (f\text{CO}_2)^2 / [\text{H}^+]^3\}^{1/2}$ . For the calculations in Figure 5-1,  $\text{CO}_2$  fugacity ( $f\text{CO}_2$ ) is fixed at  $10^{-2.539}$  atm, approximately 10 times normal atmospheric levels, following the logic in Ref. 19 and Ref. 20. At modest total phosphate concentrations typical of natural waters<sup>33</sup>, the most important phosphate complex is expected to be  $\text{GdPO}_4(\text{aq})$  (Ref. 33, p. 1135); stability constants in the EQ3/6 database<sup>12</sup> suggest that  $\text{GdHPO}_4^+$  could be important at lower pH. For all pH, the concentrations of these species can be estimated via:



Figure 5-1 gives the calculated concentrations of these species, as a function of pH. The dashed lines in Figure 5-1 show the minimum aqueous Gd concentrations that are necessary to achieve significant loss at drip rates of 0.0015, 0.015, and 0.15  $\text{m}^3/\text{year}$ . A "significant" loss is arbitrarily defined as: loss of 10% of the total Gd in the codisposal system, over a period of  $10^6$  years. The required concentrations ( $C_{min}$ ) are calculated as:

$$C_{min} = 0.1 \cdot (\text{Total moles Gd}) / ((10^6 \text{ years}) \cdot (\text{drip rate in } \text{m}^3/\text{year}) \cdot 10^3 \text{L}/\text{m}^3). \quad (8)$$

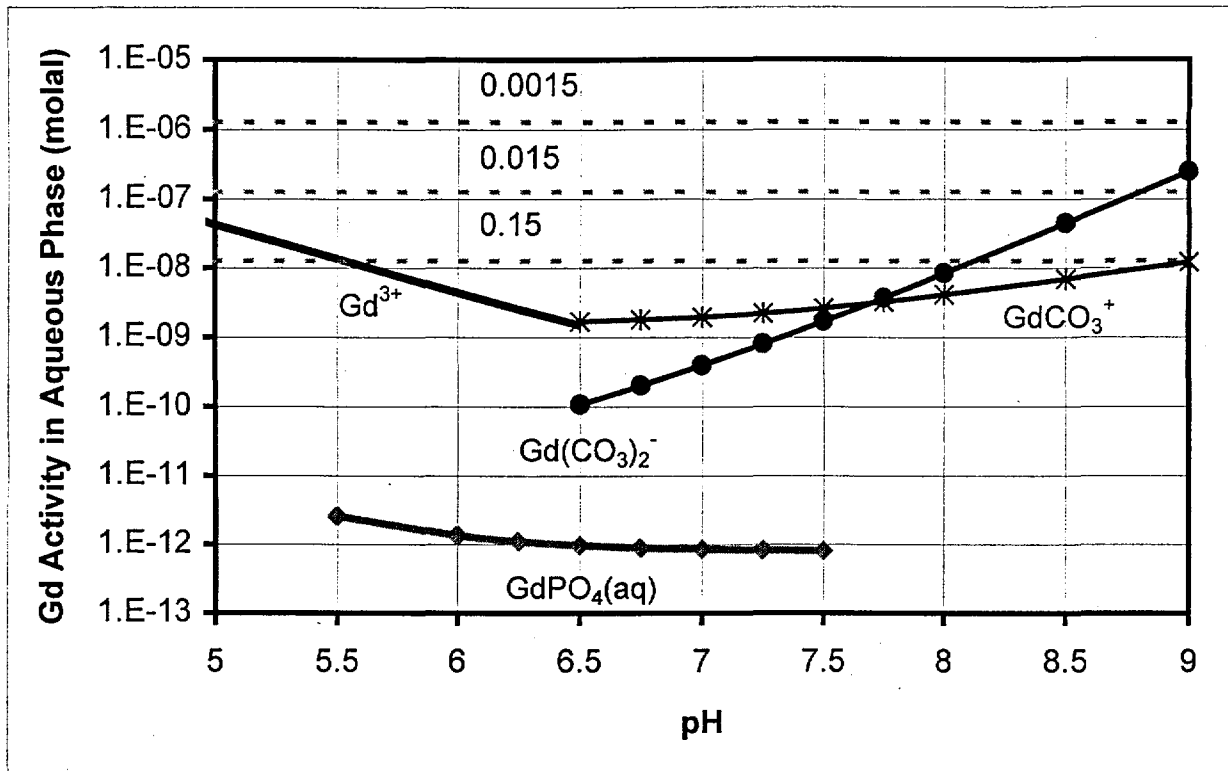


Figure 5-1. Unbroken Lines: Approximate Solubility of GdPO<sub>4</sub>·H<sub>2</sub>O, in Terms of Major Species. Dashed Lines: Solubilities Necessary to Achieve 10% Gd Loss in One Million Years at the Specified Drip Rates

At a drip rate of 0.0015 m<sup>3</sup>/year (top dashed line), the concentrations of all the plotted Gd species are too low to allow significant loss. At 0.015 m<sup>3</sup>/year (middle dashed line), only Gd(CO<sub>3</sub>)<sub>2</sub><sup>-</sup> achieves a high enough concentration for significant loss, and only with pH > 8.7 for 10<sup>6</sup> years. However, with the chosen high CO<sub>2</sub> fugacity, the long-term pH will be ~7.6<sup>19</sup>, so it is extremely unlikely that significant loss will occur (at lower CO<sub>2</sub> fugacities, a higher pH is possible, but the stability of Gd(CO<sub>3</sub>)<sub>2</sub><sup>-</sup> decreases at lower CO<sub>2</sub> fugacities). At the drip rate of 0.15 m<sup>3</sup>/year, Gd<sup>3+</sup> reaches sufficient concentrations at pH < 5.5, and Gd(CO<sub>3</sub>)<sub>2</sub><sup>-</sup> achieves adequate concentrations for loss at pH > 8. As noted before, the long-term pH is likely to be < 8, so the latter species is probably not that significant. Previous studies<sup>19,21</sup> suggest high pH can be achieved when glass degrades rapidly, but at such high drip rates, the period of high pH is limited to thousands, not millions, of years. Similarly, previous studies<sup>19,20</sup> showed that acid conditions (pH < 6) could be produced in the codisposal packages, but generally only for “short” periods ranging over hundreds of years to tens of thousands of years. Thus it appears that unusual conditions will be required to achieve significant loss of Gd, when the element is present in the package as solid GdPO<sub>4</sub>. The matrix of EQ6 run conditions (Section 5.3) has been chosen to emphasize conditions that could create either acid or alkaline conditions, and to determine if these conditions are of sufficient duration to induce Gd loss. Other components known to cause Gd complexation (e.g., the EQ6 databases contain stability constants for Gd fluoride and sulfate

complexes) should be retained in the analysis, in the event that unusual conditions cause high aqueous concentrations of these species.

Figure 5-2 plots the calculated total concentration of dissolved Gd phosphate complexes, as functions of pH and total dissolved phosphate ( $\text{HPO}_4^{2-}$  and  $\text{H}_2\text{PO}_4^-$ ), for system B. Even at high total dissolved phosphate ( $10^{-2}$  Molal), these Gd complexes never exceed concentrations much greater than  $10^{-9}$  Molal for  $4 \leq \text{pH} \leq 9$ , thus are not expected to cause significant Gd loss from the system.

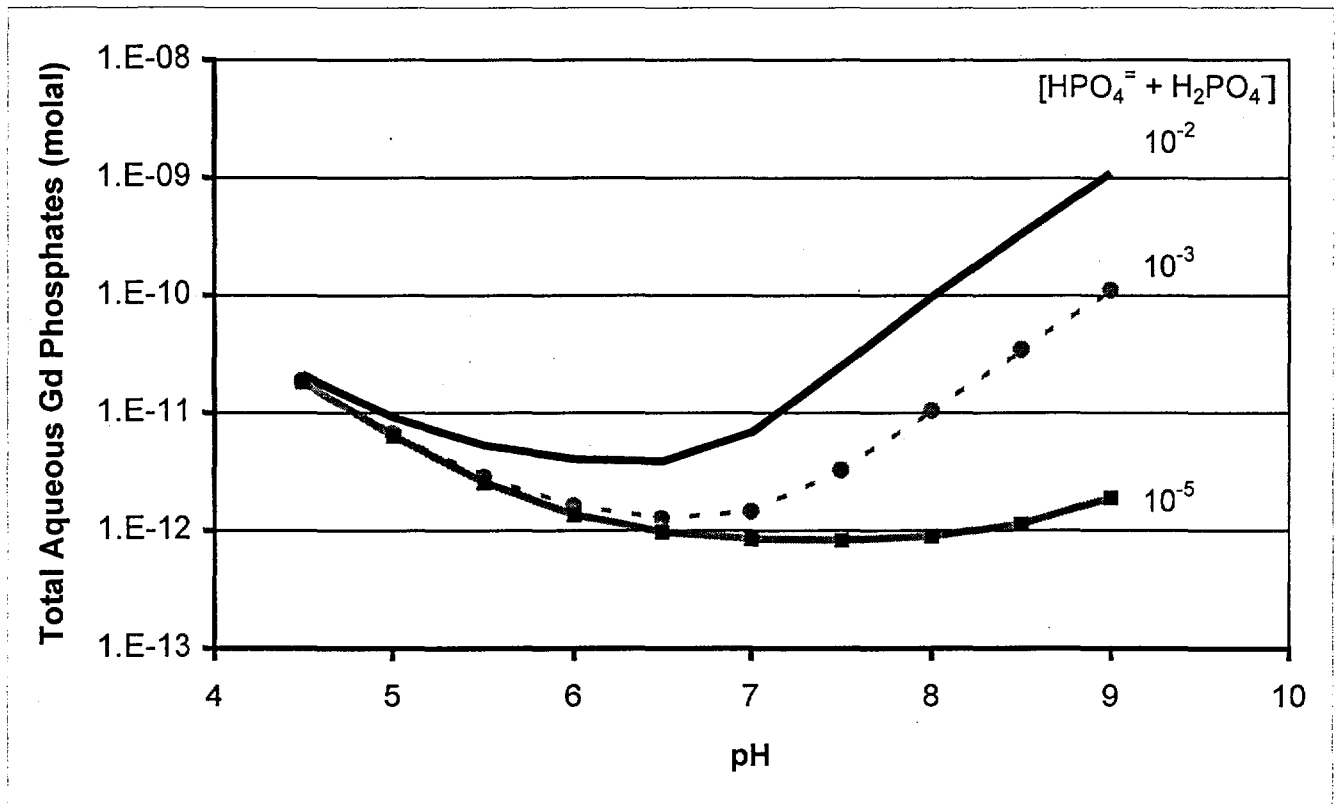


Figure 5-2. Concentrations of Phosphate Species in Equilibrium with  $\text{GdPO}_4 \cdot 2\text{H}_2\text{O}$ , for Total Phosphate Concentrations of  $10^{-5}$ ,  $10^{-3}$  and  $10^{-2}$  molal.

### 5.3.2 EQ6 Run Conditions and Nomenclature

Table 5-6 summarizes the file names and conditions used for the runs, and the total percentage Gd, Pu and U remaining at the end of the runs. Table 5-7 summarizes the total compositions of the solids in the system, normalized to silicon (which varies little with time). Attachment III gives examples of the full aqueous and total system concentration tables for the second stage of

case 10; the complete tables for all the cases are included in the electronic media, as tab-delimited text files.

In the second column from the left, Table 5-6 gives the root file names used to describe the runs. The EQ6 input files corresponding to these runs end with the extension “.6i” (e.g., f00a1111.6i is the EQ6 input file name for case 1); these input files are included with the electronic media accompanying this calculation<sup>12</sup>. Each run has associated tab-delimited text files, also included in the electronic media (e.g., f00a1111.elem\_aqu.txt for case 1). Several input files, corresponding to separate EQ6 runs, may be grouped into a “case”. Cases 1 through 8 in Table 5-6 all involve simultaneous exposure of the fuel and all package materials to J-13 water; these cases were designed to maximize exposure of the Gd-doped basket to high pH, to stress the enhanced solubility of GdPO<sub>4</sub> under alkaline conditions (the right side of Figure 5-1). In contrast, cases 9 through 14 all involve two fundamentally different stages. In the first stage of cases 9 through 14, J-13 water interacts with the outside surface of the DOE SNF canister, and with all package materials outside the canister (including the glass, GPC 304L steel, and the A516 outer web). The second stage of cases 9 through 14 begins after the HLW glass is completely degraded; the DOE SNF canister is “breached” at the beginning of the second stage, allowing the J-13 water to interact with the fuel assemblies, fuel pin cladding, the Gd-doped basket materials, the Ident 69, and the fuel components themselves (the (U,Pu)O<sub>2</sub> MOX and UO<sub>2</sub> insulator pellets). Cases 9 through 14 were designed to produce the lowest pH at long times, by removing the alkaline glass prior to exposure of the fuel and Gd-doped basket. Thus cases 9 through 14 were intended to test the enhanced Gd solubility on the left side of Figure 5-1.

Most of the important run conditions can be inferred from the root file name. The last four characters of the root consist of four digits that encode the steel, glass, fuel, and J-13 rates. The first of these digits is 1 or 2, corresponding to the average and high steel corrosion rates in Table 5-1. The second digit in this block is 1, 2 or 0, with 1 and 2 corresponding to the low and high glass corrosion rates listed in Table 5-2, and 0 corresponding to no glass present in the EQ6 run. The third digit in the block is 1, 2 or 0, with 1 and 2 corresponding to the average and high fuel dissolution rates in Table 5-3, and 0 corresponding to no fuel present in the EQ6 run. The last digit in the block encodes the choice of J-13 flush rate, with 1, 2, 3 and 4 corresponding to 0.0015 m<sup>3</sup>/year, 0.015 m<sup>3</sup>/year, 0.15 m<sup>3</sup>/year and 0.5 m<sup>3</sup>/year, respectively. The fourth character in the root name is “g” if goethite forms as the major Fe-oxide phase (that is, hematite formation is suppressed), or one of a, b, c, or “\_” (underscore) if hematite forms in place of goethite. Both hematite and goethite are observed to form in rust, though the EQ6 thermodynamic database indicates hematite is thermodynamically more stable, and hematite’s stability increases with temperature. When there are several similar file names, with fourth characters varying among a, b and c, the nomenclature indicates that the run was broken into steps, typically to improve convergence. In Table 5-6, the steps of the run are grouped together, and the designation f00{a,b,c}2122 corresponds to the three files f00a2122, f00b2122 and f00c2122. The second and third characters of the root name typically represent revisions of the basic run conditions, which occurred after mandated changes in package design, or waste form composition, during the course of the study. All FFTF root names begin with the letter “f”.

Thus, case 10 in Table 5-6 lists root file names f01g2204 / f00g2022. The first root name, f01g2204, covers the time period before the breach of the DOE SNF canister, and represents revision 01 (second and third characters). The fourth character, g, indicates this is a run in which goethite forms (hematite formation is suppressed). The fifth character is 2, and corresponds to the selection of the faster degradation rates for the A516, 304L and 316L steels in the package (Table 5-1). The sixth character is 2, corresponding to the faster glass degradation rate in Table 5-2. The seventh character is 0, corresponding to no fuel present in the EQ6 system (since the run is pre-breach, the fuel is not yet exposed to chemical corrosion). The last character is 4, corresponding to the highest J-13 flush rate of  $0.5 \text{ m}^3/\text{year}$ . The second root name, f00g2022, covers the time after breach of the DOE SNF canister, and is revision 00 (second and third characters). As always, the last block of characters, 2022, indicates the rates. The fifth character again corresponds to the faster steel corrosion rates. The time of breach for the DOE canister was chosen to correspond to a low pH plateau, that followed the complete degradation of all glass in the system (e.g., see Figure 5-27). Thus the sixth character is 0, since no glass remains in the EQ6 system (though the glass corrosion products are carried through the calculation). The seventh character corresponds to the faster fuel corrosion rate in Table 5-3, and the last corresponds to a J-13 drip rate of  $0.015 \text{ m}^3/\text{year}$ . In general, the first stage of a multi-stage run is comparatively short ( $\sim 10^3$  to  $\sim 10^4$  years), and the second stage of the run is carried out to at least  $10^5$  years. While the first stage is important in setting up the chemical conditions, the second stage is generally of greater interest for neutronics calculations, since the corrosion product compositions can vary wildly in the first stage, but achieve a quasi-steady state composition at long times.

**Table 5-6. Summary of Cases Run, Associated Input File Names, Percent Gd, Pu and U Retained, and Fe Oxide Corrosion Product**

Case	Root File Names	Gd	Pu	U	Fe Oxide
1	f00a1111	99.9	99.6	56.4	hematite
2	f00a1112	<b>99.3</b>	99.0	91.1	hematite
3	f01{a,b}1113	<b>99.3</b>	97.6	99.7	hematite
4	f00a1211	99.8	11.7	11.9	hematite
5	f00a2211	99.8	41.4	<b>0.00</b>	hematite
6	f00a2221	99.8	41.4	<b>0.00</b>	hematite
7	f00a2222	99.7	<b>6.20</b>	1.20	hematite
8	f00{a,b,c}2122	<b>99.3</b>	74.5	78.0	hematite
9	f01_2204 / f02_2022	100	99.5	99.9	hematite
9s*	f01_2204 / f02_2022	100	99.7	99.9	hematite
10	f01g2204 / f00g2022	100	98.3	99.8	goethite
10s*	fs1g2204 / fs0g2022	100	99.3	99.7	goethite
11	f01g2203 / f00g2021	100	98.3	99.9	goethite
12	f01g1203 / f00g1021	100	97.0	99.9	goethite
13**	f00g1103, fa0g1103	N/A***	N/A	N/A	goethite
14**	f00g1104	N/A	N/A	N/A	goethite

\* Cases 9s and 10s used HLW glass containing ~0.8 weight % Mg (see Section 5.3.7).  
 \*\*These two cases were not run past the breach of the DOE SNF canister, because it was determined they would not significantly enhance Gd loss (see Section 5.3.6).  
 \*\*\*Not applicable.

**Table 5-7. Volume of Corrosion Products (% of Volume inside CRB) and Moles Elements in Corrosion Products (Normalized to Silicon)**

Years*	Vol Frac	O	Al	Ca	Fe	Gd	H	K	Mn	Na	Ni	Pu	Ti	U
<b>Case 9: (f02_2022, Hematite)</b>														
50	45.4%	4.73	0.096	0.024	1.37	3.97E-6	0.55	0.034	0.054	7.07E-3	0.037	1.94E-3	0.015	5.82E-3
20502	48.6%	5.06	0.095	0.024	1.58	1.66E-4	0.55	0.031	0.060	7.36E-3	0.037	1.92E-3	0.015	5.79E-3
200517	48.47%	5.05	0.095	0.029	1.58	1.65E-4	0.55	0.017	0.060	7.18E-3	0.037	1.91E-3	0.015	5.76E-3
<b>Case 9s: (f02_2022, Hematite, 0.8 wt% Mg in Glass)</b>														
50	45.1%	4.75	0.096	0.017	1.37	3.97E-6	0.55	0.009	0.054	2.14E-3	0.055	1.94E-3	0.015	5.82E-3
20073	48.3%	5.07	0.096	0.017	1.58	1.66E-4	0.55	0.008	0.060	3.53E-3	0.054	1.93E-3	0.015	5.79E-3
200087	48.3%	5.06	0.095	0.021	1.58	1.65E-4	0.55	0.003	0.060	4.05E-3	0.054	1.92E-3	0.015	5.76E-3
<b>Case 10: (f00g2022, Goethite)</b>														
50	49.5%	5.11	0.096	0.024	1.37	3.97E-6	1.31	0.032	0.054	7.56E-3	0.041	1.94E-3	0.015	5.82E-3
20072	53.7%	5.54	0.095	0.025	1.58	1.66E-4	1.52	0.030	0.060	8.67E-3	0.040	1.90E-3	0.015	5.79E-3
200086	53.6%	5.53	0.095	0.030	1.58	1.65E-4	1.51	0.017	0.060	7.39E-3	0.040	1.89E-3	0.015	5.76E-3
<b>Case 10s: (fs0g2022, Goethite, 0.8 wt% Mg in Glass)</b>														
50	49.1%	5.12	0.096	0.017	1.37	3.87E-6	1.28	0.009	0.054	2.41E-3	0.055	1.94E-3	0.015	5.81E-3
20040	53.3%	5.54	0.095	0.017	1.58	1.66E-4	1.49	0.008	0.060	3.92E-3	0.056	1.92E-3	0.015	5.79E-3
200057	53.4%	5.53	0.095	0.021	1.58	1.65E-4	1.48	0.003	0.060	4.17E-3	0.056	1.91E-3	0.015	5.76E-3
<b>Case 11: (f00g2021, Goethite)</b>														
50	48.4%	5.00	0.096	0.020	1.32	3.98E-6	1.25	0.039	0.052	9.14E-3	0.043	1.91E-3	0.015	5.84E-3
22400	53.7%	5.55	0.096	0.020	1.59	1.66E-4	1.52	0.039	0.060	9.51E-3	0.042	1.90E-3	0.015	5.80E-3
224817	53.8%	5.55	0.096	0.021	1.59	1.66E-4	1.52	0.037	0.060	1.05E-2	0.042	1.87E-3	0.015	5.80E-3
<b>Case 12: (f00g1021, Goethite)</b>														
50	44.2%	4.58	0.097	0.022	1.11	4.00E-7	1.09	0.039	0.046	9.51E-3	0.021	1.91E-3	0.015	5.86E-3
20770	49.0%	5.08	0.096	0.021	1.35	1.65E-4	1.33	0.038	0.053	8.02E-3	0.023	1.90E-3	0.015	5.83E-3
200077	53.7%	5.55	0.096	0.022	1.59	1.66E-4	1.56	0.036	0.060	9.39E-3	0.020	1.83E-3	0.015	5.80E-3
*Years after breach of the DOE SNF canister (18" canister). For cases 9, 9s, 10 and 10s, the DOE canister breach is placed $3.8 \cdot 10^3$ years after CRB breach, in the low pH plateau. For case 11, the DOE canister breach is placed at $3.0 \cdot 10^3$ years, and for case 13, the breach is at $5.0 \cdot 10^3$ years after breach of the CRB.														

5.3.3 Comparison of Aqueous Gd, Pu, U and pH for Cases 1-12

Figures 5-3 through 5-14 give the pH and aqueous Gd, Pu and U concentrations with time in cases 1 through 12. As predicted in Figure 5-1, the highest Gd concentrations correlate with periods of low or high pH. The aqueous concentrations of all elements are given in the fxxxxxx.elem\_aqu.txt files in Ref. 12, where fxxxxxx is the root file name given in Table 5-6. A detailed analysis of cases 2 and 10 is given in Section 5.3.5.

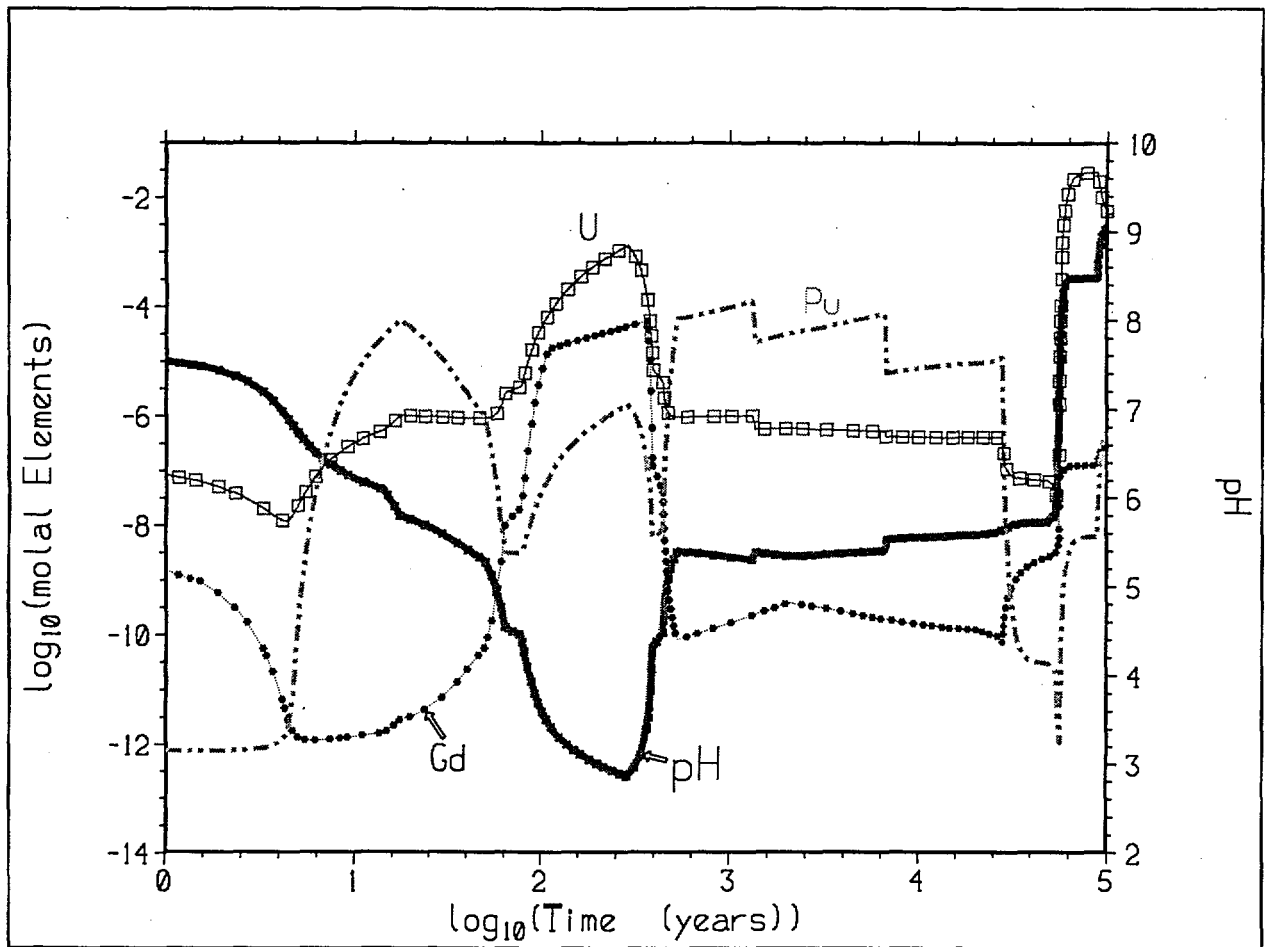


Figure 5-3. Aqueous Gd, Pu, U and pH for Case 1 (f00a1111). The pH Low (and Gd Maximum) Correspond to Degradation of A516 in the Outer Web Structure



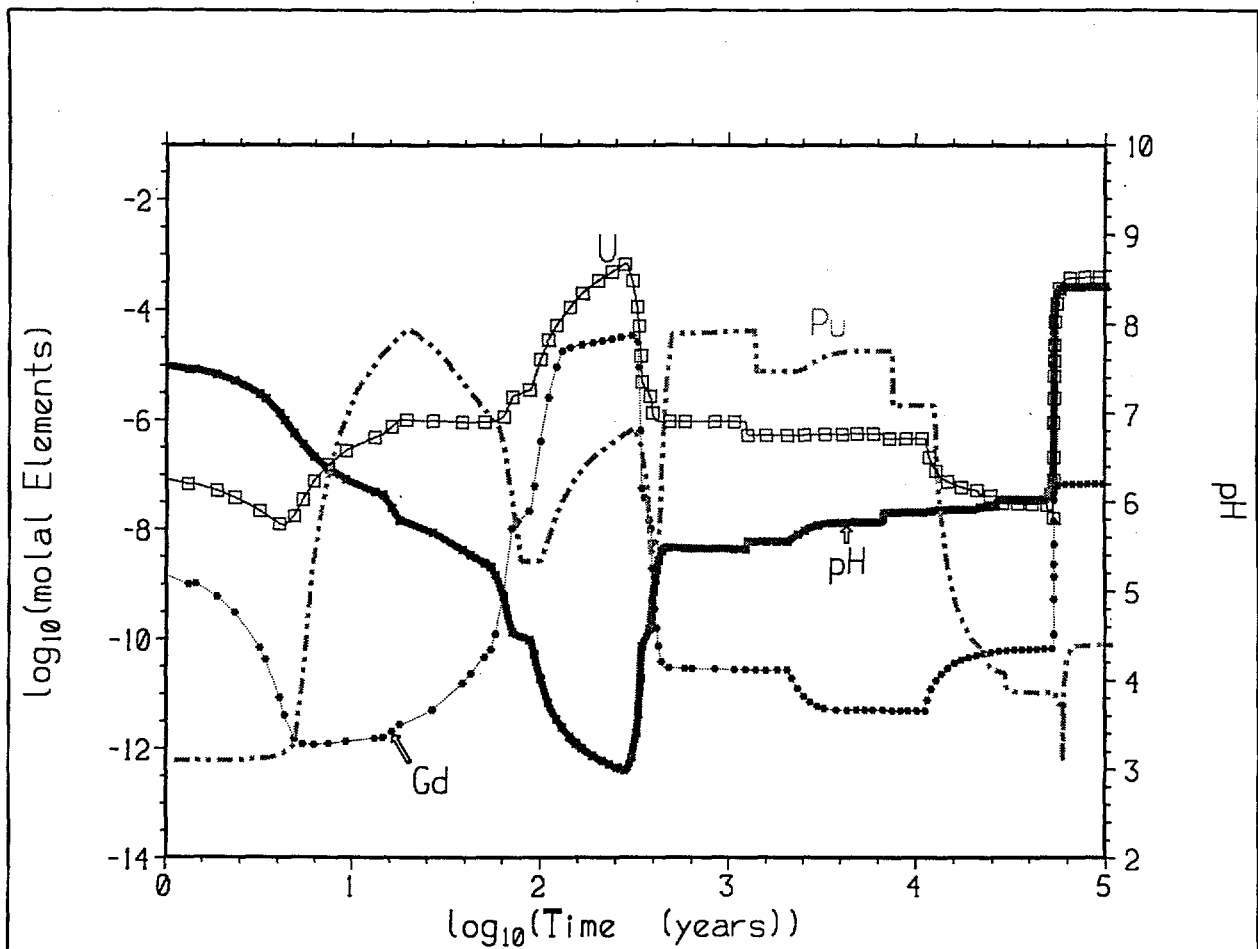


Figure 5-4. Aqueous Gd, Pu, U and pH for Case 2 (f00a1112). The pH Low (and Gd Maximum) Correspond to Degradation of A516 in the Outer Web Structure

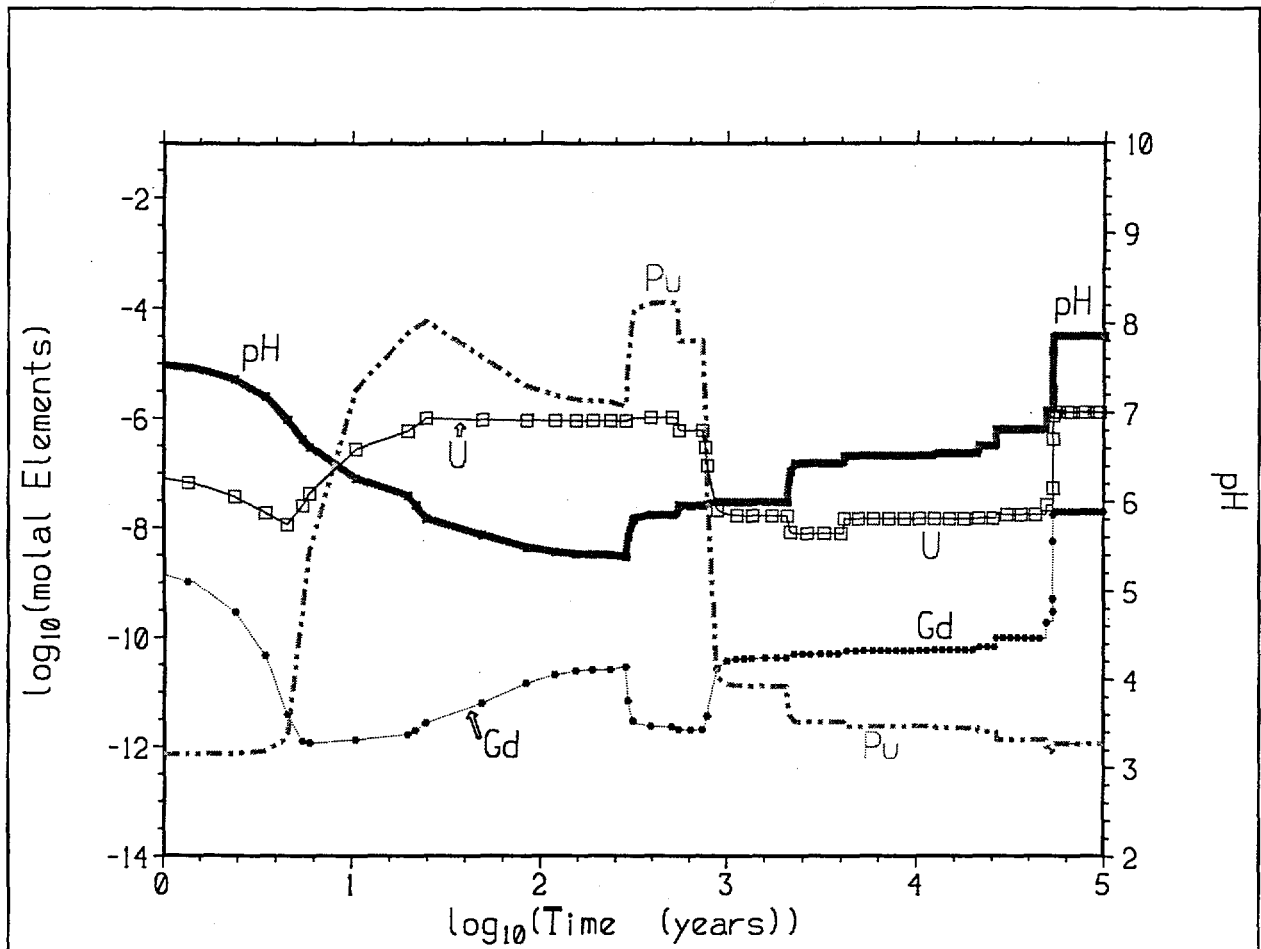


Figure 5-5. Aqueous Gd, Pu, U and pH for Case 3 (f00{a,b}1113). The High J-13 Flush Rate Prevents pH from Reaching Extreme Low Values

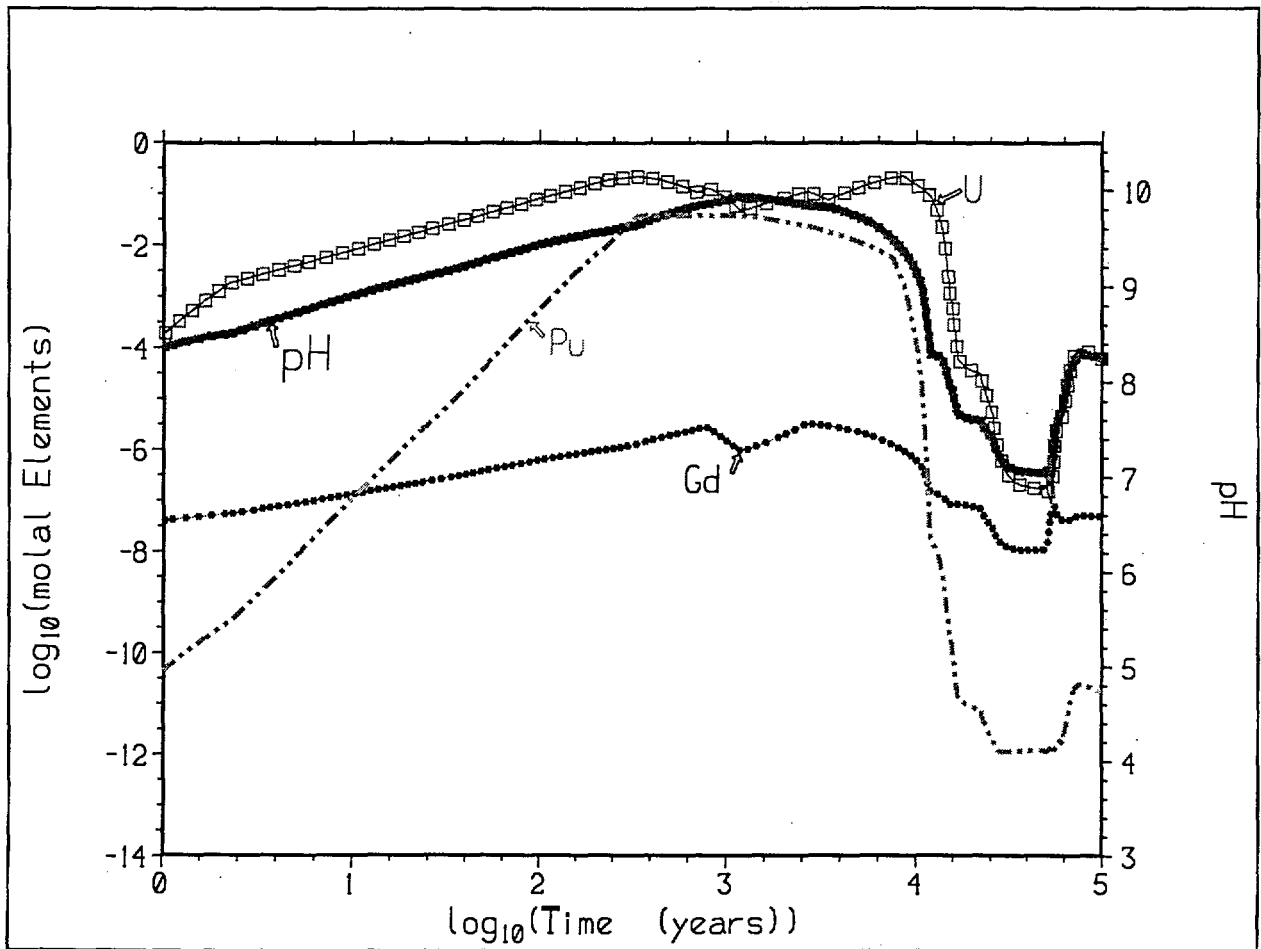


Figure 5-6. Aqueous Gd, Pu, U and pH for Case 4 (f00a1211). Because of the High Glass Degradation Rate (Compared to Figure 5-3), Acid from Steel Degradation Is Neutralized, High pH Is Reached, and U and Pu Concentrations Are High

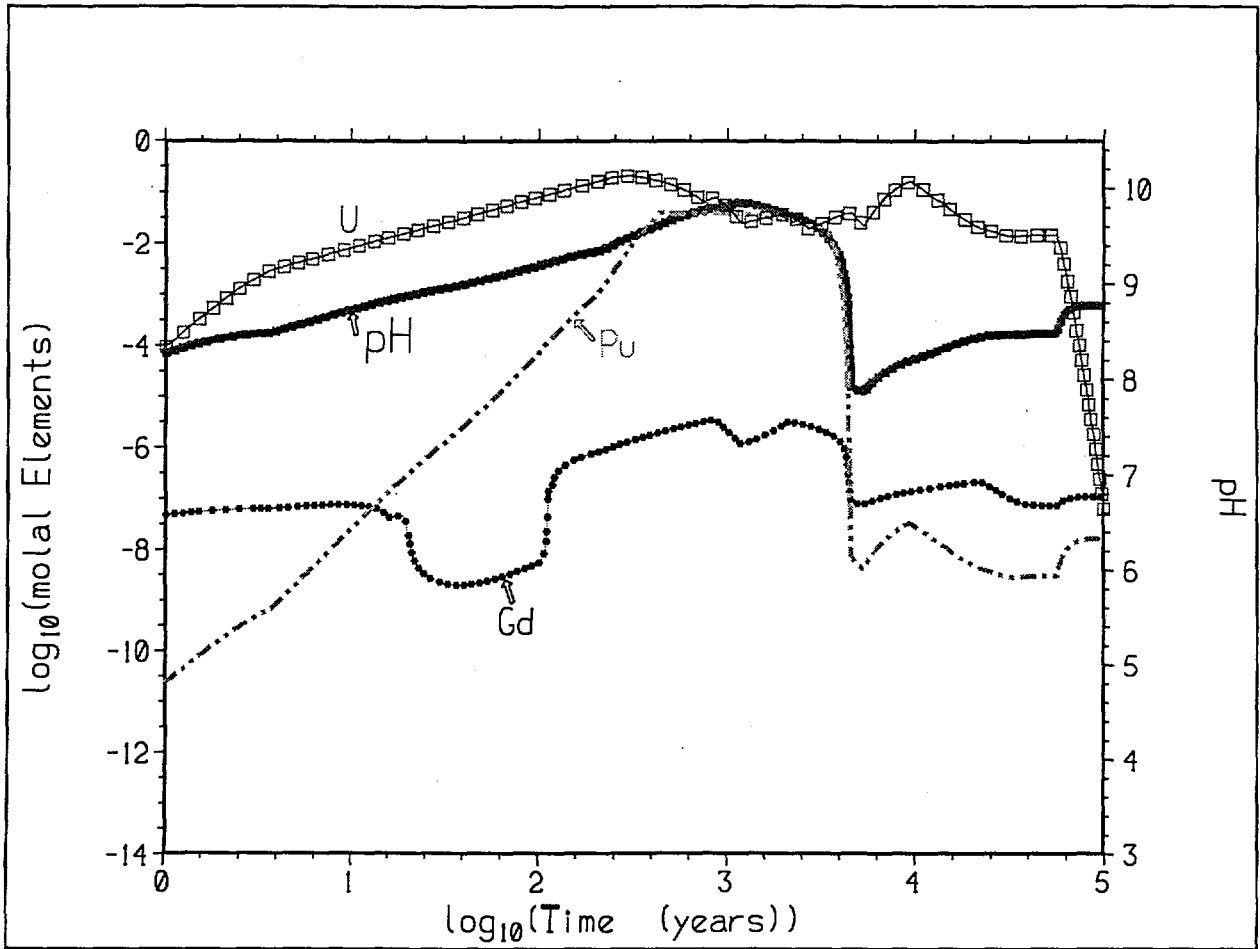


Figure 5-7. Aqueous Gd, Pu, U and pH for Case 5 (f00a2211). This Case and Case 6 Achieve 100% U Loss. The Gd Peak Is Due to Carbonate Complexes

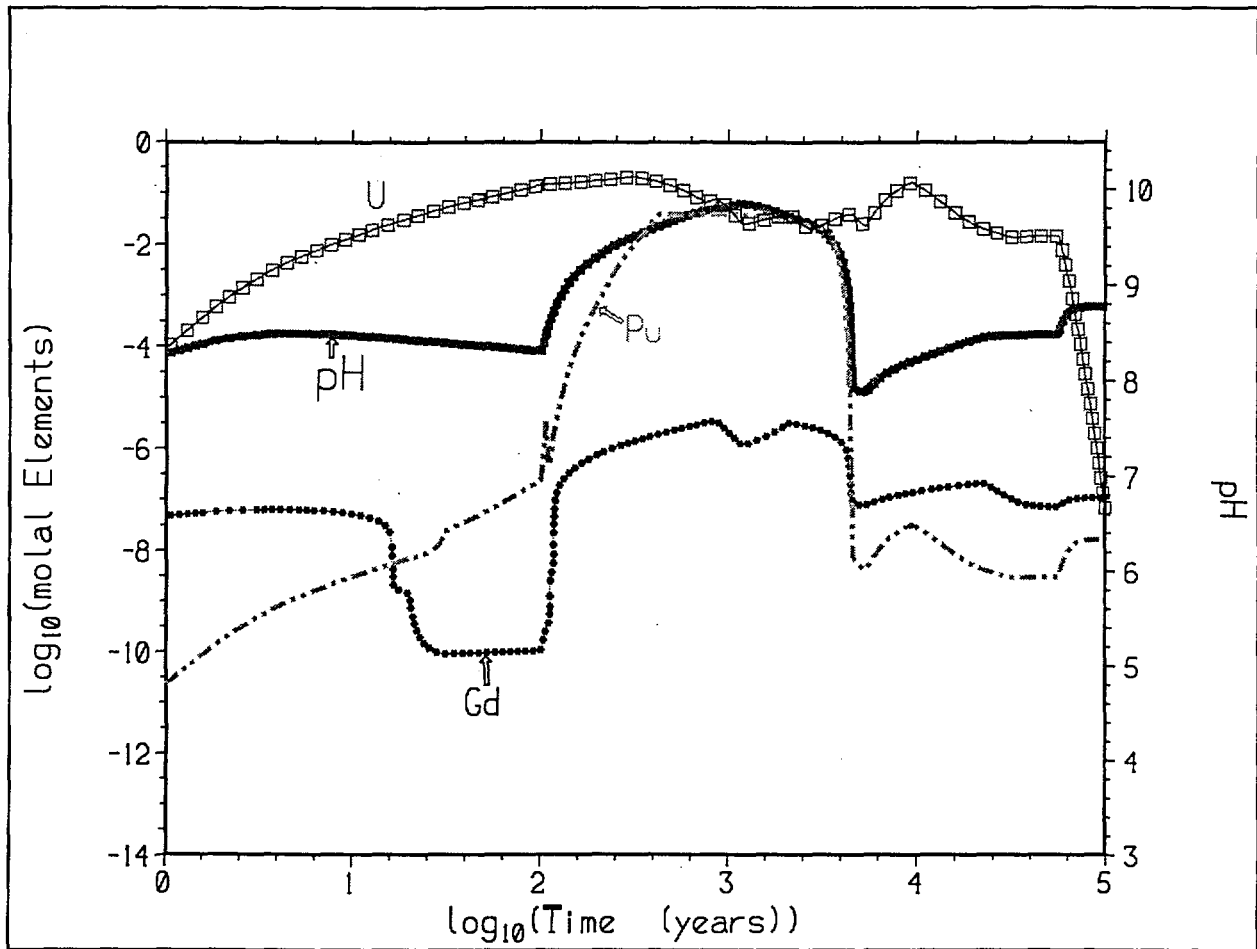


Figure 5-8. Aqueous Gd, Pu, U and pH for Case 5 (f00a2221). This Case and Case 5 Achieve 100% U Loss. The Gd Peak Is Due to Carbonate Complexes

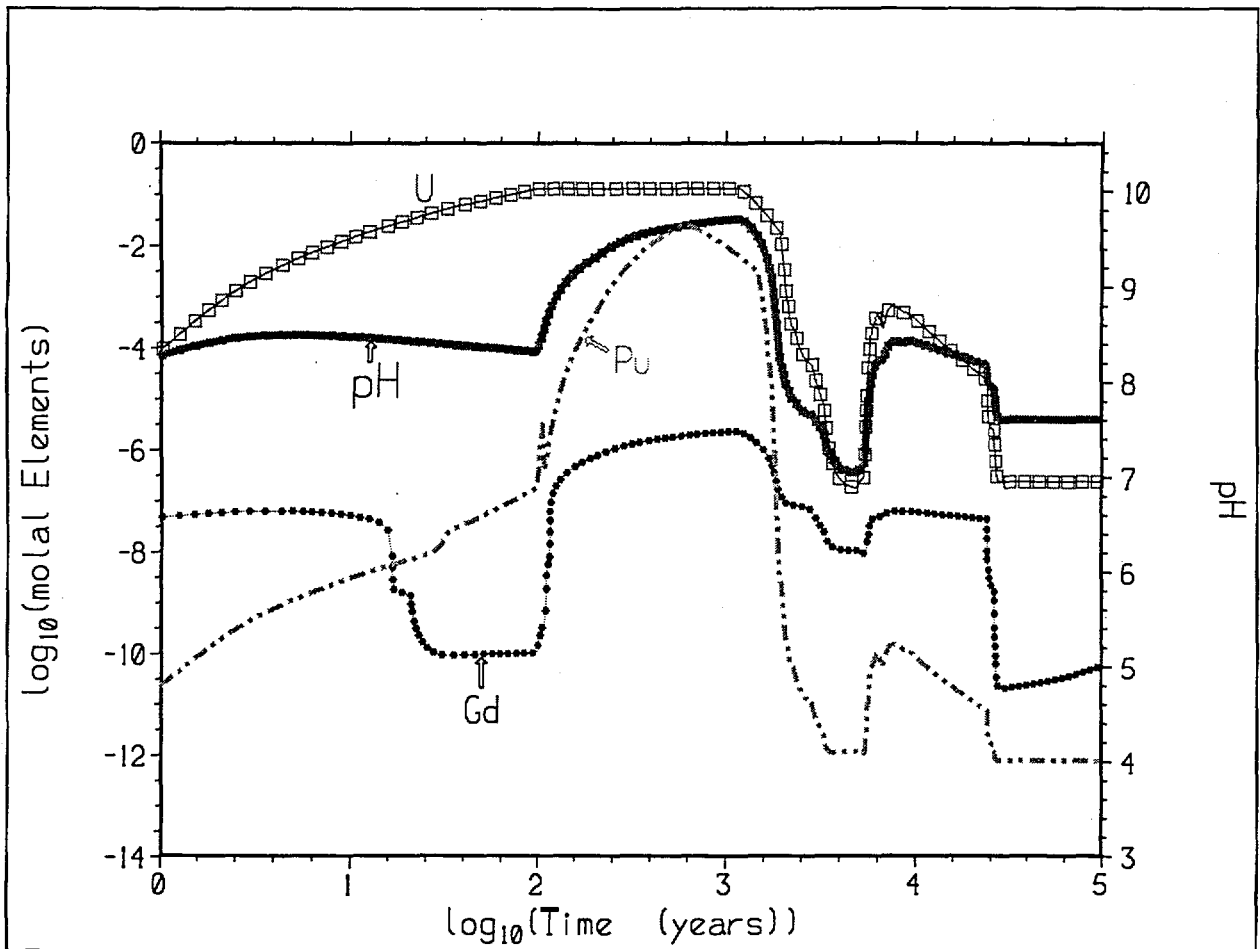


Figure 5-9. Aqueous Gd, Pu, U and pH for Case 7 (f00a2222). Total Pu and U Losses Are 93.8% and 98.8%, Respectively

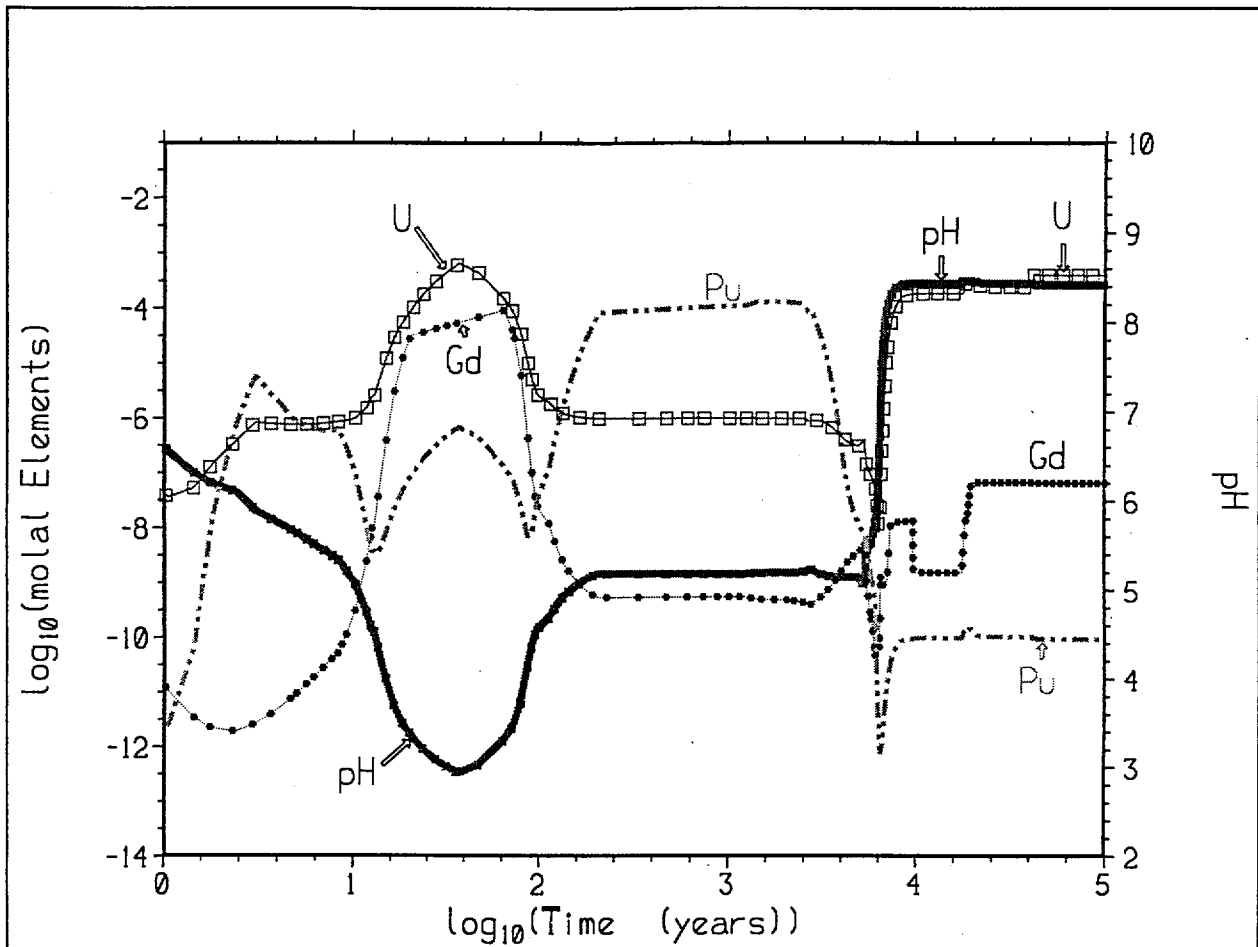


Figure 5-10. Aqueous Gd, Pu, U and pH for Case 8 (f00{a,b,c}2122). Compared to Case 7, the Lower Glass Degradation Rate Yields Lower Pu and U Loss (25.5% and 22.0%, Respectively), But Allows 0.7% Gd Loss During pH Low

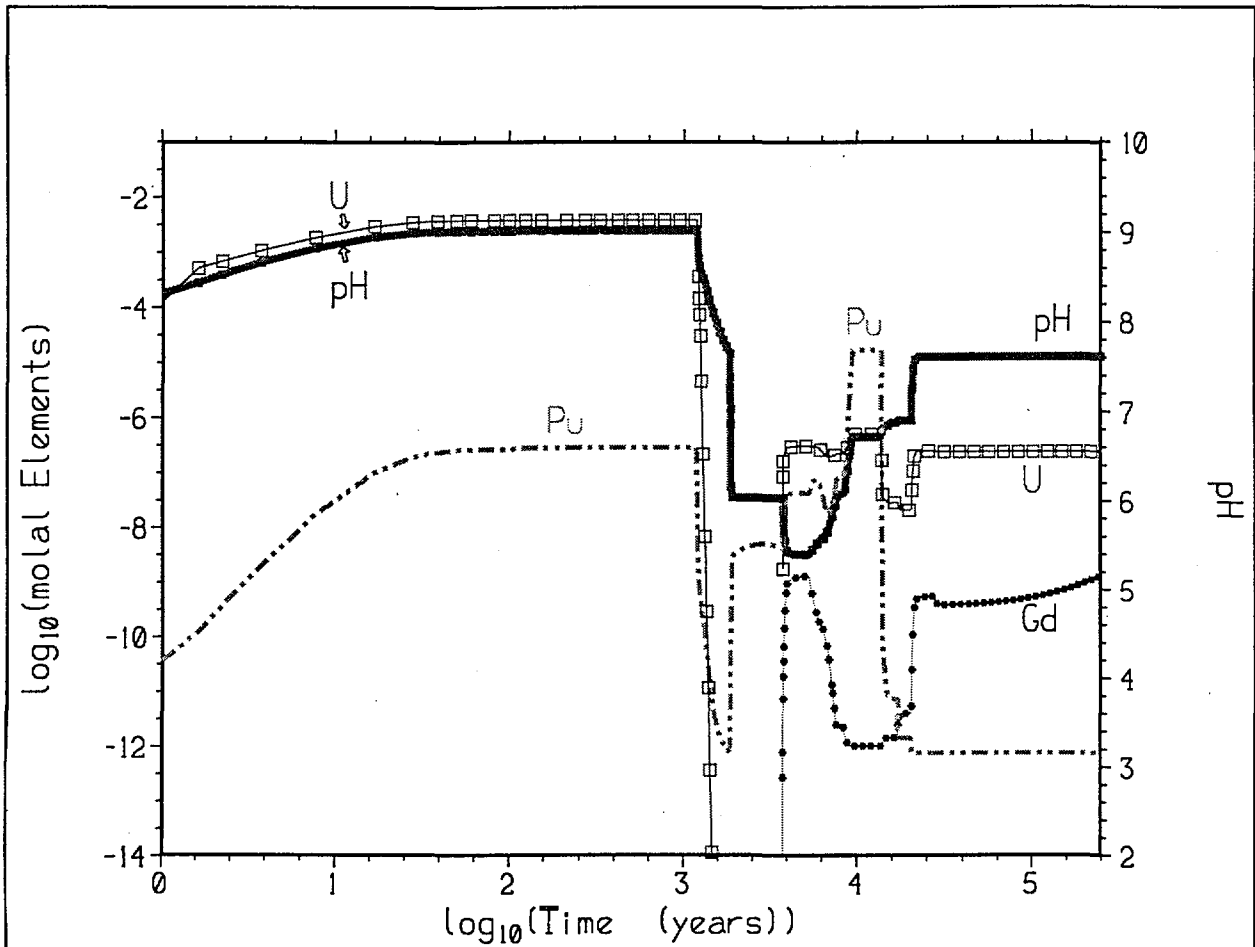


Figure 5-11. Aqueous Gd, Pu, U and pH for Case 9 (f01\_2204 / f02\_2022, Hematite). Initial High U and Pu Concentrations Are from Glass; High Initial Flush Rate Removes Glass Alkalinity. The DOE SNF Canister Is Breached at 3765 Years, Exposing More Pu and U (Fuel) and Gd-Doped Basket; Lower Flush Rate Prevents High Losses



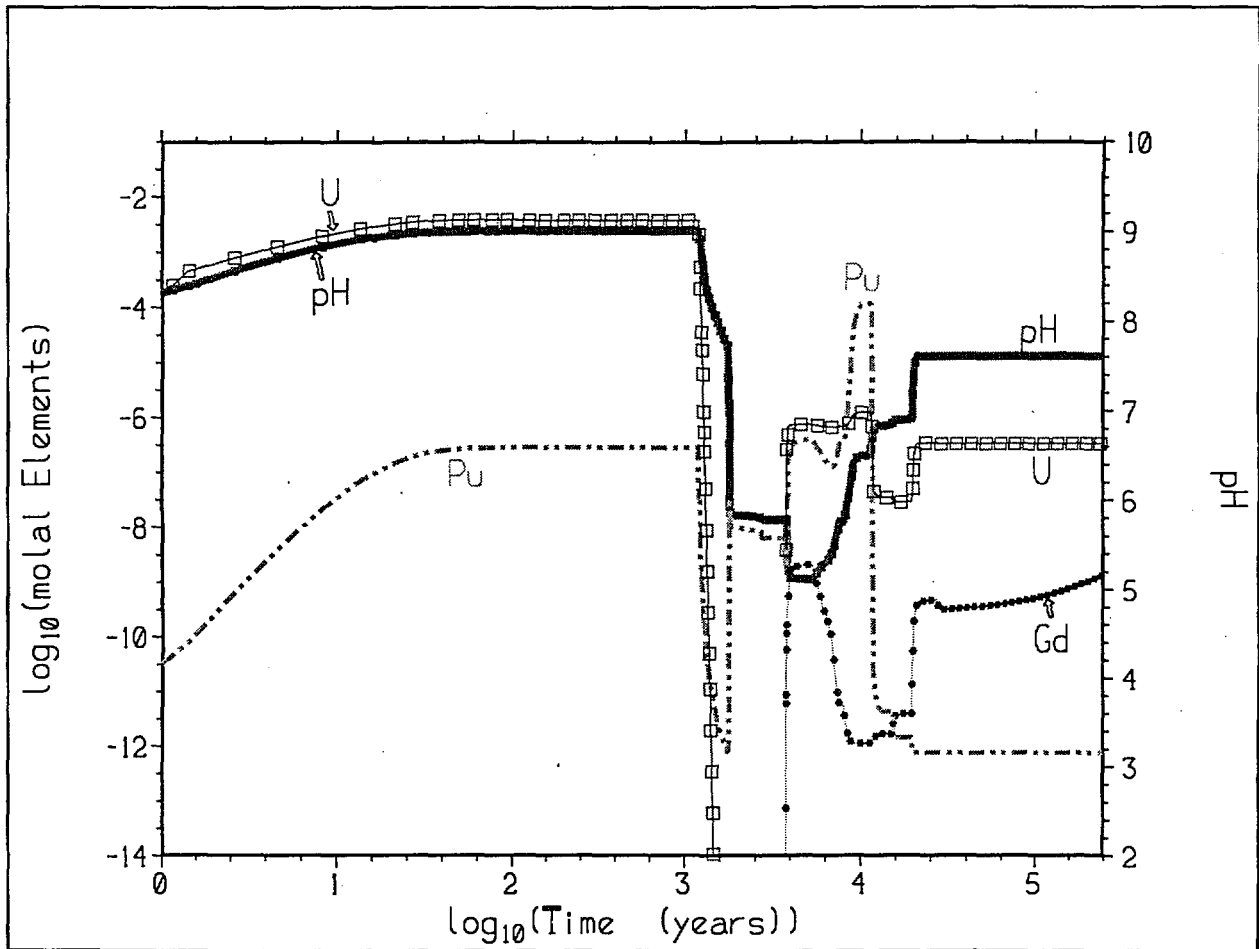


Figure 5-12. Aqueous Gd, Pu, U and pH for Case 10 (f01g2204 / f00g2022, Goethite). The DOE SNF Canister Is Breached at 3765 Years. Similar to Case 9, But Goethite Allows Slightly Lower pH Minimum

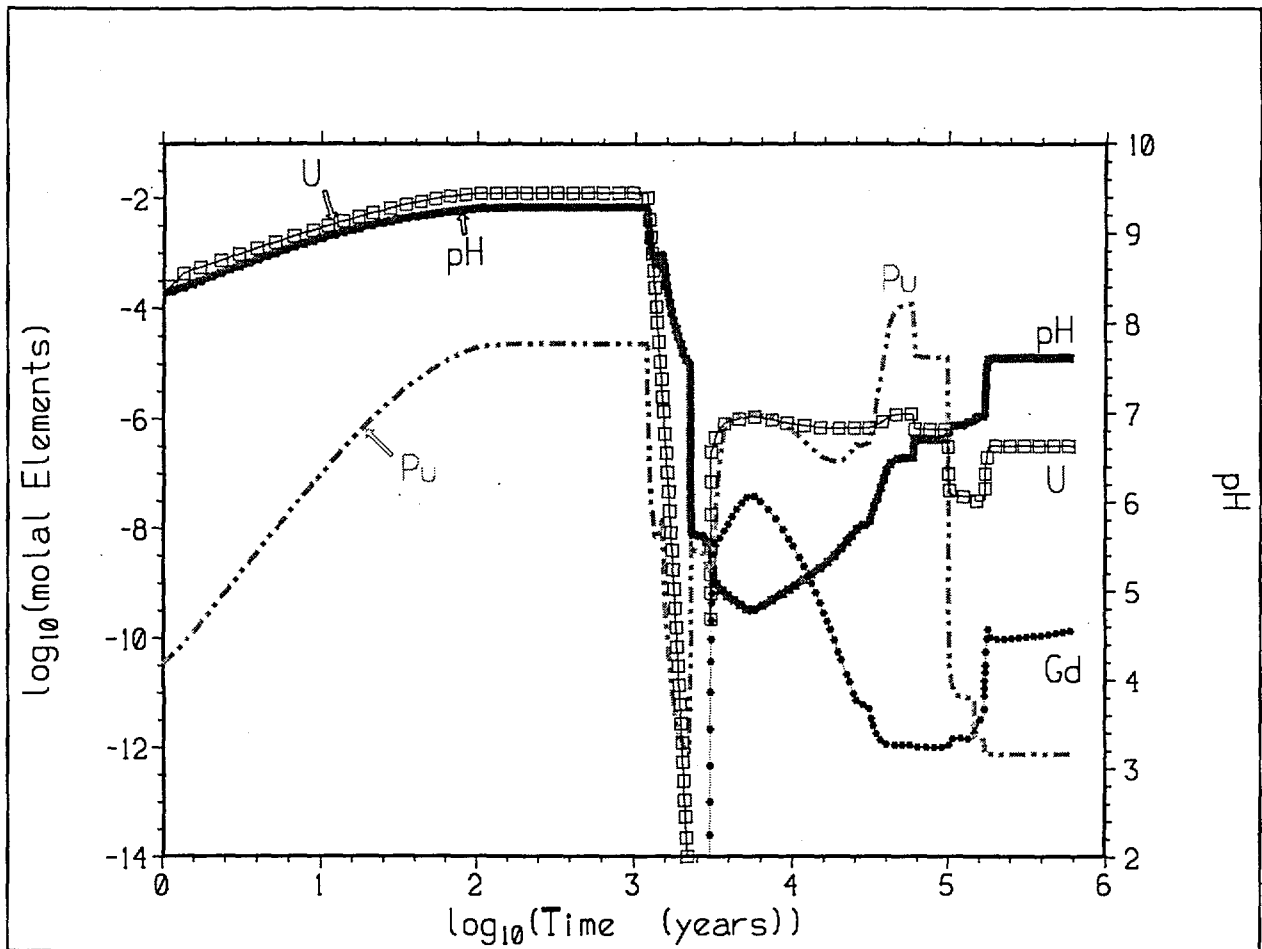


Figure 5-13. Aqueous Gd, Pu, U and pH for Case 11 (f01g2203 / f00g2021, Goethite). The DOE SNF Canister Is Breached at 3013 Years, Exposing More Pu and U (Fuel) and Gd-Doped Basket. Similar to Case 10, But Lower Flush Rates Throughout

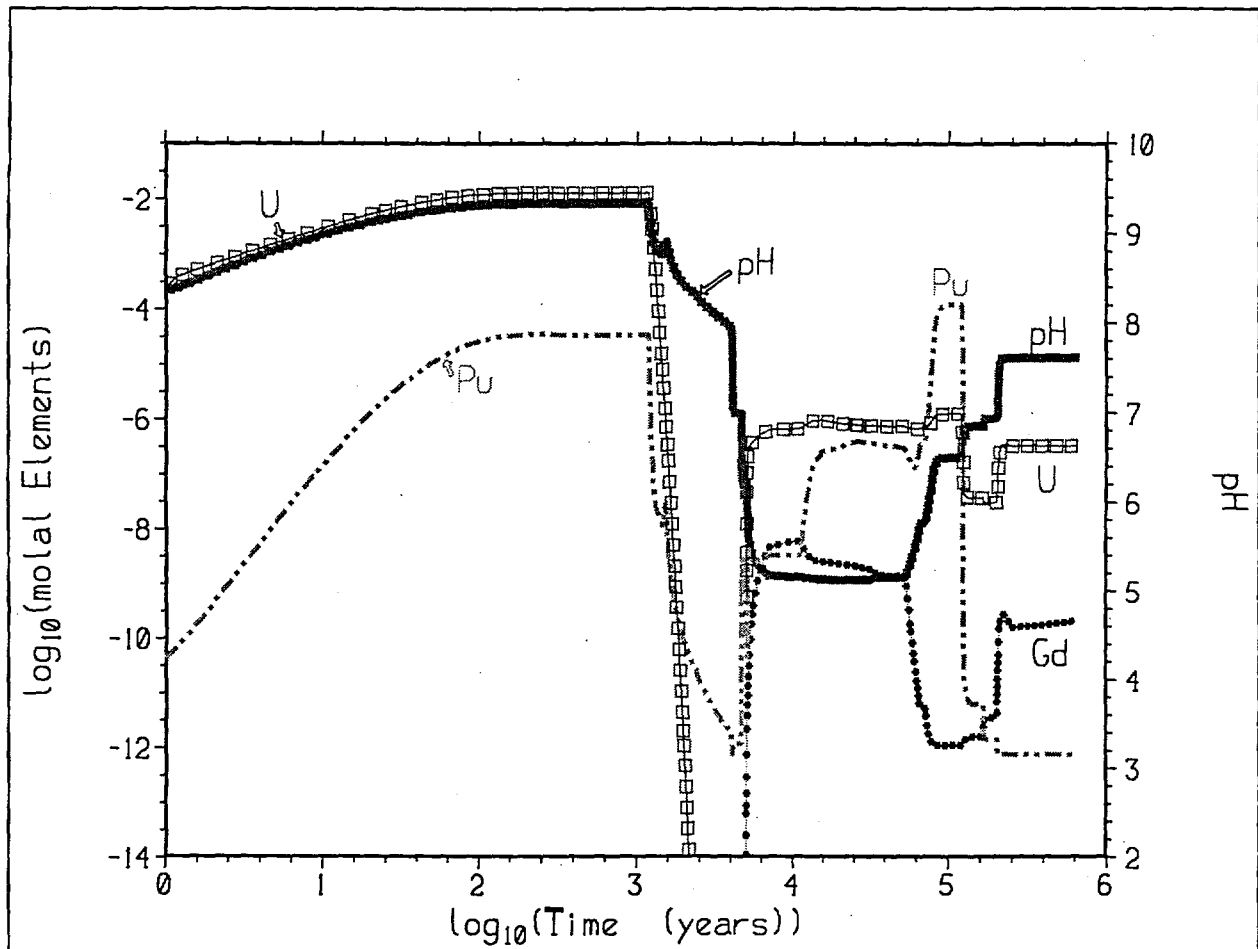


Figure 5-14. Aqueous Gd, Pu, U and pH for Case 12 (f01g1203 / f00g1021, Goethite). The DOE SNF Canister Is Breached at 5003 Years, Exposing More Pu and U (Fuel) and Gd-Doped Basket. Similar to Case 11, But Lower Steel Degradation Rates

### 5.3.4 Justification for Eliminating Multi-Stage Cases 13 and 14

Figures 5-15 through 5-17 illustrate the reasons for dropping cases 13 and 14 from consideration. The case 13 pH plateaus early ( $<10^3$  years), and the actinide concentrations remain modest, despite the early drop in pH (Figure 5-15). The early pH plateau suggest that any second stage chosen for case 13 would not likely lead to dramatic loss of Gd. The very low pH correlates with the degradation of A516 carbon steel (Figure 5-16), and is due, in part, to the oxidation of sulfur in the steel (e.g.,  $S^0 + H_2O + 1.5O_2 = SO_4^{2-} + 2H^+$ ). The maintenance of low glass dissolution rates, in the face of such low pH, is somewhat artificial; glass dissolution rates rise rapidly at low pH, and in a more realistic EQ6 run, the glass rate would be linked to pH so that the pH minimum in Figure 5-16 would probably be much shallower. The combination of

undramatic behavior, combined with the unrealistic combination of low pH and slow glass dissolution rates, eliminates case 13 from further consideration.

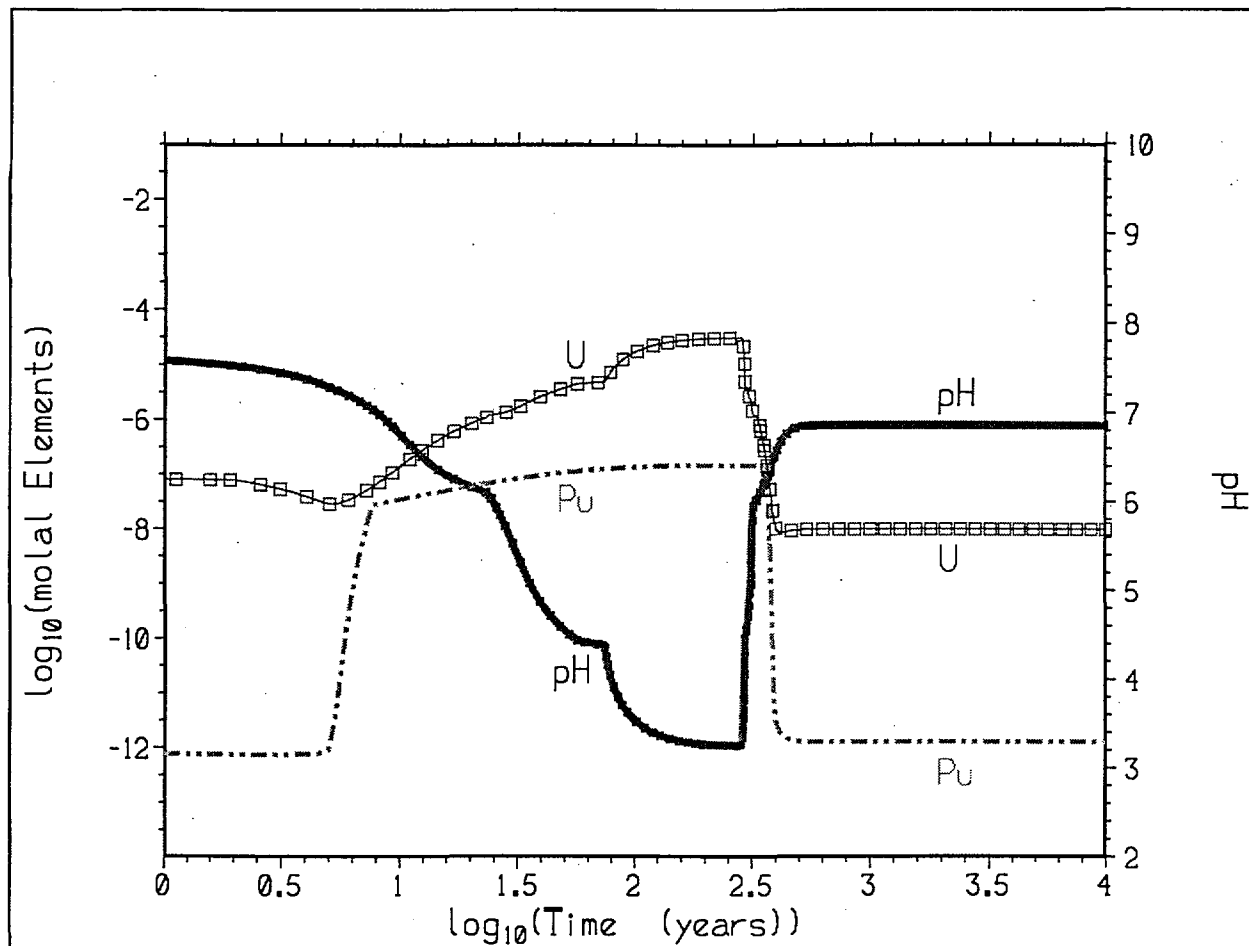


Figure 5-15. Aqueous Pu, U and pH for Eliminated Case 13 (f00g1103, Pre-Breach of DOE SNF). Despite pH Low, U and Pu Concentrations Remain Modest, and pH Plateaus Near Neutrality

In effect, case 13 has been subsumed in case 3. Case 14 (figure 5-17) proves to be even less dramatic than case 13, with an early leveling of pH to the ambient value of J-13 water, and comparatively low aqueous U and Pu.

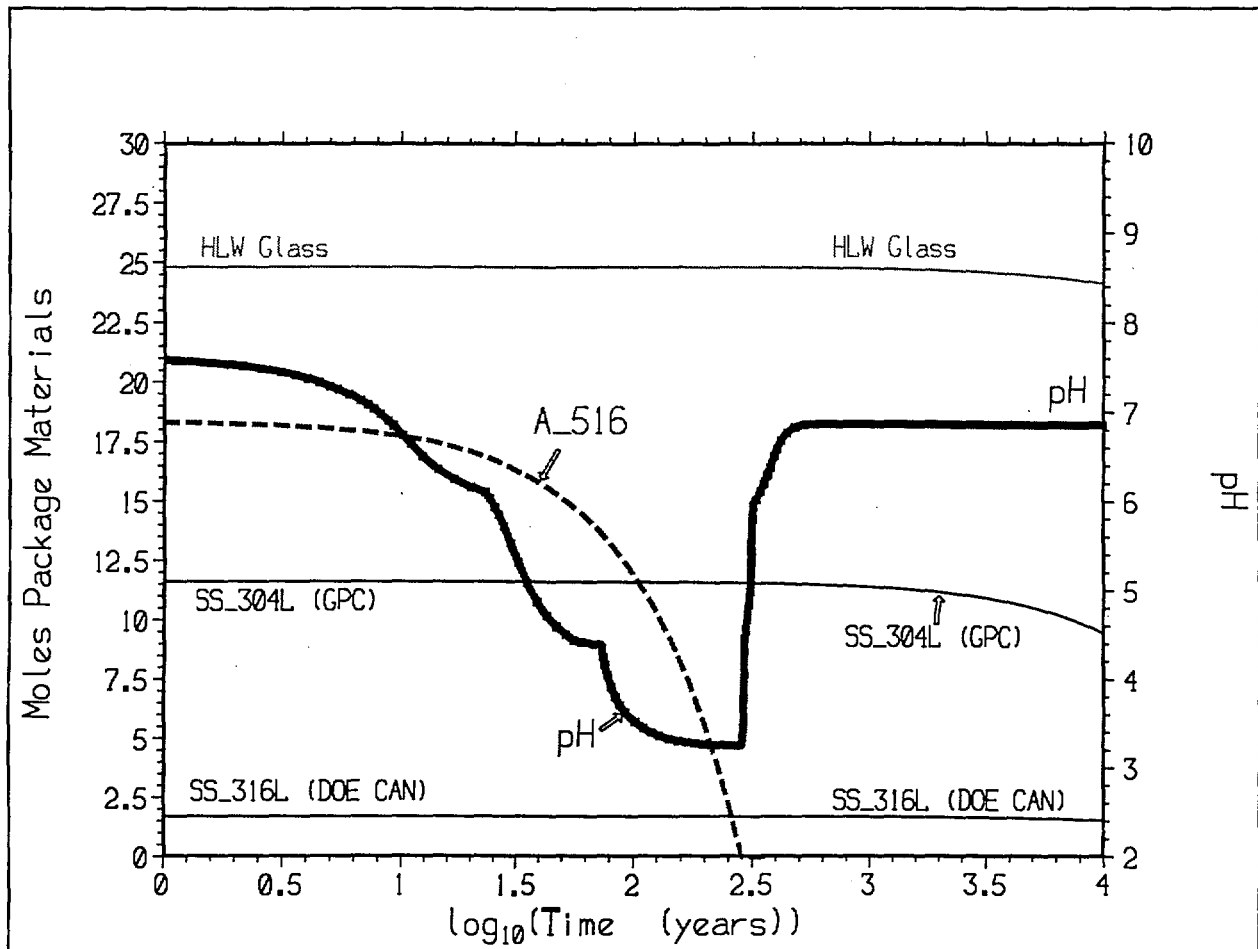


Figure 5-16. Package Materials Remaining (Per liter Initial Void Space), and pH, for Eliminated Case 13 (f00g1103, Pre-Breach of DOE SNF). The pH Low Is Due to A516 Degradation

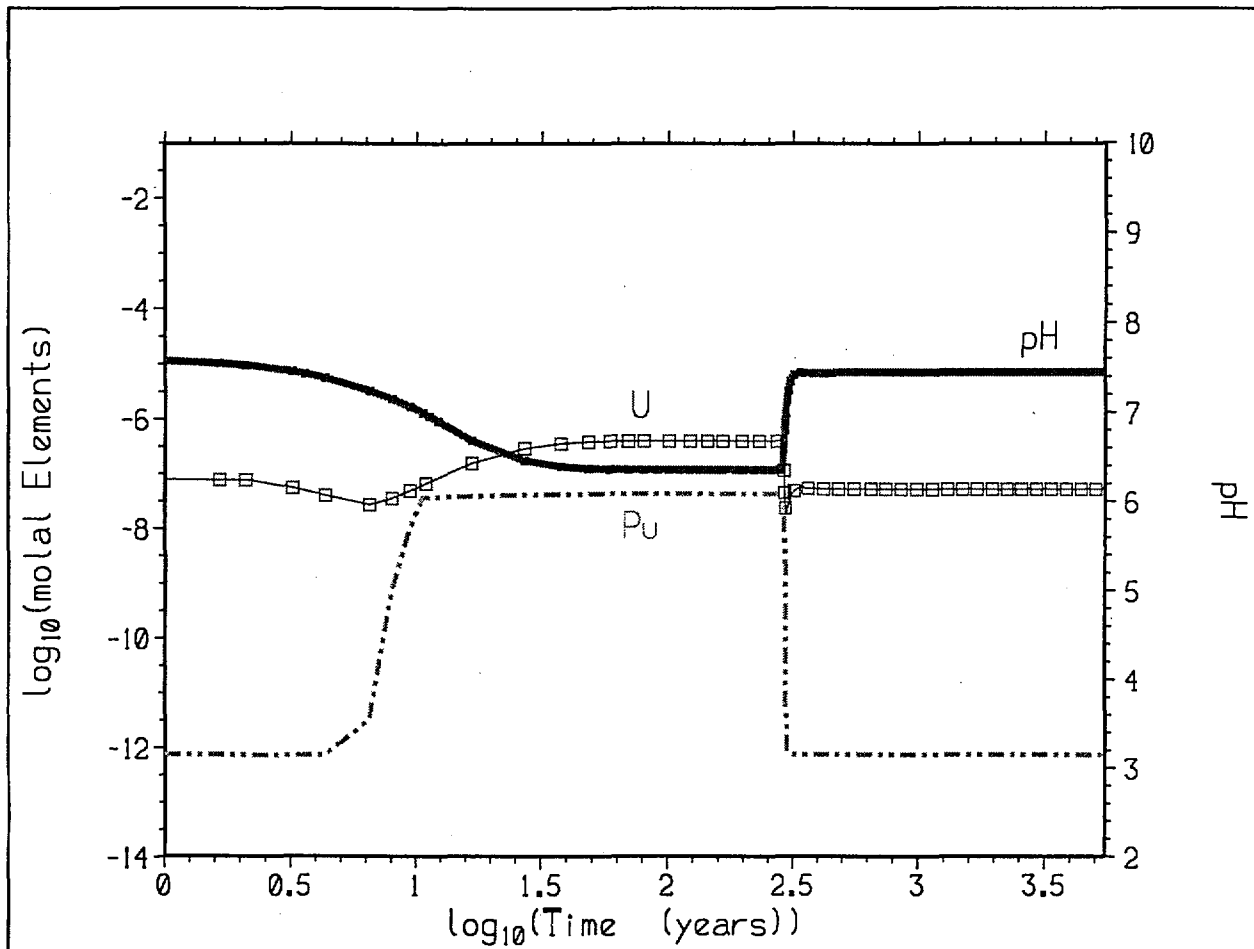


Figure 5-17. Aqueous Pu, U and pH for Eliminated Case 14 (f00g1104, Pre-Breach of DOE SNF). The High Flush Rate Prevents Extreme pH Variation

### 5.3.5 Detailed Examination of Cases 2 and 10

To understand the seemingly chaotic concentration and pH variations in Figures 5-3 through 5-14, it is useful to examine cases 2 and 10 in detail. These two cases span the observed range of Gd loss (0.7% for case 2, and 0.0% for case 10), and involve quite different scenarios and rate assumptions. Figures 5-18 through 5-22 illustrate case 2, and Figures 5-23 through 5-26 illustrate case 10. In all these figures, when units of moles are used on the left axis, the quantity is scaled relative to 1 liter of coexisting J-13 water (which is equivalent to 1 liter of initial void space in the package). To obtain the total moles of product minerals or package materials in the WP, the mole quantities in the figures must be multiplied by the package void volume (5807.028 liters, or 0.001 times the value of VVOIDS\_PREBREACH\_TOT in spreadsheet `fftf_fuel_hws.xls`).

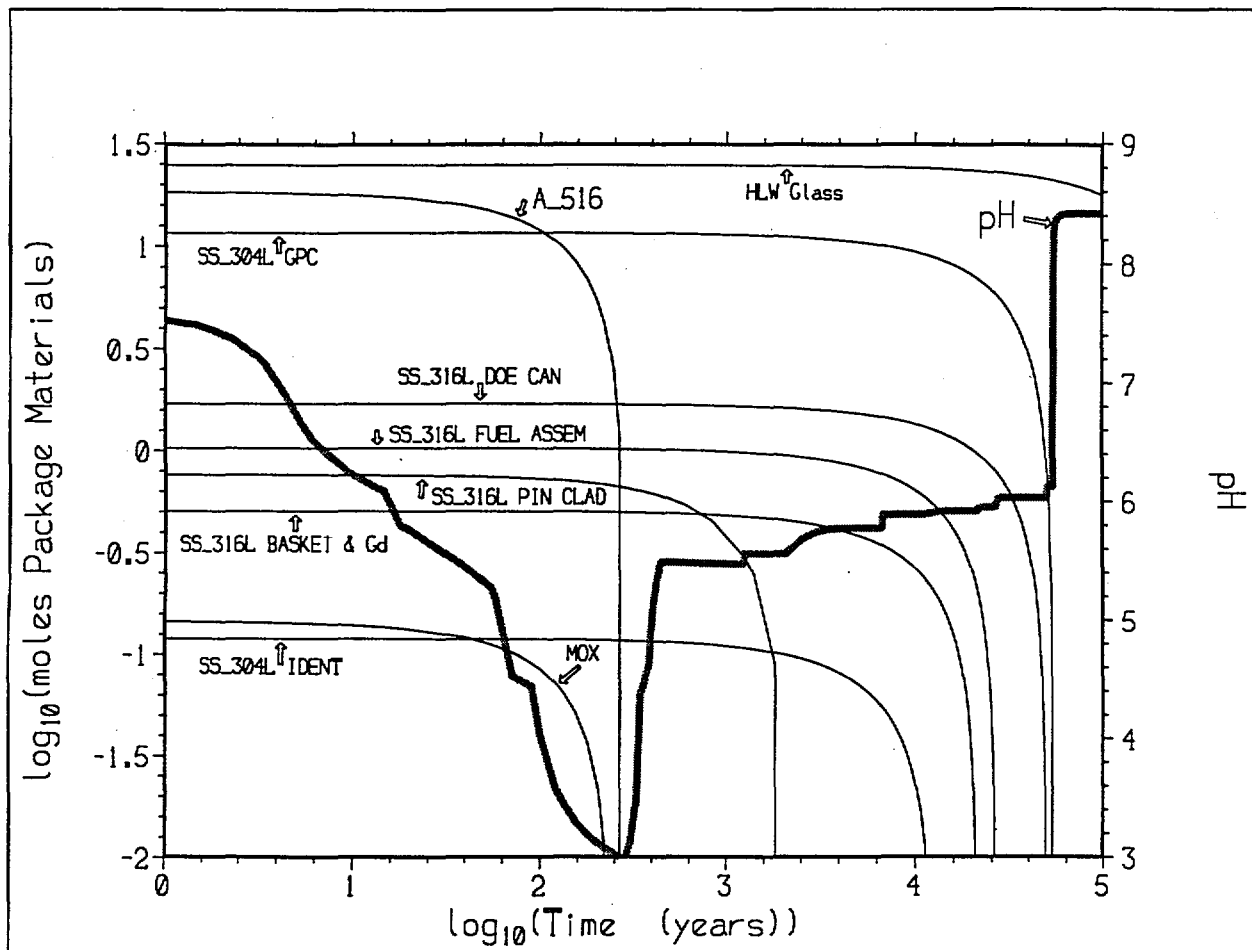


Figure 5-18. Case 2: pH and Moles Package Materials Remaining (Per liter Initial Void Space). The pH Minimum Is Associated with Degradation of Steels, Particularly A516

Figure 5-18 shows how the kinks in the pH curves correlate with the consumption of package materials. A\_516 denotes A516 carbon steel, and the quantities beginning with "SS" are the various stainless steels on the GPC, the DOE SNF canister ("DOE CAN" in Figure 5-18), the fuel assembly container, the pin cladding, and the Ident 69. While the quantity of some steel components is small (e.g., the pin cladding), the specific surface area of these steel components can be quite high, causing rapid degradation and acid production. The dramatic pH low in Figure 5-18 correlates with degradation of the A516 outer web structure, and the ultimate high pH results from a quasi-steady state equilibrium between dissolution of the glass, and the slow flushing and dilution with J-13 water. As described in Section 5.3.6, the coexistence of low pH and a slow glass dissolution rate is somewhat artificial.

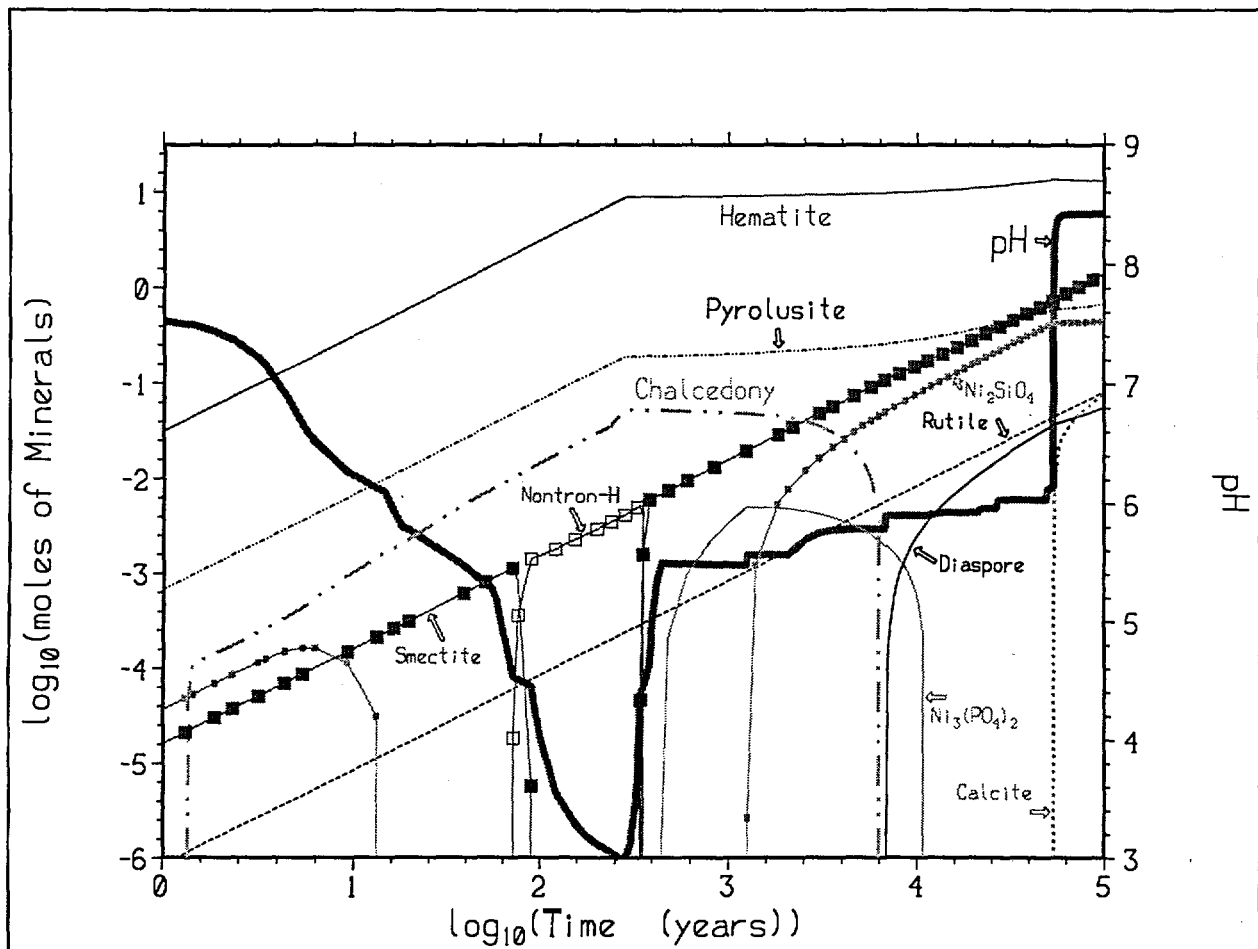


Figure 5-19. Case 2: Major Minerals and pH. In pH Minimum, Nontronite-H (Hydrogen Nontronite, Open Squares) Replaces Smectite (Solid Squares). Molar Amounts Are Per liter Initial Void Space

Figures 5-19 and 5-20 show the major and minor minerals that form with time in case 2. Since the glass degradation rate is very low, smectite clay ( $((Ca,Mg)_{0.165},(K,Na)_{0.33})Fe_2Al_{0.33}Si_{3.67}H_2O_{12}$ ) does not dominate till late in the run; however, a "mole" of smectite contains roughly four times as many atoms as a "mole" of hematite ( $Fe_2O_3$ ), so the comparison on a molar basis is somewhat deceptive. During the period of lowest pH, the smectite converts to hydrogen nontronite (Nontron-H), and buffers pH somewhat. Figure 5-20 shows the moles of minerals that control Gd, Pu and U solubility in the EQ6 calculations. Rhabdophane ( $(Gd,Sm)PO_4 \cdot H_2O$ ) dissolves completely during the extreme low pH, but reprecipitates as the pH rises. The principal U and Pu solids are soddyite ( $(UO_2)_2SiO_4 \cdot 2H_2O$ ) and  $PuO_2$ , respectively.



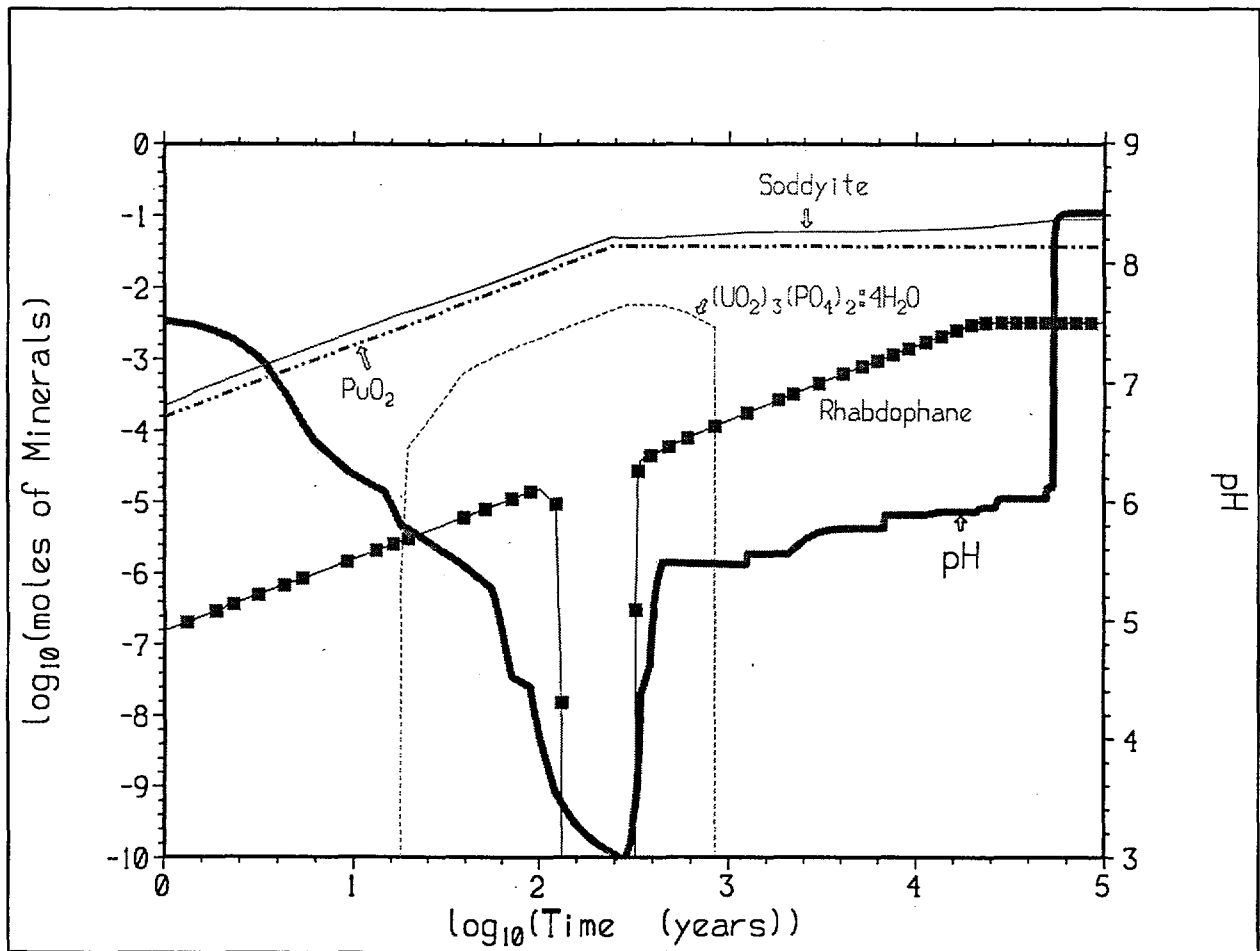


Figure 5-20. Case 2: pH and Solubility-Controlling Minerals for Gd (Rhabdophane), Pu, and U (Soddyite, U-Phosphate). Rhabdophane Completely Dissolves During pH Minimum, But Reprecipitates. Molar Amounts Are Per liter Initial Void Space

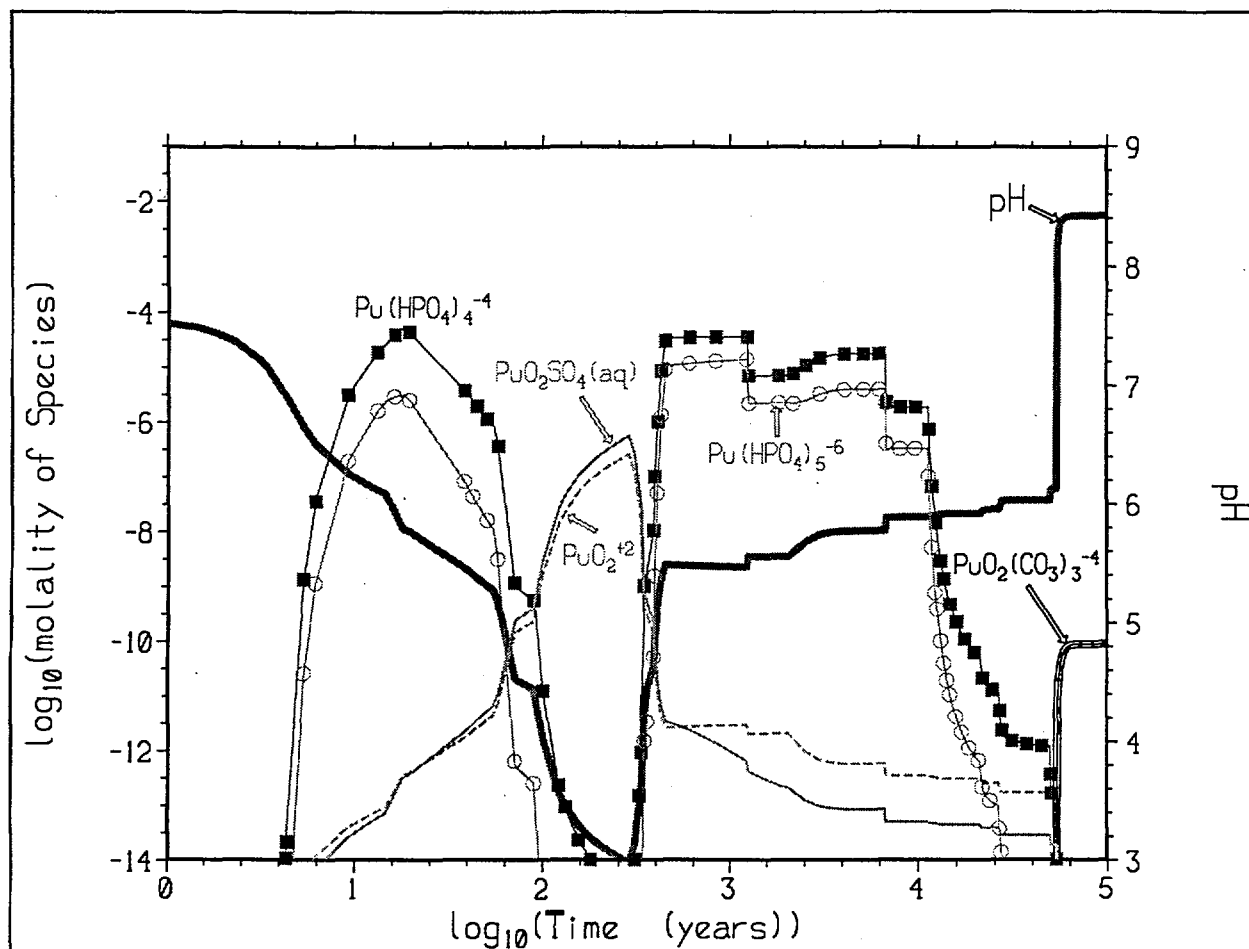
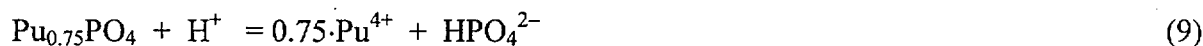


Figure 5-21. Case 2: Predicted Major Pu Species and pH

The principal aqueous Pu and Gd species for case 2 are given in Figures 5-21 and 5-22 (the species molalities are calculated by EQ6). In the lower pH periods, Pu phosphate complexes and  $\text{PuO}_2\text{SO}_4(\text{aq})$  dominate, but at  $\text{pH} > 7$ , Pu carbonate complexes are the most important dissolved Pu species. Similarly  $\text{Gd}^{3+}$  and  $\text{GdSO}_4^+$  dominate dissolved Gd during the low pH periods, and Gd carbonate complexes dominate at pH above 7.

The high calculated solubility of Pu, as phosphate complexes, deserves attention, because the current EQ6 database contains no stability constants for solid Pu orthophosphates. If such solids exist, the solubility of Pu may be overestimated. To estimate the possible influence of solid Pu phosphates, the stability constant for



was estimated from the data for the analogous Th reaction (data sources summarized in Ref. 34, pp. 13-14; most stable phosphate used). The following entry was then added temporarily to the EQ6 data0.nuc.R8a file (and the corresponding data1 file), in the "solids" section.

```

Pu.75PO4
  date last revised = 23-dec-1998
  keys = solid
    VOPrTr = 40.000 cm**3/mol (source = hws , placeholder )
*   mwt = ** g/mol
    3 chemical elements =
      1.0000 P          4.0000 O          0.7500 Pu
    4 species in data0 reaction
      -1.0000 Pu.75PO4          0.7500 Pu++++
      1.0000 HPO4--          -1.0000 H+
*   log k grid (0-25-60-100/150-200-250-300 C) =
      500.0000 -15.6782 500.0000 500.0000
      500.0000 500.0000 500.0000 500.0000
    
```

Case 2 was then re-run. The hypothetical  $\text{Pu}_{0.75}\text{PO}_4$  never precipitated, and was undersaturated by at least a factor of  $10^6$ . To the extent that this estimate reflects the stability of real solid Pu phosphates, it seems unlikely that addition of such phases, to the EQ6 database, would change the Pu solubility estimates for case 2.

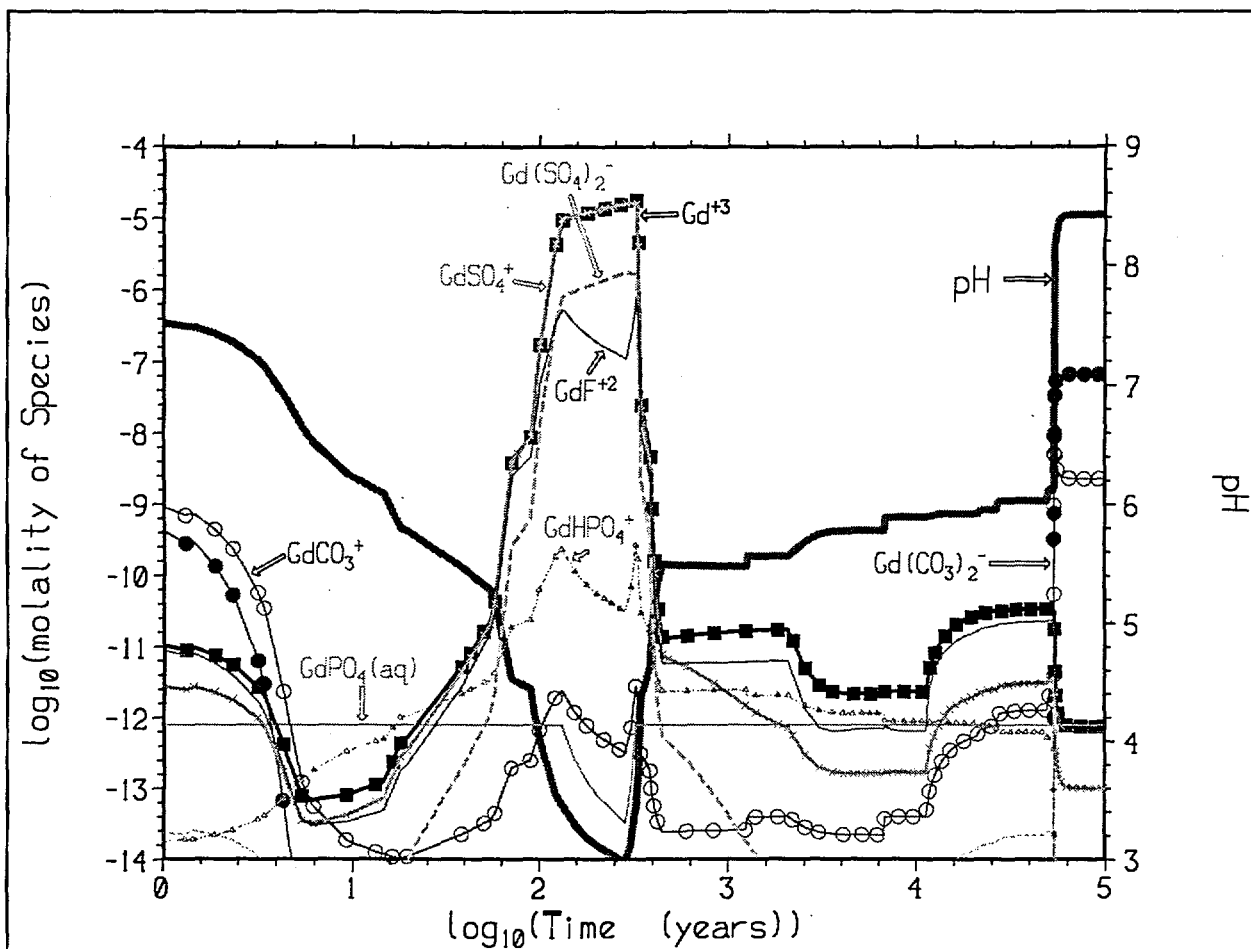


Figure 5-22. Case 2: Predicted Major Gd Species and pH. Gd-Carbonate Complexes Dominate Only at Early and Late Time. At Intermediate Time and Lower pH, Gd<sup>3+</sup> (and Gd-Phosphate Complexes) Dominate

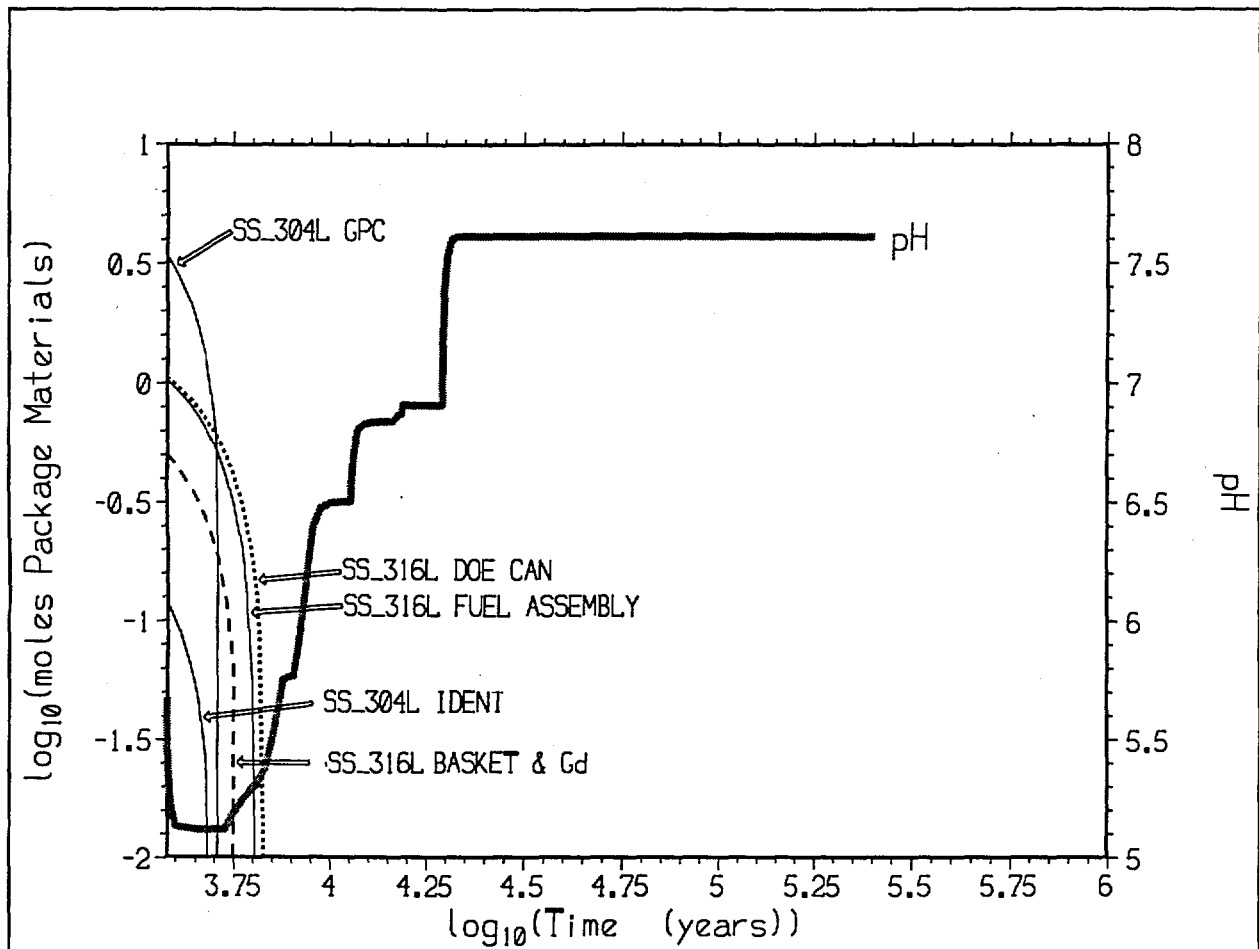


Figure 5-23. Case 10: pH and Moles Package Materials Remaining (Per liter Initial Void Space). The pH Minimum Is Associated with Degradation of Steels

The pH and moles of package materials, for the second stage of case 10, are given in Figure 5-23. The rapid degradation of the steel components, combined with the lowering of drip rate in the second stage (to 0.015 m<sup>3</sup>/year), drop the pH to ~5.1.

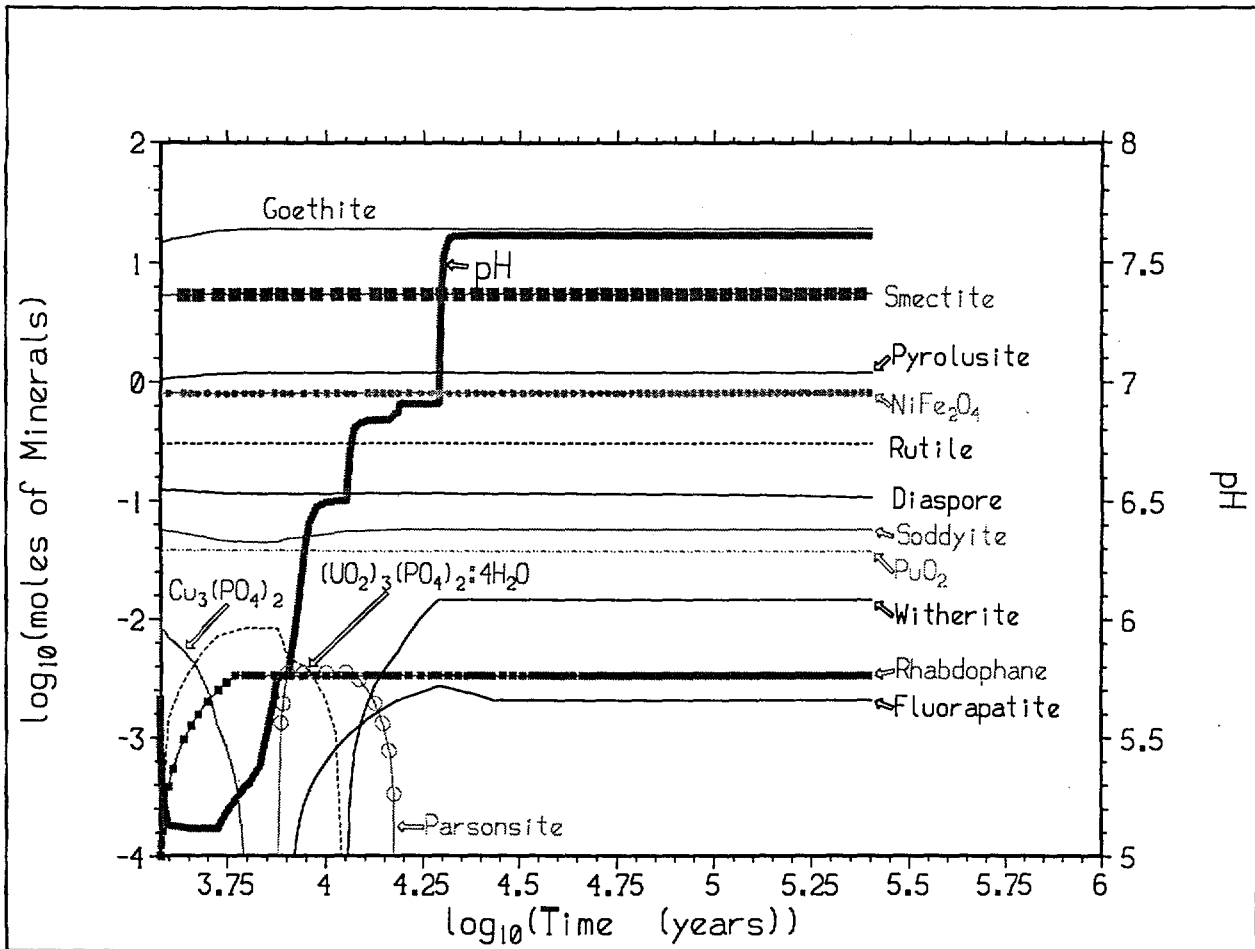


Figure 5-24. Case 10: pH and Amounts of Major and Minor Minerals Formed from Corrosion of WP (Per liter Initial Void Space). Parsonsite= $Pb_2UO_2(PO_4)_2 \cdot 2H_2O$ ; Soddyite= $(UO_2)_2SiO_4 \cdot 2H_2O$

The major corrosion products (minerals) for case 10, as well as the minerals that control Gd, Pu and U solubility, are show in Figure 5-24. By  $\sim 5 \cdot 10^4$  years, the pH and amounts of all minerals have stabilized. The amounts of smectite clay and goethite stabilize much more quickly, before  $\sim 10^4$  years.

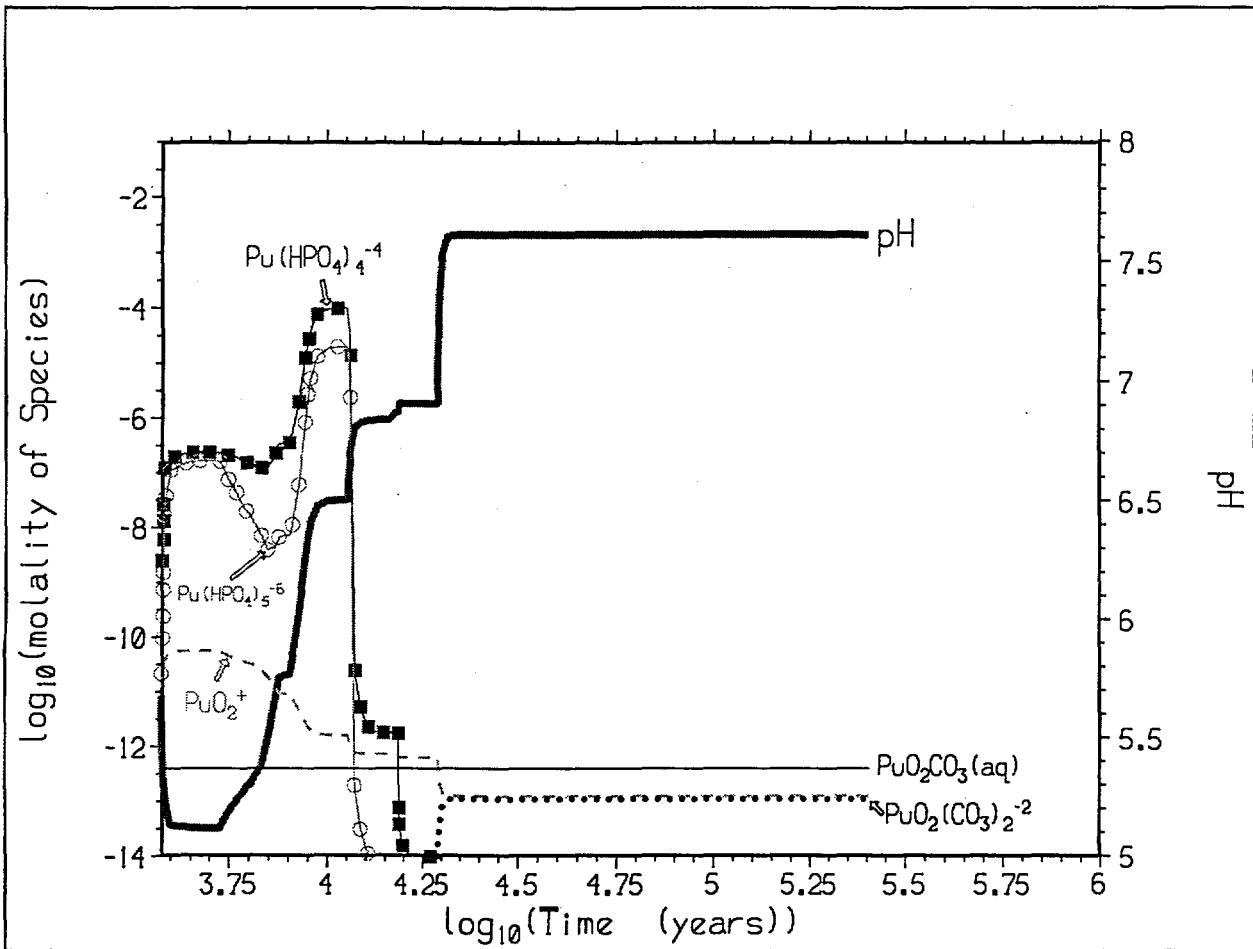


Figure 5-25. Case 10: pH and Predicted Pu Speciation. Following the pH Minimum, Pu-Phosphate Complexes Dominate as the Gd-Rich Basket Degrades. At Long Times, Pu-Carbonate Complexes Dominate

The principal Pu and Gd aqueous species, for case 10, are shown in Figures 5-25 and 5-26 (the species molalities are calculated by EQ6). As with case 2, phosphate complexes dominate Pu solubility at low pH, after the Gd-phosphate-doped basket materials degrade, and carbonate complexes dominate at higher pH. For Gd, the  $\text{Gd}^{3+}$  ion dominates at low pH, and Gd carbonate complexes dominate at high pH.

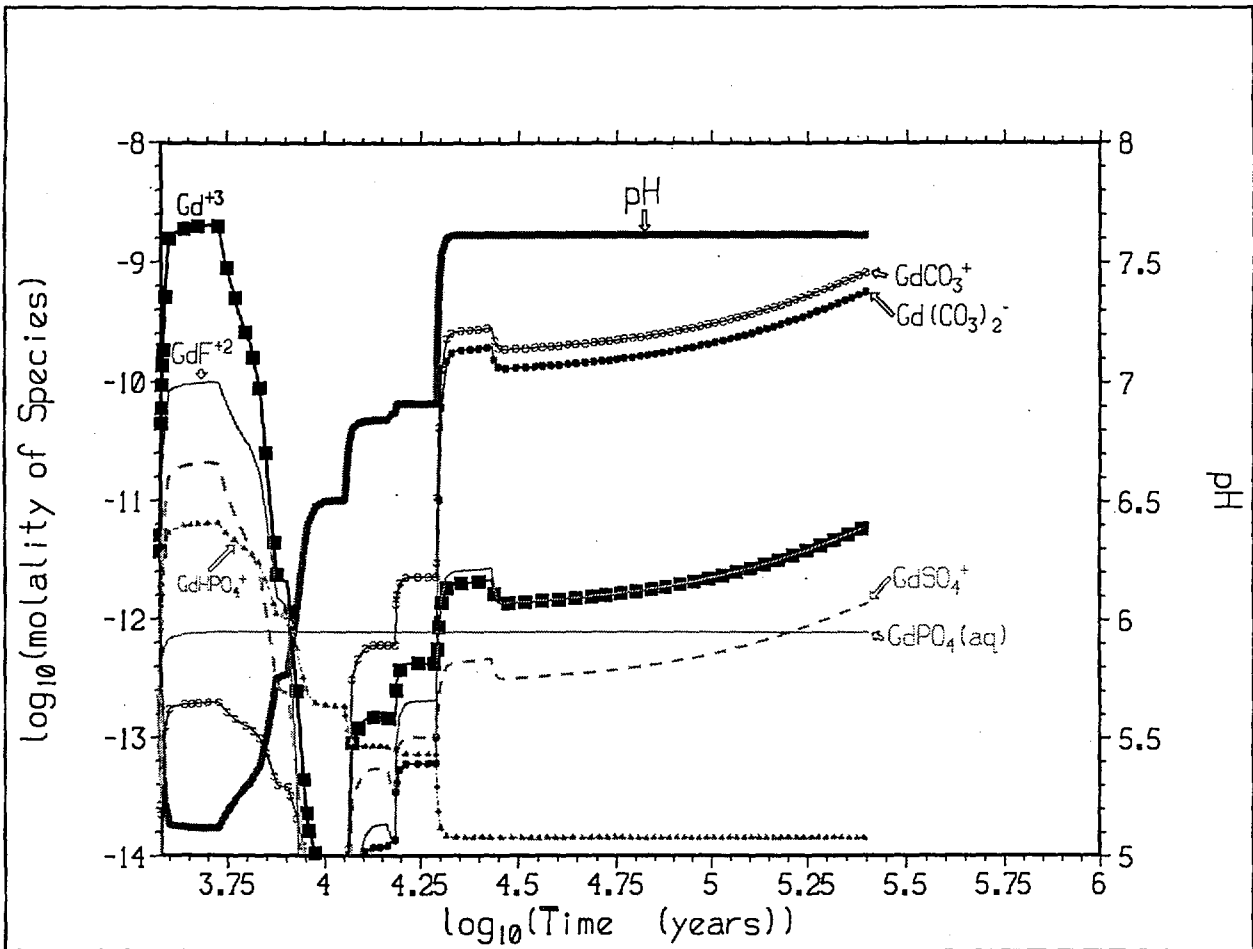


Figure 5-26. Case 10: pH and Predicted Gd Speciation.  $\text{Gd}^{3+}$  Dominates in the pH Minimum, and Gd-Carbonate Complexes Dominate at Long Times



**5.3.6 Compositions, Volumes and Masses of Clay-Like Materials Formed from Degradation of WP Materials**

In neutronics calculations, it is often desirable to know the average composition of the non-fuel portions of the degraded waste package. It is expected that the degraded package materials will comprise a clay-like mass, rich in Fe-oxides or hydroxides, and true silicate clays. The tables in this section give estimates of the total volumes and masses of the clay-like materials for cases 9 and 10. These tables were calculated with the older allpost/nxtinput method (Ref. 19, Attachment III), and were made available for neutronics calculations in an early part of the study, before the new SCFT method (Section 4.2) was available. Consequently, they are provided principally as a reference for other documents that cite the early results. The tables in this section correlate with cases 9 and 10 in Tables 5-6 and 5-7.

It is apparent from Tables 5-10 and 5-13 that the bulk composition of the clay-like material changes little with time, and also hematite and the goethite-allowed cases produce similar compositions. A comparison of Table 5-7 with Tables 5-8 and 5-11 shows slight discrepancies between the calculated % volume of the CRB. For case 9, the discrepancy amounts to 48.5% for the new method (long-term value), versus 47.9% for the old method. For case 10, the discrepancy amounts to 53.6% for the new method, versus 53.0% for the older method. These minor differences result from the fact that the new method automatically sums up molar volumes for all solids predicted by an EQ6 run (provides the solids have valid molar volumes and are real minerals, not fixed fugacity species); the old method required manual summing of volumes, and only major phases were included in the totals. Thus the new method produces slightly higher (and presumably more accurate) total volumes.

**Table 5-8. Case 9: Volumes of Minerals (liters) and Percent of Total Volume inside CRB**

Years <sup>1</sup>	Hematite <sup>2</sup>	Smectite <sup>2</sup>	Pyrolusite <sup>2</sup>	Ni <sub>2</sub> SiO <sub>4</sub>	Rutile <sup>2</sup>	Diaspore <sup>2</sup>	Total Minerals	Percent CRB <sup>3</sup>
3765	1438.76	4060.92	104.96	89.80	32.99	15.95	5743.4	44.81%
1.026E+4	1821.31	4067.53	118.33	90.36	32.99	15.37	6145.9	47.95%
1.001E+5	1819.55	4062.70	118.33	90.12	32.99	15.07	6138.8	47.90%

1. Years after the breach of the CRB. The DOE SNF breaches at ~3765 years.  
 2. Mineral formulae: Hematite=Fe<sub>2</sub>O<sub>3</sub>; Smectite=[(Ca,Mg)<sub>0.165</sub>(K,Na)<sub>0.33</sub>] Fe<sub>2</sub>Al<sub>0.33</sub> Si<sub>3.67</sub>H<sub>2</sub>O<sub>12</sub> is a "nontronite", iron-rich clay; Pyrolusite=MnO<sub>2</sub>; Rutile=TiO<sub>2</sub>; Diaspore=AlOOH.  
 3. The CRB contains 12816.382 liters (spreadsheet fff\_fuel\_hws.xls).  
 Reference input files: F01\_2204\_alln.6i, F02\_2022\_alln.6i.  
 Reference spreadsheets: fff\_fuel\_hws.xls; F02\_2204\_2022\_alln\*.xls; F03\_2022\_\*scratch.xls.

**Table 5–9. Case 9: Mass (kg) and Average Density (kg/L) of Minerals Formed within CRB**

Years <sup>1</sup>	Hematite <sup>2</sup>	Smectite <sup>2</sup>	Pyrolusite <sup>2</sup>	Ni <sub>2</sub> SiO <sub>4</sub>	Rutile <sup>2</sup>	Diaspore <sup>2</sup>	Total Minerals	Avg Density
3765	7589.3	13053.9	531.1	441.4	140.0	53.9	21809.7	3.797
1.026E+4	9607.2	13079.3	598.7	444.2	140.0	51.9	23921.4	3.892
1.001E+5	9597.9	13083.3	598.7	443.0	140.0	50.9	23913.9	3.896

1. Years after the breach of the CRB. The DOE SNF breaches at ~3765 years.  
 2. Mineral formulae: Hematite=Fe<sub>2</sub>O<sub>3</sub>; Smectite=[(Ca,Mg)<sub>0.165</sub>,(K,Na)<sub>0.33</sub>] Fe<sub>2</sub>Al<sub>0.33</sub> Si<sub>3.67</sub>H<sub>2</sub>O<sub>12</sub> is a "nontronite", iron-rich clay; Pyrolusite=MnO<sub>2</sub>; Rutile=TiO<sub>2</sub>; Diaspore=AlOOH.  
 3. The CRB contains 12816.382 liters (spreadsheet fff\_fuel\_hws.xls).  
 Reference input files: F01\_2204\_alln.6i, F02\_2022\_alln.6i.  
 Reference spreadsheets: fff\_fuel\_hws.xls; F02\_2204\_2022\_alln\*.xls; F03\_2022\_\*scratch.xls.

**Table 5–10. Case 9: Mole Percent of Major Elements in Non-Actinide Corrosion Products**

Years <sup>1</sup>	H	C	O	Na	Al	Si	Ca	K	Ti	Mn	Fe	Ni	Cu	Gd
3765	6.918	0.0000	59.75	0.0921	1.225	12.75	0.2829	0.4324	0.1954	0.6807	17.41	0.2348	0.0300	0.0000
1.026E+4	6.455	0.0002	59.80	0.0761	1.139	11.89	0.2762	0.3872	0.1819	0.7144	18.84	0.2200	0.0123	0.0020
1.001E+5	6.462	0.0088	59.82	0.0918	1.139	11.91	0.3042	0.2942	0.1818	0.7143	18.84	0.2194	0.0178	0.0020

1. Years after the breach of the CRB. The DOE SNF breaches at ~3765 years.  
 Reference input files: F01\_2204\_alln.6i, F02\_2022\_alln.6i.  
 Reference spreadsheets: fff\_fuel\_hws.xls; F02\_2204\_2022\_alln\*.xls; F03\_2022\_\*scratch.xls.

**Table 5–11. Case 10: Volumes of Minerals (liters) and Percent of Total Volume inside CRB**

Years <sup>1</sup>	Goethite <sup>2</sup>	Smectite <sup>2</sup>	Pyrolusite <sup>2</sup>	NiFe <sub>2</sub> O <sub>4</sub>	Rutile <sup>2</sup>	Diaspore <sup>2</sup>	Total Minerals	Percent CRB <sup>3</sup>
3765	1761.55	4134.53	104.96	207.23	32.99	12.38	6253.6	48.79%
1.016E+4	2287.47	4143.92	118.33	207.59	32.99	11.90	6802.2	53.07%
1.005E+5	2285.05	4139.42	118.33	207.49	32.99	11.59	6794.9	53.02%

1. Years after the breach of the CRB. The DOE SNF breaches at ~3765 years.  
 2. Mineral formulae: Goethite=FeOOH; Smectite=[(Ca,Mg)<sub>0.165</sub>,(K,Na)<sub>0.33</sub>] Fe<sub>2</sub>Al<sub>0.33</sub> Si<sub>3.67</sub>H<sub>2</sub>O<sub>12</sub> is a "nontronite", iron-rich clay; Pyrolusite=MnO<sub>2</sub>; Rutile=TiO<sub>2</sub>; Diaspore=AlOOH.  
 3. The CRB contains 12816.382 liters (spreadsheet fff\_fuel\_hws.xls).  
 Reference input files: F02\_2204\_alln.6i, F03\_2022\_alln.6i.  
 Reference spreadsheets: fff\_fuel\_hws.xls; F02\_2204\_2022\_alln\*.xls; F03\_2022\_\*scratch.xls.

**Table 5-12. Case 10: Mass (kg) and Average Density (kg/L) of Total Minerals Formed within CRB**

Years <sup>1</sup>	Goethite <sup>2</sup>	Smectite <sup>2</sup>	Pyrolusite <sup>2</sup>	NiFe <sub>2</sub> O <sub>4</sub>	Rutile <sup>2</sup>	Diaspore <sup>2</sup>	Total Minerals	Avg Density
3765	7517.8	13297.6	531.1	1090.9	140.0	41.8	22619.2	3.617
1.016E+4	9762.3	13328.9	598.7	1092.8	140.0	40.2	24963.0	3.670
1.005E+5	9752.0	13333.1	598.7	1092.3	140.0	39.2	24955.3	3.673

1. Years after the breach of the CRB. The DOE SNF breaches at ~3765 years.  
 2. Mineral formulae: Goethite=FeOOH; Smectite=[(Ca,Mg)<sub>0.165</sub>(K,Na)<sub>0.33</sub>] Fe<sub>2</sub>Al<sub>0.33</sub> Si<sub>3.67</sub>H<sub>2</sub>O<sub>12</sub> is a "nontronite", iron-rich clay; Pyrolusite=MnO<sub>2</sub>; Rutile=TiO<sub>2</sub>; Diaspore=AlOOH.  
 3. The CRB contains 12816.382 liters (spreadsheet fff\_fuel\_hws.xls).  
 Reference input files: F02\_2204\_alln.6i, F03\_2022\_alln.6i.  
 Reference spreadsheets: fff\_fuel\_hws.xls; F02\_2204\_2022\_alln\*.xls; F03\_2022\_\*scratch.xls.

**Table 5-13. Case 10: Mole Percent of Major Elements in Non-Actinide Corrosion Products**

Years <sup>1</sup>	H	C	O	Na	Al	Si	Ca	K	Ti	Mn	Fe	Ni	Gd
3765	14.23	0.0000	55.83	0.0849	1.059	11.03	0.2641	0.3482	0.1689	0.5886	15.95	0.4485	0.0000
1.016E+4	15.23	0.0000	55.28	0.0815	0.9594	10.05	0.2399	0.3110	0.1531	0.6016	16.69	0.4072	0.0017
1.005E+5	15.23	0.0074	55.30	0.0829	0.9593	10.06	0.2657	0.2400	0.1531	0.6015	16.68	0.4070	0.0017

1. Years after the breach of the CRB. The DOE SNF breaches at ~3765 years.  
 Reference input files: F02\_2204\_alln.6i, F03\_2022\_alln.6i.  
 Reference spreadsheets: fff\_fuel\_hws.xls; F02\_2204\_2022\_alln\*.xls; F03\_2022\_\*scratch.xls.

**5.3.7 Effects of Varying Glass Mg Composition**

In an aqueous system that is buffered to a fixed CO<sub>2</sub> fugacity, the degradation of glass affects pH in several ways. First, when a glass rich in alkali metals (Li, Na, K, Rb and Cs) decomposes in water, the pH and total dissolved carbonate can be driven to high values. Effectively, the solution is enriched in dissolved A<sub>2</sub>CO<sub>3</sub> (where A represents any alkali metal). Under such conditions, most actinides are highly soluble. In a flow-through system, the dissolved A<sub>2</sub>CO<sub>3</sub> is easily flushed away (solid alkali carbonates are generally very soluble). Second, a glass rich in alkaline earths (e.g., Mg, Ca, Sr and Ba) buffers pH through the precipitation and dissolution of solid carbonates, such as calcite solid solutions ((Ca,Mg,Fe)CO<sub>3</sub>). The alkalinity associated with these solids may persist longer in a flow-through system, simply because limited solubility prevents rapid removal; however the effect on pH is more modest. Third, clays formed by the degradation of the glass have some pH buffering capacity, and the composition of the clays is certainly affected by the balance of alkali metals and alkaline earths, as well as the availability of Fe, Al, and Si. Since proposed waste glass compositions vary substantially (e.g., Ref. 23 and Ref. 35), it is useful to assess the sensitivity of the EQ6 calculations to glass composition.

The glass composition in Table 5–2 was supplied “TBV” (to be verified) by the originator of Ref. 21. Ultimately, this composition traces back through Ref. 35 and Ref. 36 (Attachment II, pp. 1 and 2); these references contains a number of ambiguities, from the inclusion of an unspecified “zeolite” as part of the composition, to an ambiguous procedure for inclusion of radioactive components in the total. During the check for Ref. 21, suspicions arose that U had been added twice into the composition for Ref. 36, and that a subsequent compiler of the glass composition had inadvertently switched carbon for magnesium (the composition cited in Ref. 35 did not explicitly mention carbon, but did list Mg compounds corresponding to ~0.8% Mg). Given the factor 6 variation reported for U compositions in Savannah River glass, and the conservatism associated with high U content (see Section 5.1.1.1), the doubled U content was kept for this calculation, to maintain consistency with earlier work. However, the seemingly small Mg content could be significant, because the glass composition is otherwise very poor in alkaline earths, and the amount of glass in the WP is large. Given the uncertainty and possible importance of Mg, cases 9 and 10 were re-run with a “new” glass composition that contained 0.8 % Mg, and no carbon. Of all the cases considered in this study, cases 9 and 10 might be most sensitive to changes in Mg content, since the first stages are intended to achieve low pH by flushing away much of the alkali metals and alkaline earths. The runs with the “new” glass composition are designated cases 9s and 10s. It is notable that because of the recalculation of U and oxygen content associated with each metal, the compositions in Table 5–2 do not exactly match those in Ref. 21 (Attachment V, p. 3).

**Table 5–14. Case 9s: Mole Percent of Major Elements in Non-Actinide Corrosion Products**

Years <sup>1</sup>	H	C	O	Na	Al	Si	Ca	K	Ti	Mn	Fe	Ni	Cu	Gd	Mg
3765	6.918	0.0000	59.75	0.0280	1.225	12.75	0.2057	0.1200	0.1954	0.6807	17.41	0.3495	0.0300	0.0000	0.2686
1.026E+4	6.455	0.0002	59.80	0.0291	1.139	11.89	0.1994	0.1050	0.1819	0.7144	18.84	0.3249	0.0123	0.0020	0.2597
1.001E+5	6.462	0.0088	59.82	0.0491	1.139	11.91	0.2201	0.0616	0.1818	0.7143	18.84	0.3244	0.0178	0.0020	0.2470

1. Years after the breach of the CRB. The DOE SNF breaches at ~3765 years.  
 Reference input files: F01\_2204\_alln.6i, F02\_2022\_alln.6i.  
 Reference spreadsheets: fftf\_fuel\_hws.xls; F02\_2204\_2022\_alln\*.xls; F03\_2022\_\*scratch.xls, norm.xls.

**Table 5–15. Case 10s: Mole Percent of Major Elements in Non-Actinide Corrosion Products**

Years <sup>1</sup>	H	C	O	Na	Al	Si	Ca	K	Ti	Mn	Fe	Ni	Gd	Mg
3765	14.23	0.0000	55.83	0.0278	1.059	11.03	0.1932	0.1041	0.1689	0.5886	15.95	0.5986	0.0000	0.2215
1.016E+4	15.23	0.0000	55.28	0.0287	0.9594	10.05	0.1696	0.0876	0.1531	0.6016	16.69	0.5654	0.0017	0.2083
1.005E+5	15.23	0.0074	55.30	0.0429	0.9593	10.06	0.1883	0.0533	0.1531	0.6015	16.68	0.5651	0.0017	0.1908

1. Years after the breach of the CRB. The DOE SNF breaches at ~3765 years.  
 Reference input files: F02\_2204\_alln.6i, F03\_2022\_alln.6i.  
 Reference spreadsheets: fftf\_fuel\_hws.xls; F02\_2204\_2022\_alln\*.xls; F03\_2022\_\*scratch.xls; norm.xls

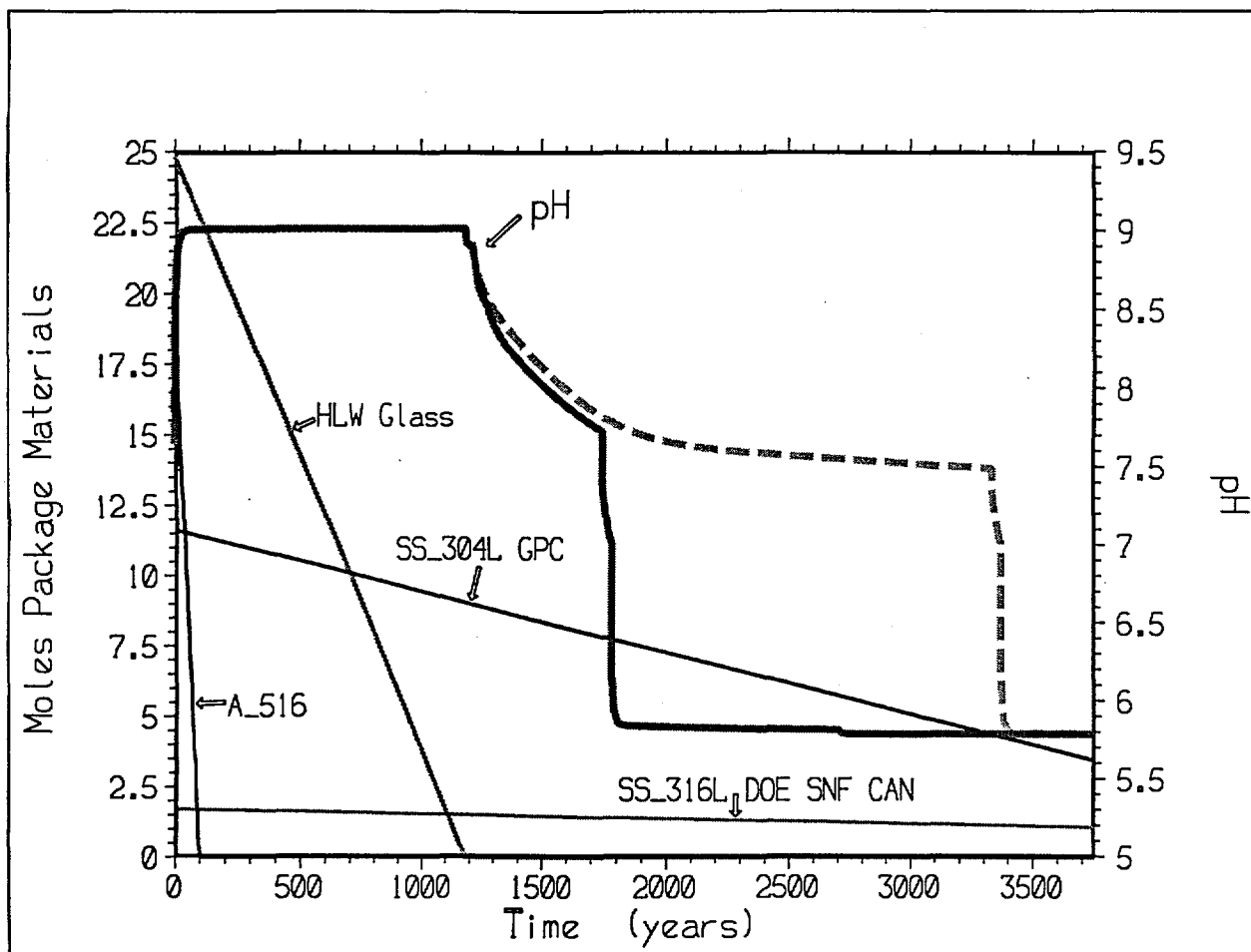


Figure 5-27. Moles Package Materials and pH for the First Stage (f00g2204 and fs0g2204) of Cases 10 and 10s. The Dashed pH Line Corresponds to Case 10s (with Added Mg) and the Unbroken pH Line Corresponds to Case 10

For the elements that affect neutronics calculations, there is little difference between cases 10 and 10s. In case 10s, 100% Gd, 99.3% Pu and 99.7% U are retained, compared to 100% Gd, 98.3% Pu and 99.8% U in case 10. The corrosion product compositions (Table 5-14) for the two cases are very similar for O, Al, Fe, Gd, H, Mn, Pu, Ti and U, somewhat similar for Ni, but markedly different for Ca, K, and Na. The differences in Ca, K and Na content are hardly surprising, since Mg readily replaces alkali metals and other alkaline earths in the smectite clay that dominates the corrosion products. It was found that between cases 9 and 9s, the ratio  $(Mg+Ca+(Na+K)/2)/Si$  varied by less than 0.2% on average. Throughout the second stage of the case 9 and 9s calculations, smectite is the only solid phase that contains Mg, Ca, K and Na in abundance, so regardless of the individual variations of these elements, the total  $(Mg+Ca+(Na+K)/2)/Si$  is held constant by the formula for the smectite (nontronite) solid solution. Cases 10 and 10s are similar. The slight increase in Ni results from the increased

average stability of trevorite ( $\text{NiFe}_2\text{O}_4$ ), which in turn results from the lower acid availability, as discussed below. Tables 5-14 and 5-15 are the Mg-“corrected” equivalents of Tables 5-10 and 5-13, respectively.

Figures 5-27 and 5-28 illustrate the relationship of pH to consumption of the HLW glass, and the formation of  $(\text{Ca},\text{Mg})\text{CO}_3$  calcite solid solution. In Figure 5-27, the first drop in pH occurs at ~1170 years, after all the HLW is exhausted, and acidity from corrosion of stainless steel (SS\_304L and SS\_316L in the figure) takes over. In Figure 5-28, one can see that the final drop to the plateau pH of ~5.8 occurs when all the calcite solid solution is consumed. Since the HLW glass in case 10s contains ~3 times as much Mg+Ca as case 10, case 10s forms more calcite and takes substantially longer to drop to the low pH plateau. The pH drop for case 10s consumes more of the acid produced by steel degradation; the resultant “acid deficit”, and the concomitant pH lag, are propagated through the second stage of case 10s.

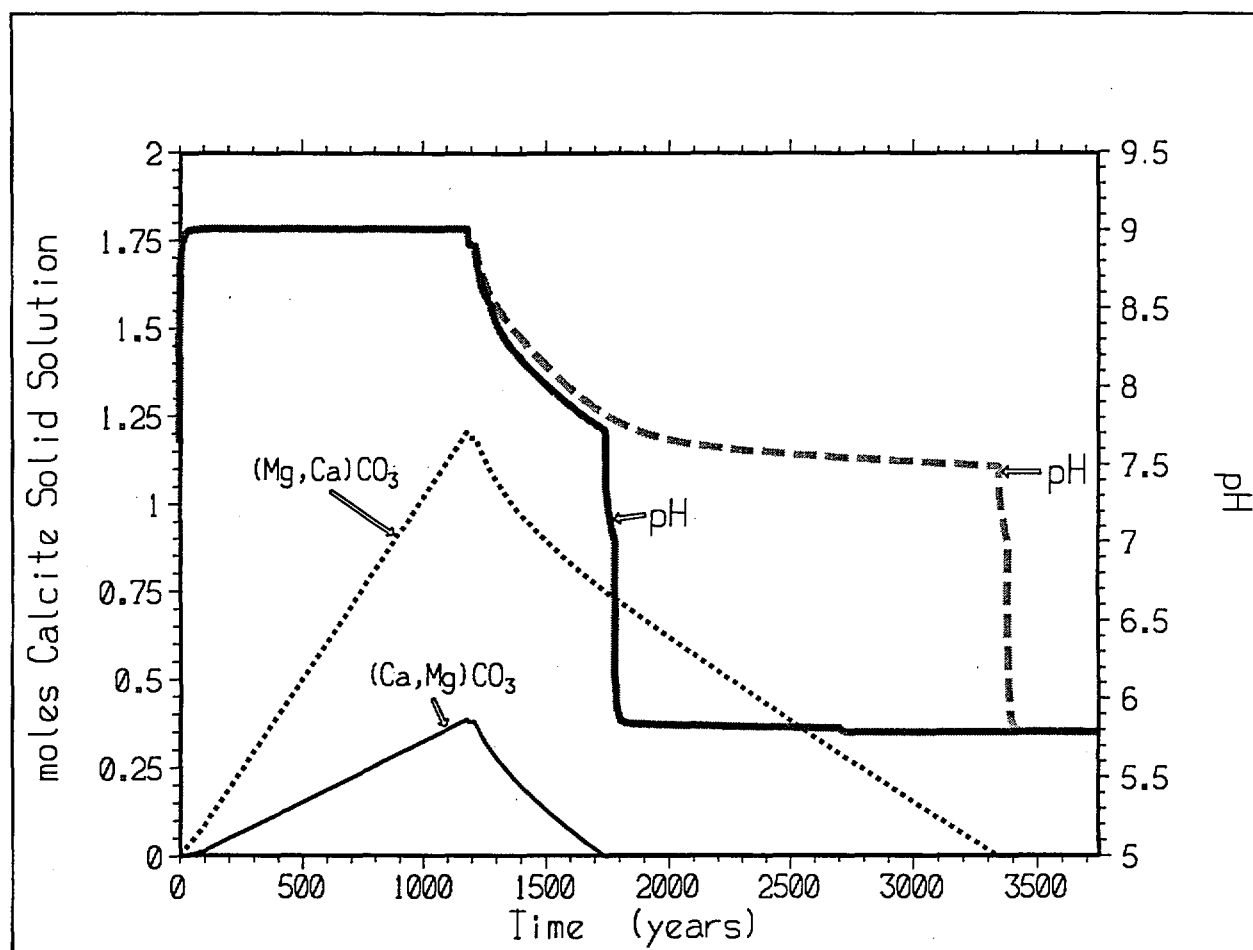


Figure 5-28. Comparison of Case 10 (Solid Lines) and Case 10s Results (Dashed Lines). Case 10s Has a Higher Mg Content, Generates More Calcite Solid Solution  $(\text{Mg},\text{Ca})\text{CO}_3$ , and Buffers pH Longer than Case 10. This Figure Is for Time before Breach of the DOE SNF Canister

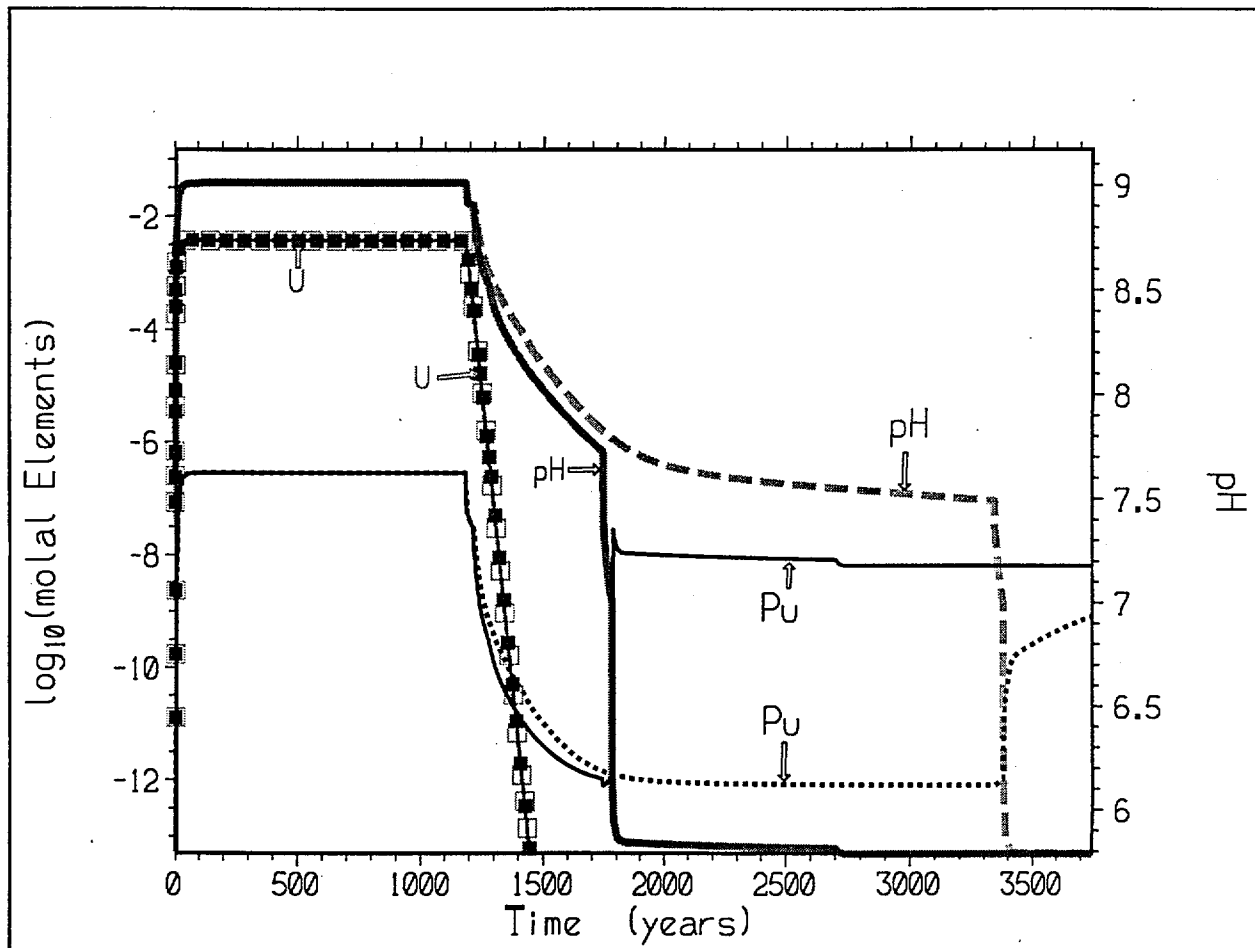


Figure 5-29. Comparison of Aqueous U, Pu and pH for Case 10 (Solid Lines) and Case 10s (Dashed). This Figure Is for Time before Breach of the DOE SNF Canister

Figure 5-29 shows how the pH differences of cases 10 and 10s ultimately affect the aqueous concentrations of U and Pu. The sudden increase in Pu solubility at ~1800 years (case 10) and 3400 years (case 10s) is a peculiar cascade effect from the consumption of calcite solid solution (Figure 5-28). Once the calcite is all consumed, the aqueous Ca drops rapidly, and fluorapatite ( $\text{Ca}_5(\text{PO}_4)_3\text{F}$ ) begins to dissolve. Dissolution of even a small fraction of the fluorapatite greatly increases the aqueous  $\text{HPO}_4^-$ , ultimately promoting the formation of stable,  $\text{Pu}(\text{HPO}_4)_n^{(2-2n)}$  complexes. As always, the predicted solubility of these species depends heavily on the quality of thermodynamic data.

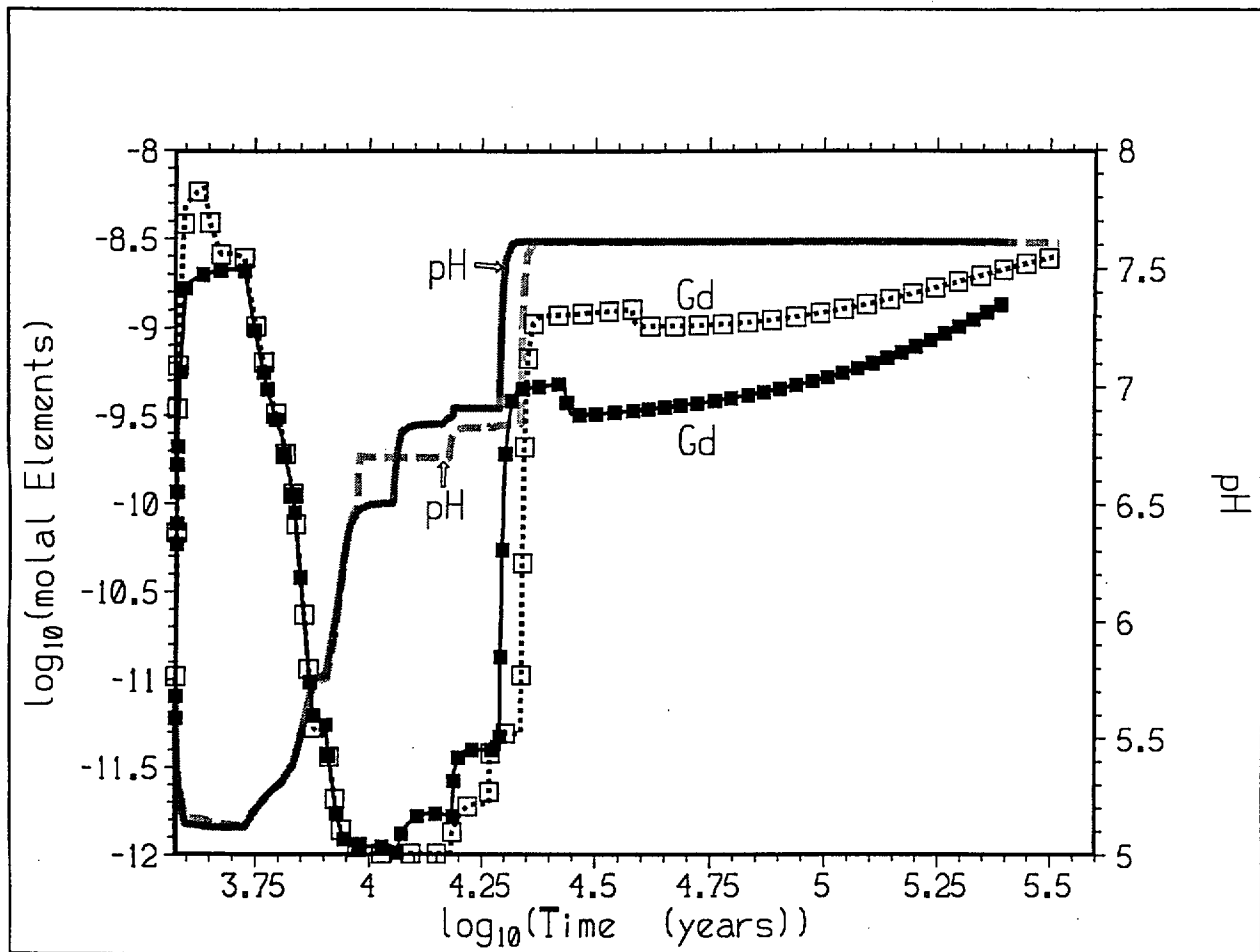


Figure 5-30. Comparison of Aqueous Gd and pH for Case 10 (Solid Lines and Symbols) and Case 10s (Dashed Lines and Open Symbols). This Figure Is for Time after Breach of the DOE SNF Canister

The second stages of cases 10 and 10s, after the breach of the DOE SNF canister (and the coincident slowing of J-13 flush rate from  $0.5$  to  $0.015 \text{ m}^3/\text{year}$ ), are compared in Figures 5-30 through 5-32. The acid deficit from the first stage propagates through as slight differences in the pH curves and concentrations of aqueous Gd, U and Pu. At long times ( $\geq 3 \cdot 10^4$  years), the pH and aqueous concentrations of cases 10 and 10s converge. Thus, while the differences in glass Mg concentrations (assumed for cases 10 and 10s) cause early differences in pH, they have little effect on the long-term behavior of the elements that are most significant in the neutronics calculations.



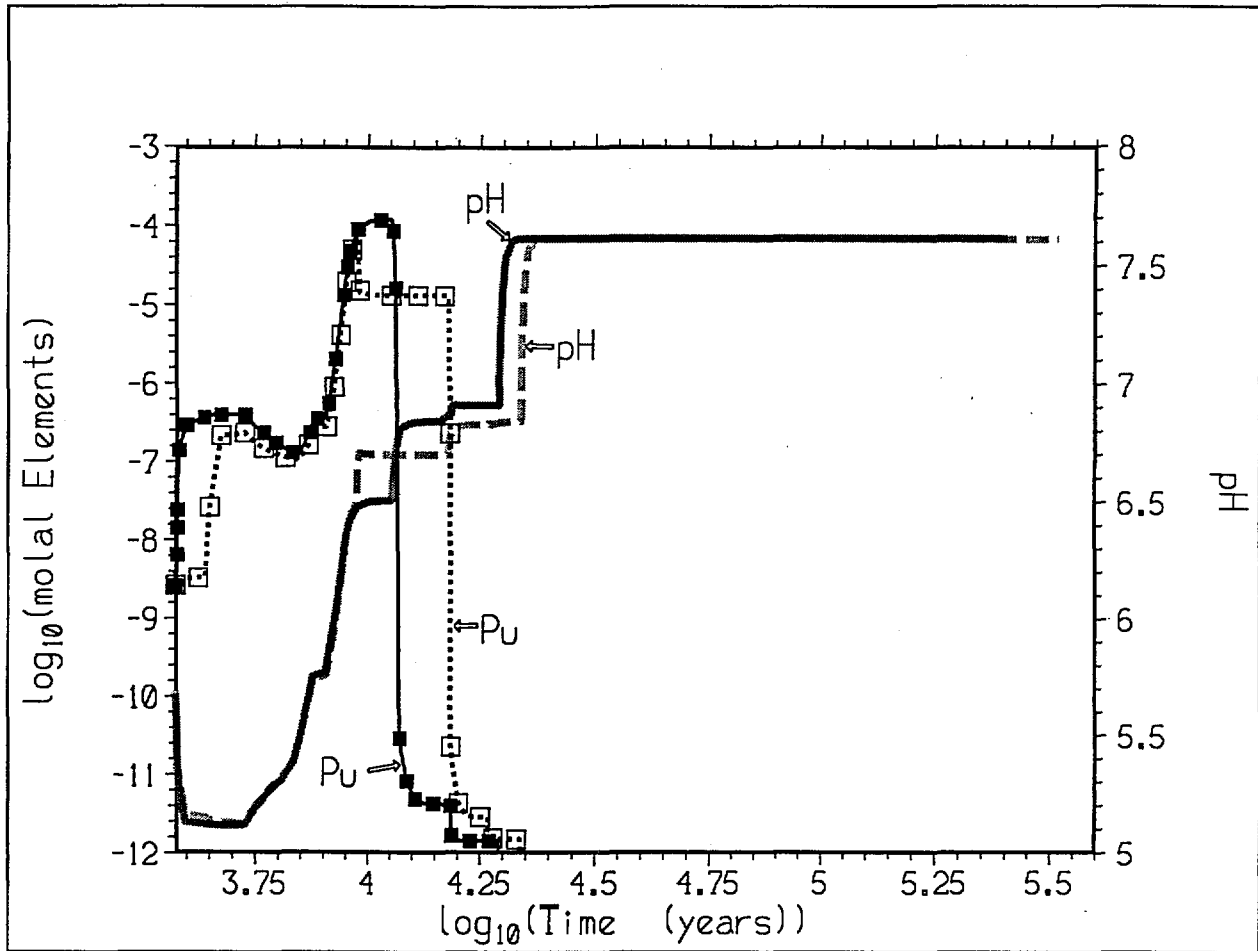


Figure 5-31. Comparison of Aqueous Pu and pH for Case 10 (Solid Lines and Symbols) and Case 10s (Dashed Lines and Open Symbols). This Figure Is for Time after Breach of the DOE SNF Canister

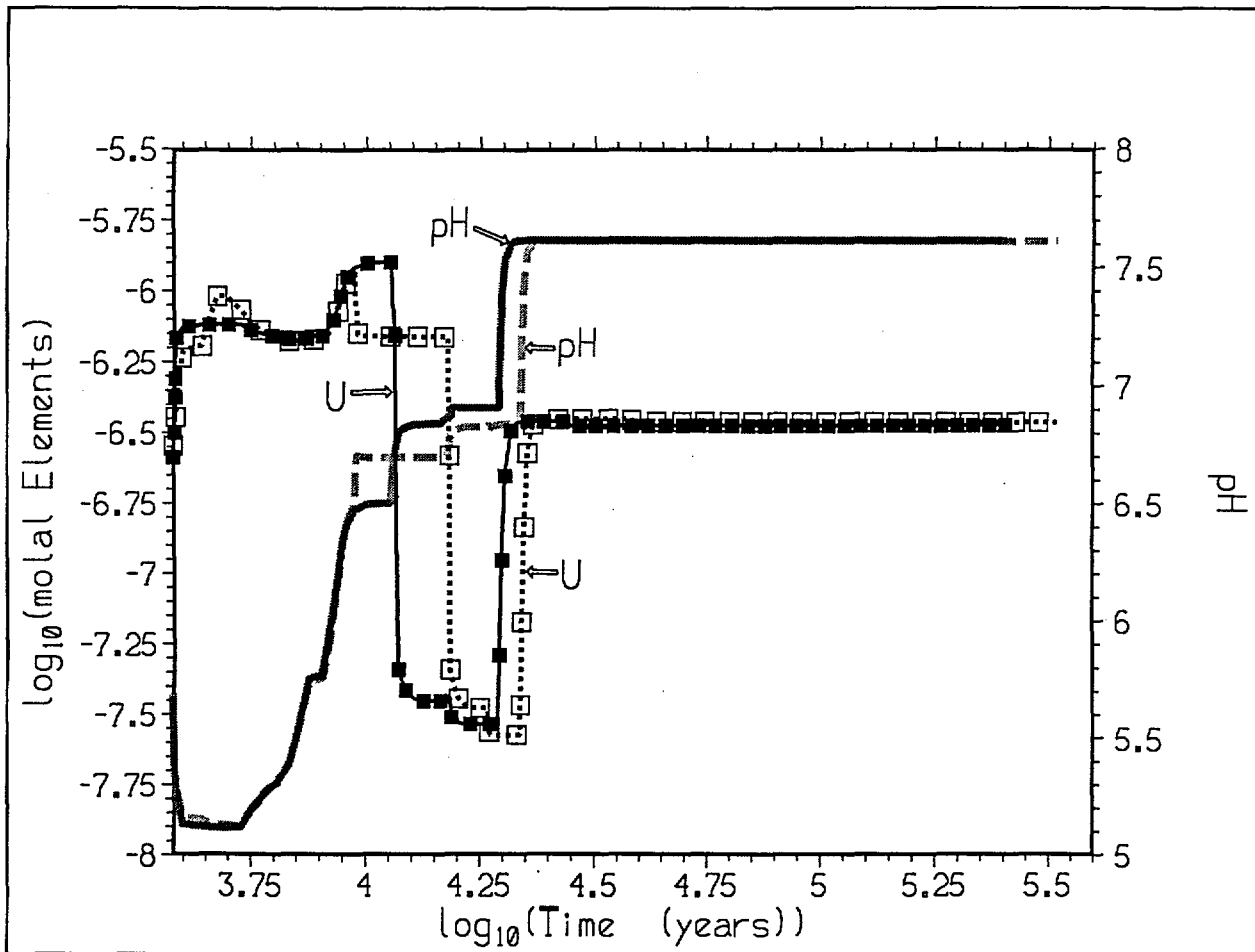


Figure 5-32. Comparison of Aqueous U and pH for Case 10 (Solid Lines and Symbols) and Case 10s (Dashed Lines and Open Symbols). This Figure Is for Time after Breach of the DOE SNF Canister

## 6. RESULTS

### 6.1 SUMMARY OF RESULTS

A principal purpose of the calculations was to assess chemical conditions that could lead to a loss of neutron absorbers (particularly Gd) from the package, as well as conditions that would allow the fissile materials to remain. Gadolinium is assumed to be present as  $\text{GdPO}_4$ , in the basket separating the fuel assemblies and derodded pins. A water with composition of J-13 well water is assumed to drip in through an opening at the top of the WP, pooling inside and eventually overflowing, allowing removal of soluble components through continual dilution. A scoping analysis (Section 5.3.1) suggested that high pH conditions, as well as acid conditions, could cause significant Gd loss; however, excess dissolved phosphate was unlikely to enhance removal of Gd from the WP.

Fourteen EQ6 reaction-path cases were constructed to span the range of possible Gd and fuel corrosion (Tables 5-5 and 5-6). Two additional cases tested effects of varying glass composition. Cases 1 through 8 tested the alkaline regime, achieving high pH by exposing the fuel to degrading glass. While cases 1 through 8 did produce the highest Gd loss, the total loss was  $\leq 0.7\%$  in  $\geq 10^5$  years; furthermore, when the glass was allowed to degrade rapidly, the alkaline conditions produced high U and Pu loss (up to 100%), reducing the chances of internal criticality. Some of these "alkaline" cases actually produced short-lived, very low pH ( $\sim 3$ ) when glass corrosion rates were set to low values, but steel corrosion rates were set to high values. These low pH values may not be realistic, since the simple glass corrosion model does not allow a feedback between pH and corrosion rate (which would tend to increase pH). Cases 9 through 12 tested the effect of exposing the Gd, Pu and U to long-lived acidic conditions (pH  $\sim 5$  to 6). The highest acidity was obtained by breaking the calculations into two stages; in the first stage, the DOE SNF canister is assumed to be intact, and only the outside of the DOE canister, the GPCs (and contained glass), and the A516 outer web structure are allowed to interact with the water dripping into the package. With a sufficiently high drip rate, the alkaline components of the glass are removed during this stage. In the second stage, the Gd-doped basket, fuel, and other components within the DOE SNF canister are exposed to J-13 water at a much lower drip rate, allowing pH to drop. When hematite formation was suppressed (in favor of goethite), somewhat lower pH was achieved. None of cases 9 through 12 caused significant loss of Gd, and none produced more than a few percent loss of Pu or U.

For two-stage cases, it was found that small variations in the Mg content of the glass caused shifts in the times of peak pH and aqueous Gd, Pu and U concentrations. The cause of these shifts was the production of solid alkaline-earth carbonates, which consume some of the acid produced by steel degradation, and delay the onset of the low pH plateau. Clays formed with the Mg-rich glass had higher Mg contents; however, the clay  $(\text{Mg}+\text{Ca}+(\text{Na}+\text{K})/2)/\text{Si}$  varied by only a fraction of a percent among the cases (as would be expected, since one clay phase dominates, and this ratio is fixed by structural and charge balance). The fractions of O, Si, Al, Ti, Fe, Mn,

Gd, Pu and U in the corrosion products were nearly constant (except for the early stages of runs with very low glass corrosion rates).

The predicted major corrosion products are: an Fe-rich smectite clay (nontronite); hematite or goethite; pyrolusite; rutile; and  $\text{Ni}_2\text{SiO}_4$  or  $\text{NiFe}_2\text{O}_4$ . The smectite and Fe oxide typically comprise over 90% of the corrosion product volume. If interaction with J-13 water continues for  $> 10^4$  years, corrosion products may fill ~50% of the volume within the CRB; given the poor packing and high porosity of clay aggregates, volume fraction occupied by corrosion products plus occluded water may be much greater than 50%. The Gd enters into rhabdophane (hydrated  $\text{GdPO}_4$ ) as the basket corrodes, the Pu enters  $\text{PuO}_2$ , and the dominant U solid is soddyite ( $(\text{UO}_2)_2(\text{SiO}_4) \cdot 2\text{H}_2\text{O}$ ).

As the basket corrodes, high aqueous  $\text{HPO}_4^{=}$  concentrations may be achieved. A somewhat surprising result of this study is the prediction that  $\text{HPO}_4^{=}$  complexes may dominate Pu solubility during periods of low pH. However, high dissolved phosphate levels are not entirely due to the basket; the HLW glass contains ~3 times the phosphate of the Gd-doped basket, and the abundant carbon steel also contains trace phosphate.

## 6.2 TBV DISCLAIMER

Existing (qualified and unqualified) data were used in the development of the results presented in this section. Therefore, the use of any data from this calculation for input into documents supporting procurement, fabrication, or construction is required to be identified and tracked as TBV in accordance with appropriate procedures.

---

## 7. REFERENCES

- 1 Idaho National Engineering and Environmental Laboratory (INEEL) 1998. *FFTF (MOX) Fuel Characteristics for Disposal Criticality Analysis*. DOE/SNF/REP-032 Rev 0. Idaho Falls, Idaho: Idaho National Engineering and Environmental Laboratory. 241492.
- 2 Bergsman, K.H. 1994. *Hanford Spent Fuel Inventory Baseline*. WHC-SD-SNF-TI-001 REV 0. Richland, Washington: Westinghouse Hanford Company. 227655.
- 3 Civilian Radioactive Waste Management System (CRWMS) Management & Operating Contractor (M&O) 1998. *Total System Performance Assessment-Viability Assessment (TSPA-VA) Analyses Technical Basis Document. Chapter 10, Disruptive Events*. B00000000-01717-4301-00010 REV 00. Las Vegas, Nevada: M&O. MOL.19980724.0399.
- 4 CRWMS M&O 1998. *Evaluation of Codisposal Viability for Aluminum-Clad DOE-Owned Spent Fuel: Phase II. Degraded Codisposal Waste Package Internal Criticality*. BBA000000-01717-5705-00017 REV 01. Las Vegas, Nevada: M&O. MOL.19980616.0098.
- 5 National Research Council of the National Academy of Sciences 1995. *Technical Bases for Yucca Mountain Standards*. Washington, District of Columbia: National Academy Press. 104273.
- 6 Harrar, J.E.; Carley, J. F.; Isherwood, W. F.; and Raber, E. 1990. *Report of the Committee to Review the Use of J-13 Well Water in Nevada Nuclear Waste Storage Investigations*. UCID-21867. Livermore, California: Lawrence Livermore National Laboratory. MOL.19980416.0660
- 7 Wolery, T.J. 1992. *EQ3/6, A Software Package for Geochemical Modeling of Aqueous Systems: Package Overview and Installation Guide (Version 7.0)*. UCRL-MA-110662 PT I. Livermore, California: Lawrence Livermore National Laboratory. 205087.
- 8 Daveler, S.A. and Wolery, T.J. 1992. *EQPT, A Data File Preprocessor for the EQ3/6 Software Package: User's Guide, and Related Documentation (Version 7.0)*. UCRL-MA-110662 PT II. Livermore, California: Lawrence Livermore National Laboratory. 205240.
- 9 Wolery, T.J. 1992. *EQ3NR, A Computer Program for Geochemical Aqueous Speciation-Solubility Calculations: Theoretical Manual, User's Guide, and Related Documentation (Version 7.0)*. UCRL-MA-110662 PT III. Livermore, California: Lawrence Livermore National Laboratory. 205154.

- 
- 10 Wolery, T.J. and Daveler, S.A. 1992. *EQ6, A Computer Program for Reaction Path Modeling of Aqueous Geochemical Systems: Theoretical Manual, User's Guide, and Related Documentation (Version 7.0)*. UCRL-MA-110662 PT IV. Livermore, California: Lawrence Livermore National Laboratory. 205002.
  - 11 Spahiu, K. and Bruno, J. 1995. *A selected thermodynamic database for REE to be used in HLNW performance assessment exercises*. SKB Technical Report 95-35. Stockholm, Sweden: Swedish Nuclear Fuel and Waste Management Co. 225493.
  - 12 CRWMS M&O 1998. *Electronic Media for BBA000000-01717-0210-00028 REV 00*. QIC-80 DT 350 Tape. MOL.19981229.0082.
  - 13 CRWMS M&O 1998. *Viability Assessment of a Repository at Yucca Mountain. Volume 3: Total system Performance Assessment*. Figures 3-20 to 3-22. B00000000-01717-4301-00003 REV 01. Las Vegas, Nevada: M&O. MOL.19981007.0030.
  - 14 Firsching, F.H. and Brune, S.N. 1991. Solubility Products of the Trivalent Rare-Earth Phosphates. *Jour. Chem. Eng. Data*, 36, 93-95. American Chemical Society. 240863.
  - 15 Yang, I.C.; Rattray, G.W.; and Yu, P. 1996. *Interpretation of Chemical and Isotopic Data from Boreholes in the Unsaturated-Zone at Yucca Mountain, Nevada*. WRIR 96-4058. Denver, Colorado: U.S. Geological Survey. MOL.19980528.0216.
  - 16 Weast, R.C., ed. 1977. *CRC Handbook of Chemistry and Physics, 58th Ed.* Cleveland, Ohio: CRC Press, Inc. 242376.
  - 17 CRWMS M&O 1996. *Second Waste Package Probabilistic Criticality Analysis: Generation and Evaluation of Internal Criticality Configurations*. BBA000000-01717-2200-00005 REV 00. Las Vegas, Nevada: M&O. MOL19960924.0193.
  - 18 CRWMS M&O 1998. *EQ3/6 Software Installation and Testing Report for Pentium Based Personal Computers (PCs)*. CSCI: LLYMP9602100. Las Vegas, Nevada: M&O. MOL.19980813.0191.
  - 19 CRWMS M&O 1998. *EQ6 Calculations for Chemical Degradation of Pu-Ceramic Waste Packages*. BBA000000-01717-0210-00018 REV 00. Las Vegas, Nevada: M&O. MOL.19980918.0004.
  - 20 CRWMS M&O 1998. *EQ6 Calculations for Chemical Degradation of PWR and MOX Spent Fuel Waste Packages*. BBA000000-01717-0210-00009 REV 00. Las Vegas, Nevada: M&O. MOL.19980701.0483.
  - 21 CRWMS M&O 1998. *Dose Calculations for the Codisposal WP of DHLW Canisters*

- 
- and the Fast Flux Test Facility (FFTF) Fuel.* BBA000000-01717-00019 REV 00. Las Vegas, Nevada: M&O. MOL.19980911.0001.
- 22 DOE/RW 1992. *Characteristics of Potential Repository Wastes.* DOE/RW-0184-R1 vol. 1, p. 3.3-15, Table 3.3.8. Oak Ridge, Tennessee: Martin Marietta Energy Systems, Inc. HQO.19910827.0001.
- 23 Bibler, N.E.; Ray, J.W.; Fellingner, T.L.; Hodoh, O.B.; Beck, R.S.; and Lien, O.G. 1998. *Characterization of Radioactive Glass Currently Being Produced by the Defense Waste Processing Facility at Savannah River Site.* WSRC-MS-97-00617, Table I. Aiken, South Carolina: Westinghouse Savannah River Company. 240859.
- 24 CRWMS M&O 1995. *Total System Performance Assessment - 1995: An Evaluation of the Potential Yucca Mountain Repository.* B00000000-01717-2200-00136 REV 01. Las Vegas, Nevada: M&O. MOL.19960724.0188.
- 25 CRWMS M&O 1998. *Controlled Design Assumptions Document.* B00000000-01717-4600-00032 REV 05. Las Vegas, Nevada: M&O. MOL.19980804.0481.
- 26 Inco Alloys International 1985. Inconel Alloy 625, pp. 11-15. Hereford, England: Inco Alloys International. 241920.
- 27 CRWMS M&O 1998. *Unsaturated-Zone Flow: Preliminary Draft Section 2.3 of TSPA-VA Document.* B00000000-01717-2200-00201. Las Vegas, Nevada: M&O. MOL.19980428.0202.
- 28 CRWMS M&O 1996. *Status Report on Degraded Mode Criticality Analysis of Immobilized Plutonium Waste Forms in a Geologic Repository.* A00000000-01717-5705-00013 REV 00. Vienna, Virginia: M&O. MOL.19970625.0445.
- 29 CRWMS M&O 1997. *Degraded Mode Criticality Analysis of Immobilized Plutonium Waste Forms in a Geologic Repository.* A00000000-01717-5705-00014 REV 01. Las Vegas, Nevada: M&O. MOL.19980422.0911.
- 30 Roberts, W.L., Jr.; Rapp, G.R., Jr.; and Weber, J. 1974. *Encyclopedia of Minerals.* New York, New York: van Nostrand Reinhold Co. 238571.
- 31 CRWMS M&O 1996. *Material Compositions and Number Densities For Neutronics Calculations.* BBA000000-01717-0200-00002 REV 00. Las Vegas, Nevada: M&O. MOL.19960624.0023.
- 32 Walker, E.W.; Parrington, J.R.; and Feiner, F. 1989. *Nuclides and Isotopes, 14th ed., Chart of the Nuclides.* San Jose, California: General Electric Co. 201637.

- 33 Lee, J.H. and Byrne, R.H. 1992. Examination of Comparative Rare Earth Element Complexation Behavior Using Linear Free-Energy Relationships. *Geochim. Cosmochim. Acta*, 56, 1127-1137. Pergamon Press Ltd. 240861.
- 34 Stockman, H.W.; Nagy, K.L.; and Morris, C.E. 1995. *Long-Term Modeling of Glass Waste in Portland Cement- and Clay-Based Matrices*. SAND95-2730 RS-8232-2/960009, Section 4.1.5, pp. 13-14. Albuquerque, New Mexico: Sandia National Laboratories. 240806.
- 35 Stout, R.B. and Leider, H.R. (eds.) 1991. *Preliminary Waste Forms Characteristics Report Version 1.0*, p. 2.2.1.4-11. Livermore, California: LLNL. MOL.19940726.0118.
- 36 CRWMS M&O 1996. *DHLW Glass Waste Package Criticality Analysis*. BBAC00000-01717-0200-00001 REV 00. Las Vegas, Nevada: M&O. MOL.19960919.0237.



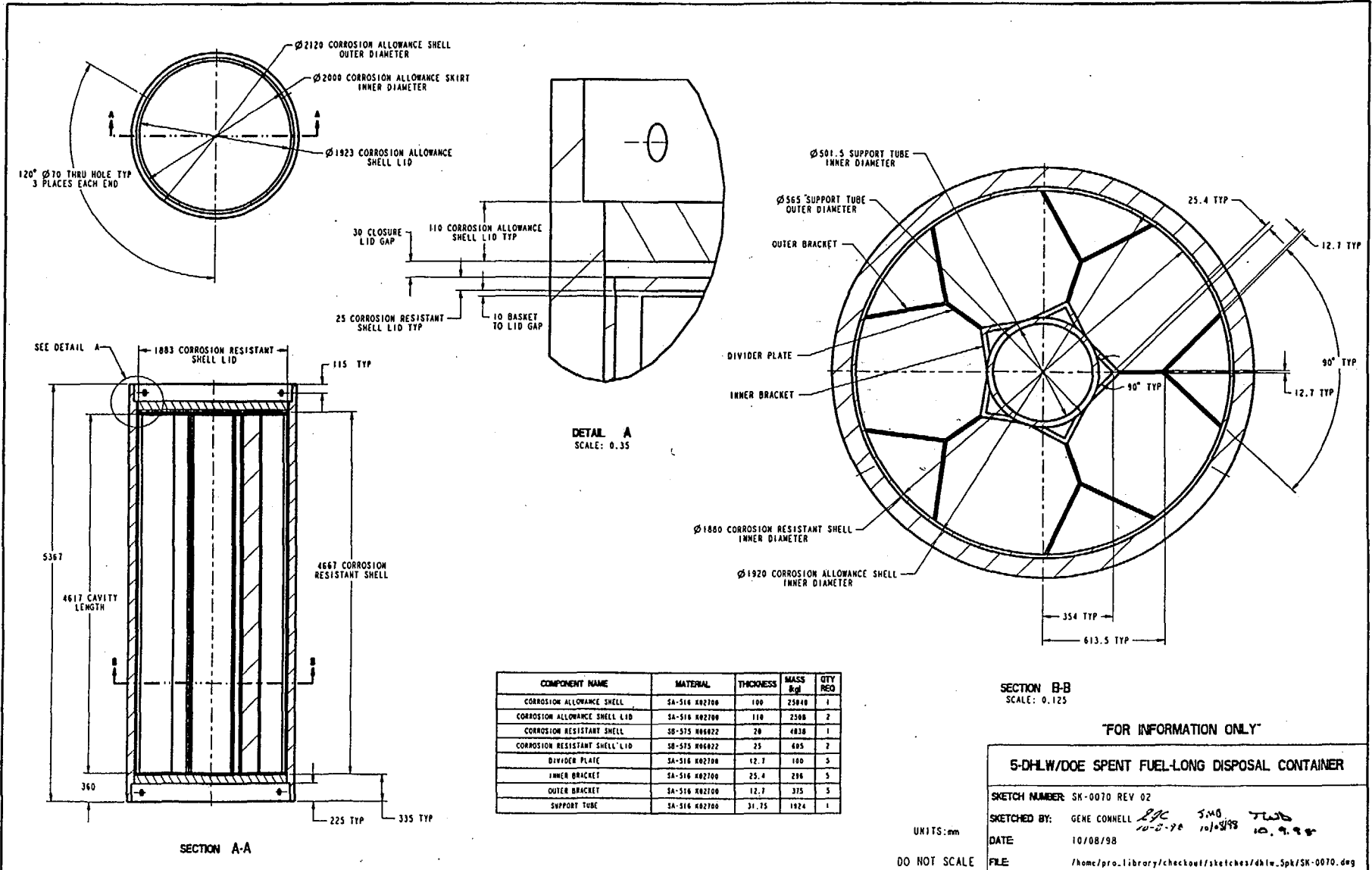
**8. ATTACHMENTS**

**Attachment I. Sketch SK-0070 REV 02 (1 page)**

**Attachment II. Sketch SK-0109 REV 01 (1 page)**

**Attachment III. Sample Output Tables for Case 10 (F00g2022.6i) (8 pages)**

**Attachment IV. Listing of Files on Electronic Media (4 pages, Ref. 12)**



COMPONENT NAME	MATERIAL	THICKNESS	MASS kg	QTY REQ
CORROSION ALLOWANCE SHELL	SA-516 R02700	100	25810	1
CORROSION ALLOWANCE SHELL LID	SA-516 R02700	110	2300	2
CORROSION RESISTANT SHELL	SA-575 R06022	20	4830	1
CORROSION RESISTANT SHELL LID	SA-575 R06022	25	405	2
DIVIDER PLATE	SA-516 R02700	12.7	100	5
INNER BRACKET	SA-516 R02700	25.4	216	5
OUTER BRACKET	SA-516 R02700	12.7	375	5
SUPPORT TUBE	SA-516 R02700	31.75	1924	1

SECTION B-B  
SCALE: 0.125

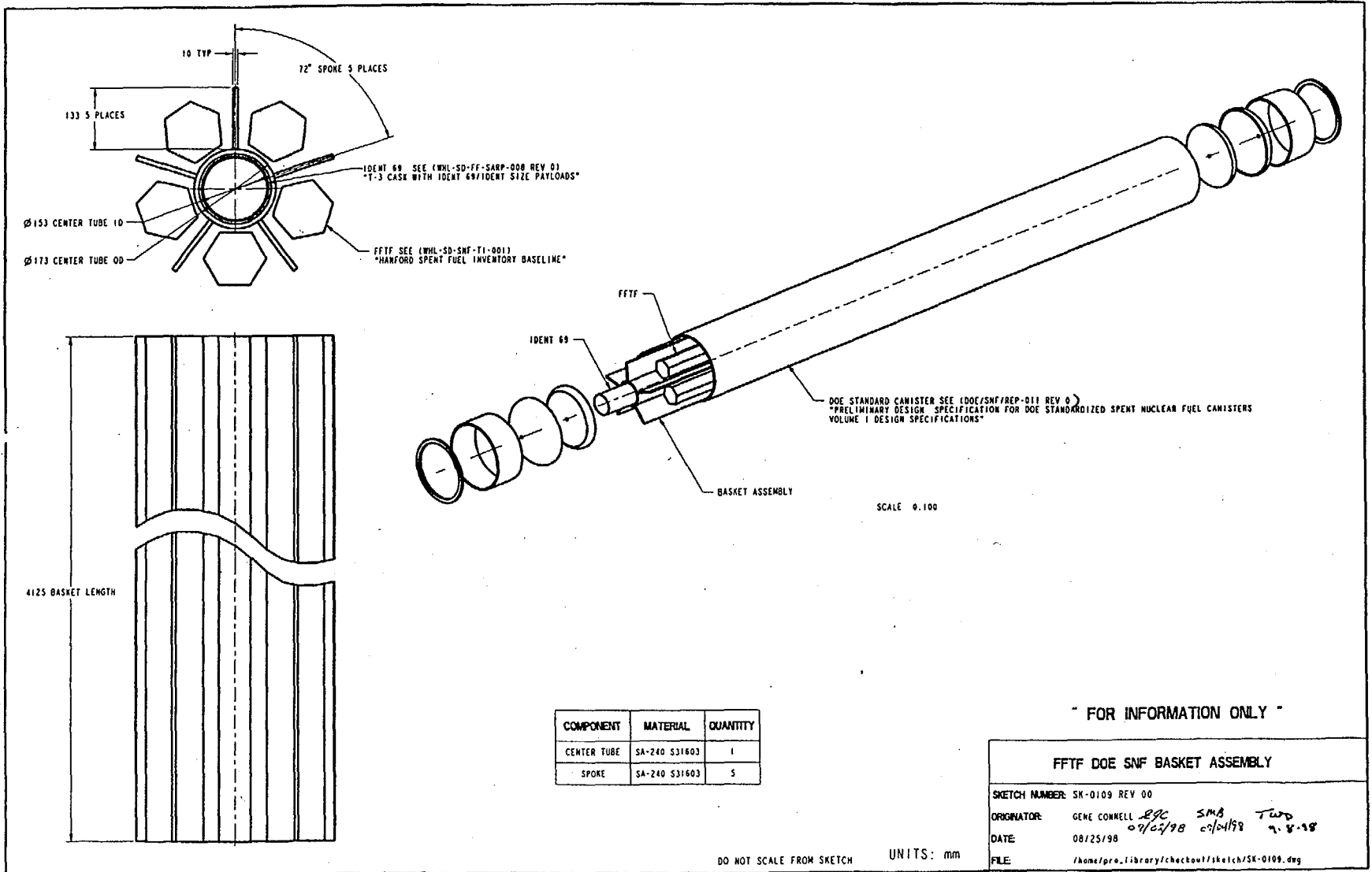
"FOR INFORMATION ONLY"

5-DHLW/DOE SPENT FUEL-LONG DISPOSAL CONTAINER

SKETCH NUMBER: SK-0070 REV 02  
 SKETCHED BY: GENE CONNELL *gpc* 5:48 10-8-98 *TWB* 10-9-98  
 DATE: 10/08/98  
 FILE: /home/pro.library/checkout/stitches/4hlw.5pk/SK-0070.dwg

UNITS: mm

DO NOT SCALE



COMPONENT	MATERIAL	QUANTITY
CENTER TUBE	SA-240 S31603	1
SPOKE	SA-240 S31603	5

" FOR INFORMATION ONLY "

FFTF DOE SNF BASKET ASSEMBLY

SKETCH NUMBER: SK-0109 REV 00  
 ORIGINATOR: GENE CONNELL *EGC* *SMB* *TWO*  
 DATE: 08/25/98 *09/02/98* *09/04/98* *9.8.98*  
 FILE: /home/pro.library/checkout/sketch/SK-0109.dwg

DO NOT SCALE FROM SKETCH UNITS: mm

**ATTACHMENT III. SAMPLE OUTPUT TABLES FOR CASE 10 (F00g2022.6i)**

**Table III-1. Sample f00g2022.elem\_tot.txt File**

MOLES in minerals, aqu & special react																	
data0.nuc.R8a																	
EQ6 input file name= F00g2022.6i																	
Description= React J-13 water with metals in an FFTF waste package.																	
Years	zi	pH	VolSolid (cc)	O	Ag	Al	B	Ba	Ca	Cl	Cr	Cu	F	Fe	Gd	H	C
3.76E+03	3.76E+02	5.79E-00	1.13E+03	1.56E+02	1.08E-02	1.90E-00	1.24E-05	1.46E-02	4.73E-01	1.10E-02	1.34E-00	2.70E-02	1.14E-04	3.14E+01	3.29E-03	1.36E+02	9.57E-03
3.76E+03	3.76E+02	5.79E-00	1.13E+03	1.56E+02	1.08E-02	1.90E-00	1.24E-05	1.46E-02	4.73E-01	1.10E-02	1.34E-00	2.70E-02	1.14E-04	3.14E+01	3.29E-03	1.36E+02	9.57E-03
3.77E+03	3.76E+02	5.58E-00	1.13E+03	1.56E+02	1.08E-02	1.90E-00	1.24E-05	1.46E-02	4.73E-01	1.10E-02	1.34E-00	2.70E-02	1.14E-04	3.14E+01	3.29E-03	1.36E+02	9.49E-03
3.79E+03	3.76E+02	5.44E-00	1.13E+03	1.56E+02	1.08E-02	1.90E-00	1.24E-05	1.46E-02	4.73E-01	1.10E-02	1.34E-00	2.70E-02	1.14E-04	3.14E+01	3.29E-03	1.36E+02	9.33E-03
3.80E+03	3.77E+02	5.36E-00	1.14E+03	1.56E+02	1.08E-02	1.90E-00	1.24E-05	1.46E-02	4.73E-01	1.10E-02	1.33E-00	2.69E-02	1.14E-04	3.14E+01	3.29E-03	1.36E+02	9.17E-03
3.81E+03	3.77E+02	5.33E-00	1.14E+03	1.57E+02	1.08E-02	1.90E-00	1.24E-05	1.46E-02	4.73E-01	1.10E-02	1.33E-00	2.69E-02	1.14E-04	3.14E+01	3.29E-03	1.36E+02	9.08E-03
3.81E+03	3.77E+02	5.33E-00	1.14E+03	1.57E+02	1.08E-02	1.90E-00	1.24E-05	1.46E-02	4.73E-01	1.10E-02	1.33E-00	2.69E-02	1.14E-04	3.14E+01	3.29E-03	1.36E+02	9.07E-03
3.83E+03	3.77E+02	5.29E-00	1.14E+03	1.57E+02	1.08E-02	1.90E-00	1.24E-05	1.46E-02	4.73E-01	1.10E-02	1.33E-00	2.68E-02	1.14E-04	3.14E+01	3.29E-03	1.36E+02	8.94E-03
3.97E+03	3.78E+02	5.13E-00	1.14E+03	1.58E+02	1.08E-02	1.90E-00	1.24E-05	1.46E-02	4.73E-01	1.10E-02	1.28E-00	2.56E-02	1.14E-04	3.14E+01	3.29E-03	1.37E+02	7.56E-03
4.53E+03	3.82E+02	5.12E-00	1.16E+03	1.61E+02	1.07E-02	1.90E-00	1.24E-05	1.46E-02	4.73E-01	1.10E-02	9.47E-01	1.86E-02	1.14E-04	3.14E+01	3.29E-03	1.38E+02	5.07E-03
5.01E+03	3.84E+02	5.12E-00	1.17E+03	1.63E+02	1.07E-02	1.90E-00	1.24E-05	1.46E-02	4.74E-01	1.09E-02	6.52E-01	1.26E-02	1.14E-04	3.14E+01	3.29E-03	1.39E+02	2.94E-03
5.33E+03	3.86E+02	5.12E-00	1.18E+03	1.65E+02	1.07E-02	1.90E-00	1.24E-05	1.46E-02	4.74E-01	1.09E-02	4.50E-01	8.47E-03	1.14E-04	3.14E+01	3.29E-03	1.40E+02	1.54E-03
5.87E+03	3.88E+02	5.23E-00	1.18E+03	1.65E+02	1.07E-02	1.90E-00	1.24E-05	1.46E-02	4.74E-01	1.09E-02	2.26E-01	3.79E-03	1.14E-04	3.14E+01	3.29E-03	1.40E+02	8.37E-04
5.93E+03	3.88E+02	5.25E-00	1.18E+03	1.65E+02	1.07E-02	1.90E-00	1.24E-05	1.46E-02	4.74E-01	1.09E-02	2.09E-01	3.42E-03	1.14E-04	3.14E+01	3.29E-03	1.41E+02	7.74E-04
6.31E+03	3.90E+02	5.30E-00	1.18E+03	1.65E+02	1.07E-02	1.90E-00	1.24E-05	1.46E-02	4.75E-01	1.09E-02	1.27E-01	1.57E-03	1.14E-04	3.14E+01	3.29E-03	1.41E+02	3.83E-04
6.40E+03	3.90E+02	5.31E-00	1.18E+03	1.65E+02	1.07E-02	1.90E-00	1.24E-05	1.46E-02	4.75E-01	1.09E-02	1.12E-01	1.26E-03	1.14E-04	3.14E+01	3.29E-03	1.41E+02	2.97E-04
6.46E+03	3.90E+02	5.32E-00	1.18E+03	1.66E+02	1.07E-02	1.90E-00	1.24E-05	1.46E-02	4.75E-01	1.09E-02	1.02E-01	1.07E-03	1.14E-04	3.14E+01	3.29E-03	1.41E+02	2.68E-04
6.80E+03	3.91E+02	5.38E-00	1.18E+03	1.66E+02	1.07E-02	1.90E-00	1.24E-05	1.46E-02	4.75E-01	1.09E-02	6.01E-02	4.31E-04	1.14E-04	3.14E+01	3.29E-03	1.41E+02	1.10E-04
7.53E+03	3.93E+02	5.75E-00	1.18E+03	1.66E+02	1.07E-02	1.90E-00	1.24E-05	1.46E-02	4.75E-01	1.09E-02	2.70E-02	5.97E-05	1.14E-04	3.14E+01	3.29E-03	1.41E+02	1.26E-04
7.79E+03	3.94E+02	5.76E-00	1.18E+03	1.66E+02	1.07E-02	1.90E-00	1.24E-05	1.46E-02	4.76E-01	1.09E-02	2.34E-02	2.94E-05	1.14E-04	3.14E+01	3.29E-03	1.41E+02	1.27E-04
8.01E+03	3.94E+02	5.77E-00	1.18E+03	1.66E+02	1.07E-02	1.90E-00	1.24E-05	1.46E-02	4.76E-01	1.09E-02	2.01E-02	1.60E-05	1.17E-04	3.14E+01	3.29E-03	1.41E+02	1.27E-04
8.95E+03	3.97E+02	6.36E-00	1.18E+03	1.66E+02	1.07E-02	1.90E-00	1.24E-05	1.46E-02	4.76E-01	1.09E-02	1.50E-02	1.27E-06	3.19E-04	3.14E+01	3.29E-03	1.41E+02	2.05E-04
1.13E+04	4.03E+02	6.50E-00	1.19E+03	1.66E+02	1.07E-02	1.90E-00	1.24E-05	1.46E-02	4.78E-01	1.09E-02	1.40E-02	1.65E-09	1.01E-03	3.14E+01	3.29E-03	1.41E+02	2.48E-04
1.13E+04	4.03E+02	6.52E-00	1.19E+03	1.66E+02	1.07E-02	1.90E-00	1.24E-05	1.46E-02	4.78E-01	1.09E-02	1.39E-02	1.62E-09	1.01E-03	3.14E+01	3.29E-03	1.41E+02	2.56E-04
1.18E+04	4.04E+02	6.80E-00	1.19E+03	1.66E+02	1.07E-02	1.90E-00	1.24E-05	1.46E-02	4.78E-01	1.09E-02	1.36E-02	4.42E-10	1.15E-03	3.14E+01	3.29E-03	1.41E+02	1.06E-03
1.22E+04	4.05E+02	6.83E-00	1.19E+03	1.66E+02	1.07E-02	1.90E-00	1.24E-05	1.46E-02	4.79E-01	1.10E-02	1.32E-02	1.30E-10	1.28E-03	3.14E+01	3.29E-03	1.41E+02	1.65E-03
1.46E+04	4.11E+02	6.84E-00	1.19E+03	1.66E+02	1.07E-02	1.90E-00	1.24E-05	1.46E-02	4.81E-01	1.19E-02	1.07E-02	1.48E-13	1.90E-03	3.14E+01	3.29E-03	1.41E+02	4.77E-03
1.53E+04	4.13E+02	6.87E-00	1.19E+03	1.66E+02	1.07E-02	1.90E-00	1.24E-05	1.46E-02	4.81E-01	1.22E-02	9.79E-03	1.96E-14	2.09E-03	3.14E+01	3.29E-03	1.41E+02	5.71E-03
1.54E+04	4.13E+02	6.91E-00	1.19E+03	1.66E+02	1.07E-02	1.90E-00	1.24E-05	1.46E-02	4.81E-01	1.22E-02	9.65E-03	1.49E-14	2.12E-03	3.14E+01	3.29E-03	1.41E+02	5.96E-03
1.80E+04	4.20E+02	6.91E-00	1.19E+03	1.66E+02	1.07E-02	1.90E-00	1.24E-05	1.46E-02	4.83E-01	1.20E-02	5.87E-03	8.51E-18	2.55E-03	3.14E+01	3.29E-03	1.41E+02	1.18E-02
1.95E+04	4.24E+02	6.91E-00	1.19E+03	1.66E+02	1.07E-02	1.90E-00	1.24E-05	1.46E-02	4.84E-01	1.17E-02	3.76E-03	1.33E-19	2.77E-03	3.14E+01	3.29E-03	1.41E+02	1.50E-02
2.38E+04	4.35E+02	7.61E-00	1.19E+03	1.66E+02	1.07E-02	1.90E-00	1.24E-05	1.46E-02	4.87E-01	1.20E-02	1.54E-03	1.67E-22	2.50E-03	3.14E+01	3.29E-03	1.41E+02	1.66E-02
2.70E+04	4.43E+02	7.61E-00	1.18E+03	1.66E+02	1.06E-02	1.90E-00	1.24E-05	1.46E-02	4.89E-01	1.22E-02	1.65E-04	1.67E-22	2.22E-03	3.14E+01	3.29E-03	1.41E+02	1.66E-02
2.96E+04	4.50E+02	7.61E-00	1.18E+03	1.66E+02	1.06E-02	1.90E-00	1.24E-05	1.46E-02	4.91E-01	1.23E-02	9.32E-08	1.67E-22	2.19E-03	3.14E+01	3.29E-03	1.41E+02	1.66E-02

I-III







Table III-2. Sample f00g2022.elem\_aqu.txt File

This xls file gives MOLES in aqueous phase

data0.nuc.R8a

EQ6 input file name= F00g2022.6i

Description= React J-13 water with metals in an FFTF waste package.

Years	zi	pH	Eh	fO2	IonStr	O	Ag	Al	B	Ba	Ca	Cl	Cr	Cu	F	Fe	Gd	H
3.76E+03	3.76E+02	5.79E+00	8.77E-01	2.10E-01	1.15E-02	5.55E+01	1.48E-06	4.91E-06	1.24E-05	2.96E-07	7.65E-05	2.03E-04	5.42E-03	1.92E-04	1.14E-04	1.72E-11	3.57E-22	1.11E+02
3.76E+03	3.76E+02	5.79E+00	8.77E-01	2.10E-01	1.15E-02	5.55E+01	1.48E-06	4.91E-06	1.24E-05	2.96E-07	7.65E-05	2.03E-04	5.42E-03	1.92E-04	1.14E-04	1.72E-11	3.19E-17	1.11E+02
3.77E+03	3.76E+02	5.58E+00	8.89E-01	2.10E-01	3.06E-02	5.55E+01	1.62E-06	1.19E-05	1.24E-05	2.85E-07	1.25E-04	2.03E-04	1.45E-02	5.94E-04	1.14E-04	2.70E-11	8.08E-12	1.11E+02
3.79E+03	3.76E+02	5.44E+00	8.97E-01	2.10E-01	7.29E-02	5.55E+01	1.82E-06	1.89E-05	1.24E-05	3.11E-07	2.61E-04	2.03E-04	3.44E-02	1.45E-03	1.14E-04	3.90E-11	7.69E-11	1.11E+02
3.80E+03	3.77E+02	5.36E+00	9.02E-01	2.10E-01	1.15E-01	5.55E+01	1.96E-06	2.31E-05	1.24E-05	3.45E-07	4.32E-04	2.03E-04	5.36E-02	1.87E-03	1.14E-04	4.79E-11	1.66E-10	1.11E+02
3.81E+03	3.77E+02	5.33E+00	9.04E-01	2.10E-01	1.39E-01	5.55E+01	2.02E-06	2.49E-05	1.24E-05	3.64E-07	5.42E-04	2.03E-04	6.45E-02	1.83E-03	1.14E-04	5.27E-11	1.86E-10	1.11E+02
3.81E+03	3.77E+02	5.33E+00	9.04E-01	2.10E-01	1.42E-01	5.55E+01	2.03E-06	2.52E-05	1.24E-05	3.66E-07	5.41E-04	2.03E-04	6.59E-02	1.82E-03	1.14E-04	5.34E-11	1.89E-10	1.11E+02
3.83E+03	3.77E+02	5.29E+00	9.06E-01	2.10E-01	1.76E-01	5.56E+01	2.10E-06	2.75E-05	1.24E-05	3.93E-07	5.13E-04	2.03E-04	8.09E-02	1.78E-03	1.14E-04	6.01E-11	2.11E-10	1.11E+02
3.97E+03	3.78E+02	5.13E+00	9.15E-01	2.10E-01	4.74E-01	5.59E+01	2.54E-06	3.88E-05	1.24E-05	5.49E-07	2.42E-04	2.04E-04	2.13E-01	4.71E-03	1.14E-04	9.56E-11	1.67E-09	1.10E+02
4.53E+03	3.82E+02	5.12E+00	9.16E-01	2.10E-01	5.06E-01	5.60E+01	2.57E-06	3.98E-05	1.24E-05	5.52E-07	4.37E-05	2.04E-04	2.37E-01	4.88E-03	1.14E-04	9.95E-11	2.06E-09	1.10E+02
5.01E+03	3.84E+02	5.12E+00	9.16E-01	2.10E-01	5.12E-01	5.60E+01	2.58E-06	4.00E-05	1.24E-05	5.52E-07	4.42E-05	2.04E-04	2.42E-01	4.94E-03	1.14E-04	1.00E-10	2.15E-09	1.10E+02
5.33E+03	3.86E+02	5.12E+00	9.16E-01	2.10E-01	5.05E-01	5.60E+01	2.57E-06	3.98E-05	1.24E-05	5.49E-07	4.36E-05	2.04E-04	2.39E-01	4.87E-03	1.14E-04	9.94E-11	2.10E-09	1.10E+02
5.87E+03	3.88E+02	5.23E+00	9.09E-01	2.10E-01	2.39E-01	5.57E+01	2.24E-06	3.14E-05	1.24E-05	4.46E-07	2.10E-05	2.04E-04	1.08E-01	2.35E-03	1.14E-04	7.12E-11	5.61E-10	1.11E+02
5.93E+03	3.88E+02	5.25E+00	9.09E-01	2.10E-01	2.21E-01	5.57E+01	2.20E-06	3.06E-05	1.24E-05	4.37E-07	1.94E-05	2.04E-04	9.99E-02	2.18E-03	1.14E-04	6.88E-11	4.90E-10	1.11E+02
6.31E+03	3.90E+02	5.30E+00	9.06E-01	2.10E-01	1.55E-01	5.56E+01	2.06E-06	2.71E-05	1.24E-05	4.00E-07	4.78E-05	2.03E-04	6.86E-02	1.57E-03	1.14E-04	5.86E-11	2.75E-10	1.11E+02
6.40E+03	3.90E+02	5.31E+00	9.05E-01	2.10E-01	1.48E-01	5.56E+01	2.05E-06	2.67E-05	1.24E-05	3.97E-07	5.19E-05	2.03E-04	6.53E-02	1.26E-03	1.14E-04	5.75E-11	2.57E-10	1.11E+02
6.46E+03	3.90E+02	5.32E+00	9.04E-01	2.10E-01	1.34E-01	5.56E+01	2.01E-06	2.58E-05	1.24E-05	3.88E-07	5.56E-05	2.03E-04	5.92E-02	1.07E-03	1.14E-04	5.52E-11	2.19E-10	1.11E+02
6.80E+03	3.91E+02	5.38E+00	9.01E-01	2.10E-01	8.71E-02	5.56E+01	1.87E-06	2.21E-05	1.24E-05	3.55E-07	6.82E-05	2.03E-04	3.83E-02	4.31E-04	1.14E-04	4.60E-11	1.11E-10	1.11E+02
7.53E+03	3.93E+02	5.75E+00	8.79E-01	2.10E-01	1.27E-02	5.55E+01	1.49E-06	5.93E-06	1.24E-05	3.32E-07	7.46E-05	2.03E-04	5.33E-03	5.97E-05	1.14E-04	1.89E-11	6.28E-12	1.11E+02
7.79E+03	3.94E+02	5.76E+00	8.78E-01	2.10E-01	1.21E-02	5.55E+01	1.48E-06	5.53E-06	1.24E-05	3.11E-07	8.24E-05	2.03E-04	5.50E-03	2.94E-05	1.14E-04	1.84E-11	5.85E-12	1.11E+02
8.01E+03	3.94E+02	5.77E+00	8.78E-01	2.10E-01	1.18E-02	5.55E+01	1.48E-06	4.65E-06	1.24E-05	3.04E-07	8.17E-05	2.03E-04	5.56E-03	1.60E-05	1.06E-04	1.83E-11	5.61E-12	1.11E+02
8.95E+03	3.97E+02	6.36E+00	8.43E-01	2.10E-01	2.77E-03	5.55E+01	1.36E-06	2.35E-09	1.24E-05	9.11E-07	2.76E-05	2.03E-04	4.42E-04	1.27E-06	4.81E-08	7.01E-12	1.16E-12	1.11E+02
1.13E+04	4.03E+02	6.50E+00	8.34E-01	2.10E-01	3.07E-03	5.55E+01	1.37E-06	2.12E-09	1.24E-05	2.68E-06	2.73E-05	2.03E-04	1.29E-04	1.65E-09	2.96E-09	6.00E-12	1.12E-12	1.11E+02
1.13E+04	4.03E+02	6.52E+00	8.33E-01	2.10E-01	3.01E-03	5.55E+01	1.37E-06	2.06E-09	1.24E-05	2.61E-06	2.72E-05	2.03E-04	1.29E-04	1.62E-09	2.32E-09	5.87E-12	1.11E-12	1.11E+02
1.18E+04	4.04E+02	6.80E+00	8.17E-01	2.10E-01	2.27E-03	5.55E+01	1.35E-06	1.87E-09	1.24E-05	7.02E-07	2.58E-05	2.03E-04	3.61E-04	4.42E-10	4.21E-06	4.65E-12	1.33E-12	1.11E+02
1.22E+04	4.05E+02	6.83E+00	8.15E-01	2.10E-01	2.36E-03	5.55E+01	2.58E-06	1.95E-09	1.24E-05	6.29E-07	2.67E-05	9.07E-05	3.99E-04	1.30E-10	8.08E-06	4.59E-12	1.52E-12	1.11E+02
1.46E+04	4.11E+02	6.84E+00	8.14E-01	2.10E-01	2.45E-03	5.55E+01	4.32E-06	2.02E-09	1.24E-05	5.84E-07	2.72E-05	5.11E-05	4.28E-04	1.48E-13	1.34E-05	4.54E-12	1.71E-12	1.11E+02
1.53E+04	4.13E+02	6.87E+00	8.13E-01	2.10E-01	2.39E-03	5.55E+01	4.61E-06	2.10E-09	1.24E-05	5.08E-07	2.60E-05	4.75E-05	4.81E-04	1.96E-14	1.08E-05	4.47E-12	1.67E-12	1.11E+02
1.54E+04	4.13E+02	6.91E+00	8.10E-01	2.10E-01	2.68E-03	5.55E+01	2.77E-06	2.38E-09	1.24E-05	4.37E-07	3.31E-05	8.41E-05	5.59E-04	1.49E-14	3.44E-05	4.39E-12	2.92E-12	1.11E+02
1.80E+04	4.20E+02	6.91E+00	8.11E-01	2.10E-01	2.86E-03	5.55E+01	1.14E-06	2.71E-09	1.24E-05	4.43E-07	3.85E-05	2.63E-04	5.59E-04	8.51E-18	5.39E-05	4.40E-12	3.98E-12	1.11E+02
1.95E+04	4.24E+02	6.91E+00	8.10E-01	2.10E-01	2.87E-03	5.55E+01	1.14E-06	2.72E-09	1.24E-05	4.41E-07	3.83E-05	2.63E-04	5.62E-04	1.33E-19	5.45E-05	4.39E-12	3.97E-12	1.11E+02
2.38E+04	4.35E+02	7.61E+00	7.69E-01	2.10E-01	3.54E-03	5.55E+01	1.58E-06	8.85E-09	1.24E-05	1.75E-08	8.11E-05	1.69E-04	1.69E-04	1.67E-22	1.48E-04	3.65E-12	4.62E-10	1.11E+02
2.70E+04	4.43E+02	7.61E+00	7.69E-01	2.10E-01	3.53E-03	5.55E+01	1.57E-06	8.85E-09	1.24E-05	1.75E-08	8.34E-05	1.70E-04	1.65E-04	1.67E-22	1.47E-04	3.65E-12	4.83E-10	1.11E+02
2.96E+04	4.50E+02	7.61E+00	7.69E-01	2.10E-01	3.04E-03	5.55E+01	1.37E-06	8.79E-09	1.24E-05	1.72E-08	6.77E-05	2.03E-04	9.32E-08	1.67E-22	1.14E-04	3.65E-12	3.20E-10	1.11E+02

III-5







Years	C	P	K	Li	Mg	Mn	Mo	N	Na	Ni	Np	Pb	Pu	S	Si	Sm	Ti	U
8.19E+04	2.04E-03	4.10E-08	5.80E-04	1.67E-22	3.54E-07	1.94E-15	1.67E-22	1.42E-04	2.04E-03	4.02E-07	1.67E-22	1.92E-09	7.76E-13	1.92E-04	2.48E-05	4.53E-12	2.26E-10	3.35E-07
8.77E+04	2.04E-03	3.94E-08	5.73E-04	1.67E-22	3.79E-07	1.94E-15	1.67E-22	1.42E-04	2.04E-03	4.02E-07	1.67E-22	1.97E-09	7.75E-13	1.92E-04	2.47E-05	4.72E-12	2.26E-10	3.36E-07
9.35E+04	2.04E-03	3.78E-08	5.66E-04	1.67E-22	4.05E-07	1.94E-15	1.67E-22	1.42E-04	2.04E-03	4.02E-07	1.67E-22	2.01E-09	7.75E-13	1.92E-04	2.47E-05	4.92E-12	2.26E-10	3.36E-07
9.93E+04	2.04E-03	3.63E-08	5.60E-04	1.67E-22	4.31E-07	1.94E-15	1.67E-22	1.42E-04	2.04E-03	4.02E-07	1.67E-22	2.07E-09	7.75E-13	1.92E-04	2.47E-05	5.12E-12	2.26E-10	3.36E-07
1.05E+05	2.04E-03	3.49E-08	5.53E-04	1.67E-22	4.60E-07	1.94E-15	1.67E-22	1.42E-04	2.05E-03	4.02E-07	1.67E-22	2.12E-09	7.75E-13	1.92E-04	2.47E-05	5.34E-12	2.26E-10	3.36E-07
1.11E+05	2.04E-03	3.35E-08	5.47E-04	1.67E-22	4.89E-07	1.94E-15	1.67E-22	1.42E-04	2.05E-03	4.02E-07	1.67E-22	2.17E-09	7.75E-13	1.92E-04	2.47E-05	5.56E-12	2.26E-10	3.36E-07
1.17E+05	2.04E-03	3.22E-08	5.40E-04	1.67E-22	5.20E-07	1.94E-15	1.67E-22	1.42E-04	2.05E-03	4.02E-07	1.67E-22	2.23E-09	7.75E-13	1.92E-04	2.47E-05	5.79E-12	2.26E-10	3.36E-07
1.23E+05	2.04E-03	3.09E-08	5.34E-04	1.67E-22	5.52E-07	1.94E-15	1.67E-22	1.42E-04	2.05E-03	4.02E-07	1.67E-22	2.28E-09	7.75E-13	1.92E-04	2.47E-05	6.04E-12	2.26E-10	3.36E-07
1.28E+05	2.04E-03	2.97E-08	5.27E-04	1.67E-22	5.86E-07	1.94E-15	1.67E-22	1.42E-04	2.05E-03	4.02E-07	1.67E-22	2.34E-09	7.75E-13	1.92E-04	2.47E-05	6.29E-12	2.26E-10	3.36E-07
1.34E+05	2.04E-03	2.85E-08	5.21E-04	1.67E-22	6.21E-07	1.94E-15	1.67E-22	1.42E-04	2.05E-03	4.02E-07	1.67E-22	2.40E-09	7.75E-13	1.92E-04	2.46E-05	6.55E-12	2.26E-10	3.36E-07
1.40E+05	2.04E-03	2.74E-08	5.15E-04	1.67E-22	6.58E-07	1.94E-15	1.67E-22	1.42E-04	2.05E-03	4.02E-07	1.67E-22	2.46E-09	7.75E-13	1.92E-04	2.46E-05	6.82E-12	2.26E-10	3.36E-07
1.46E+05	2.04E-03	2.63E-08	5.09E-04	1.67E-22	6.96E-07	1.94E-15	1.67E-22	1.42E-04	2.05E-03	4.03E-07	1.67E-22	2.52E-09	7.75E-13	1.92E-04	2.46E-05	7.10E-12	2.26E-10	3.36E-07
1.52E+05	2.04E-03	2.53E-08	5.03E-04	1.67E-22	7.36E-07	1.94E-15	1.67E-22	1.42E-04	2.06E-03	4.03E-07	1.67E-22	2.58E-09	7.75E-13	1.92E-04	2.46E-05	7.39E-12	2.26E-10	3.37E-07
1.57E+05	2.04E-03	2.43E-08	4.97E-04	1.67E-22	7.77E-07	1.94E-15	1.67E-22	1.42E-04	2.06E-03	4.03E-07	1.67E-22	2.64E-09	7.75E-13	1.92E-04	2.46E-05	7.69E-12	2.26E-10	3.37E-07
1.63E+05	2.04E-03	2.34E-08	4.90E-04	1.67E-22	8.20E-07	1.95E-15	1.67E-22	1.42E-04	2.06E-03	4.03E-07	1.67E-22	2.71E-09	7.75E-13	1.92E-04	2.46E-05	8.00E-12	2.26E-10	3.37E-07
1.69E+05	2.04E-03	2.25E-08	4.84E-04	1.67E-22	8.65E-07	1.95E-15	1.67E-22	1.42E-04	2.06E-03	4.03E-07	1.67E-22	2.77E-09	7.75E-13	1.92E-04	2.46E-05	8.32E-12	2.26E-10	3.37E-07
1.75E+05	2.04E-03	2.17E-08	4.78E-04	1.67E-22	9.11E-07	1.95E-15	1.67E-22	1.42E-04	2.06E-03	4.03E-07	1.67E-22	2.84E-09	7.75E-13	1.92E-04	2.45E-05	8.65E-12	2.26E-10	3.37E-07
1.81E+05	2.04E-03	2.09E-08	4.72E-04	1.67E-22	9.59E-07	1.95E-15	1.67E-22	1.42E-04	2.06E-03	4.03E-07	1.67E-22	2.90E-09	7.75E-13	1.92E-04	2.45E-05	8.99E-12	2.26E-10	3.37E-07
1.86E+05	2.04E-03	2.01E-08	4.66E-04	1.67E-22	1.01E-06	1.95E-15	1.67E-22	1.42E-04	2.06E-03	4.03E-07	1.67E-22	2.97E-09	7.75E-13	1.92E-04	2.45E-05	9.34E-12	2.26E-10	3.37E-07
1.92E+05	2.04E-03	1.94E-08	4.60E-04	1.67E-22	1.06E-06	1.95E-15	1.67E-22	1.42E-04	2.06E-03	4.03E-07	1.67E-22	3.04E-09	7.75E-13	1.92E-04	2.45E-05	9.70E-12	2.26E-10	3.37E-07
1.98E+05	2.04E-03	1.87E-08	4.54E-04	1.67E-22	1.11E-06	1.95E-15	1.67E-22	1.42E-04	2.06E-03	4.03E-07	1.67E-22	3.11E-09	7.75E-13	1.92E-04	2.45E-05	1.01E-11	2.26E-10	3.37E-07
2.04E+05	2.04E-03	1.80E-08	4.48E-04	1.67E-22	1.17E-06	1.95E-15	1.67E-22	1.42E-04	2.06E-03	4.03E-07	1.67E-22	3.18E-09	7.75E-13	1.92E-04	2.45E-05	1.05E-11	2.26E-10	3.37E-07
2.10E+05	2.04E-03	1.74E-08	4.42E-04	1.67E-22	1.23E-06	1.95E-15	1.67E-22	1.42E-04	2.06E-03	4.04E-07	1.67E-22	3.25E-09	7.75E-13	1.92E-04	2.45E-05	1.08E-11	2.26E-10	3.38E-07
2.15E+05	2.04E-03	1.68E-08	4.36E-04	1.67E-22	1.29E-06	1.95E-15	1.67E-22	1.42E-04	2.06E-03	4.04E-07	1.67E-22	3.32E-09	7.75E-13	1.92E-04	2.44E-05	1.12E-11	2.26E-10	3.38E-07
2.21E+05	2.04E-03	1.62E-08	4.31E-04	1.67E-22	1.35E-06	1.95E-15	1.67E-22	1.42E-04	2.05E-03	4.04E-07	1.67E-22	3.40E-09	7.75E-13	1.92E-04	2.44E-05	1.16E-11	2.26E-10	3.38E-07
2.27E+05	2.04E-03	1.57E-08	4.25E-04	1.67E-22	1.41E-06	1.95E-15	1.67E-22	1.42E-04	2.05E-03	4.04E-07	1.67E-22	3.47E-09	7.75E-13	1.92E-04	2.44E-05	1.21E-11	2.26E-10	3.38E-07
2.33E+05	2.04E-03	1.52E-08	4.19E-04	1.67E-22	1.47E-06	1.95E-15	1.67E-22	1.42E-04	2.05E-03	4.04E-07	1.67E-22	3.54E-09	7.75E-13	1.92E-04	2.44E-05	1.25E-11	2.26E-10	3.38E-07
2.39E+05	2.04E-03	1.47E-08	4.13E-04	1.67E-22	1.54E-06	1.95E-15	1.67E-22	1.42E-04	2.05E-03	4.04E-07	1.67E-22	3.62E-09	7.75E-13	1.92E-04	2.44E-05	1.29E-11	2.26E-10	3.38E-07
2.45E+05	2.04E-03	1.42E-08	4.07E-04	1.67E-22	1.61E-06	1.95E-15	1.67E-22	1.42E-04	2.05E-03	4.04E-07	1.67E-22	3.69E-09	7.75E-13	1.92E-04	2.44E-05	1.34E-11	2.26E-10	3.38E-07
2.50E+05	2.04E-03	1.37E-08	4.01E-04	1.67E-22	1.68E-06	1.95E-15	1.67E-22	1.42E-04	2.05E-03	4.04E-07	1.67E-22	3.76E-09	7.75E-13	1.92E-04	2.44E-05	1.38E-11	2.26E-10	3.38E-07
2.54E+05	2.04E-03	1.35E-08	3.98E-04	1.67E-22	1.72E-06	1.95E-15	1.67E-22	1.42E-04	2.05E-03	4.04E-07	1.67E-22	3.81E-09	7.75E-13	1.92E-04	2.44E-05	1.41E-11	2.26E-10	3.38E-07

## ATTACHMENT IV. LISTING OF FILES ON ELECTRONIC MEDIA

This attachment contains the MS-DOS directory for files placed on the electronic media. The files are of 9 types:

- 1) Excel files (extension = xls), called out in the text and tables;
- 2) EQ6 input files (extension = 6i), as discussed in Section 5.3.2, for the SCFT mode; these have 8-character names f???????.6i;
- 3) EQ6 input files (extension = 6i) for the older allpost/nxtinput method, with 13-character names f???????.alln.6i;
- 4) EQ6 output files (text, extension = 6o);
- 5) Tab-delimited text files (extension = txt), with names f???????.elem?????.txt. as discussed in Section 5.3.2; these contain total aqueous moles (\*.elem\_aqu.txt), total moles in minerals and aqueous phase (\*.elem\_m\_a.txt), total moles in minerals, aqueous phase, and remain special reactants (\*.elem\_tot.txt), and the total moles in minerals alone (\*.elem\_min.txt). The \*.elem\_tot.txt and \*.elem\_min.txt also have the volume in cm<sup>3</sup> of the minerals and total solids (including special reactants) in the system;
- 6) FORTRAN source files (extension = for) for the version of EQ6 used in the calculations; and
- 7) MS-DOS/Win95/Win98 executables (extension = exe) for the version of EQ6 and runeq6 used in the calculations, and the autoexec.bat file that sets up the environment;
- 8) EQ6 data files used for the calculations, with the text file data0.nuc.R8a, and the binary version data1.nuc; and
- 9) A copy of this calculation document, 327fftf.doc, as of 12-29-1998.

```
Volume in drive C has no label
Volume Serial Number is 07CE-0408
Directory of C:\WINDOWS\DESKTOP\electronic media 327fftf
```

```
..                <DIR>          12-28-98  1:04p  .
..                <DIR>          12-28-98  1:04p  ..
FA0G1103 6I       40,935  12-07-98  1:35p  fa0g1103.6i
F00_1103 6I       39,425  10-01-98  12:42p  F00_1103.6I
F00_1203 6I       39,351  09-25-98  8:13a  f00_1203.6i
F00_1204 6I       39,055  09-25-98  8:13a  F00_1204.6i
F00A1111 6I       48,461  11-30-98  9:19p  f00a1111.6i
F00A1112 6I       48,461  11-30-98  9:54p  f00a1112.6i
F00A1113 6I       48,313  11-30-98  9:59p  F00A1113.6I
F00A1211 6I       48,535  12-02-98  3:29p  f00a1211.6i
F00A2122 6I       48,897  12-02-98  3:37p  f00a2122.6i
F00A2211 6I       48,609  12-02-98  3:41p  f00a2211.6i
F00A2221 6I       48,683  12-02-98  3:45p  f00a2221.6i
F00A2222 6I       48,757  12-02-98  4:00p  f00a2222.6i
F00B2122 6I       45,479  12-02-98  4:22p  f00b2122.6i
F00C2122 6I       37,621  12-02-98  4:33p  f00c2122.6i
F00G1103 6I       40,533  12-02-98  4:35p  F00g1103.6i
F00G1104 6I       40,525  12-02-98  4:38p  F00g1104.6i
F00G2203 6I       40,451  12-02-98  4:44p  F00g2203.6i
F00X2122 6I       48,971  11-29-98  7:01p  f00x2122.6i
F01!1103 6I       39,499  10-01-98  12:50p  F01!1103.6I
F01_1103 6I       39,425  10-01-98  12:42p  F01_1103.6I
F01_1203 6I       39,351  09-24-98  6:40p  F01_1203.6I
F01_1204 6I       39,055  09-22-98  1:22p  F01_1204.6I
F01_2022 6I       45,378  12-02-98  5:04p  f01_2022.6i
```

F01_2204	6I	39,869	12-02-98	5:23p	F01_2204.6I
F01A1113	6I	48,377	12-03-98	10:37a	f01a1113.6i
F01B1113	6I	49,068	12-02-98	5:07p	f01b1113.6i
F02_2022	6I	47,889	12-14-98	6:24p	F02_2022.6I
F00!1103	6I	39,499	10-01-98	12:50p	F00!1103.6I
F00G2022	6I	45,240	11-30-98	1:22p	f00g2022.6i
F00G2204	6I	40,165	11-30-98	10:18a	F00g2204.6I
F00G1021	6I	46,342	12-02-98	10:09p	f00g1021.6i
F01G1203	6I	40,673	12-02-98	9:44p	F01g1203.6i
F00G2021	6I	46,054	12-02-98	10:01p	f00g2021.6i
F01G2203	6I	40,520	12-02-98	8:25p	F01g2203.6i
FS0G2204	6I	40,313	12-10-98	1:44a	FS0G2204.6I
FS0A1112	6I	48,535	12-10-98	1:43a	FS0A1112.6I
FS!A1112	6I	48,609	12-10-98	2:56p	fs!a1112.6i
FS0A2222	6I	48,831	12-11-98	9:17a	fs0a2222.6i
FS0G2022	6I	45,602	12-11-98	8:05a	fs0g2022.6i
FS1_2204	6I	39,963	12-14-98	5:55p	fs1_2204.6i
FS2_2022	6I	44,976	12-14-98	6:35p	fs2_2022.6i
FA0G11-1	TXT	13,056	12-02-98	6:58p	fa0g1103.elem_aqu.txt
FA0G11-2	TXT	12,367	12-02-98	6:58p	fa0g1103.elem_min.txt
FA0G11-3	TXT	12,380	12-02-98	6:58p	fa0g1103.elem_tot.txt
FA0G11-4	TXT	12,375	12-02-98	6:58p	fa0g1103.elem_m_a.txt
F00A11-1	TXT	31,746	12-02-98	7:15p	f00a1111.elem_aqu.txt
F00A11-2	TXT	30,049	12-02-98	7:15p	f00a1111.elem_min.txt
F00A11-3	TXT	30,062	12-02-98	7:15p	f00a1111.elem_tot.txt
F00A11-4	TXT	30,057	12-02-98	7:15p	f00a1111.elem_m_a.txt
F00A11-5	TXT	35,306	12-02-98	7:40p	f00a1112.elem_aqu.txt
F00A11-6	TXT	33,417	12-02-98	7:40p	f00a1112.elem_min.txt
F00A11-7	TXT	33,430	12-02-98	7:40p	f00a1112.elem_tot.txt
F00A11-8	TXT	33,425	12-02-98	7:40p	f00a1112.elem_m_a.txt
F00A21-1	TXT	12,380	12-02-98	8:06p	f00a2122.elem_tot.txt
F00A12-1	TXT	27,523	12-02-98	7:56p	f00a1211.elem_min.txt
F00A12-2	TXT	27,536	12-02-98	7:56p	f00a1211.elem_tot.txt
F00A12-3	TXT	27,531	12-02-98	7:56p	f00a1211.elem_m_a.txt
F00A12-4	TXT	29,076	12-02-98	7:56p	f00a1211.elem_aqu.txt
F00A21-2	TXT	12,367	12-02-98	8:06p	f00a2122.elem_min.txt
F00A21-3	TXT	12,375	12-02-98	8:06p	f00a2122.elem_m_a.txt
F00A21-4	TXT	13,056	12-02-98	8:06p	f00a2122.elem_aqu.txt
F00A22-1	TXT	28,799	12-02-98	8:41p	f00a2221.elem_tot.txt
F00A22-2	TXT	27,523	12-02-98	8:22p	f00a2211.elem_min.txt
F00A22-3	TXT	27,536	12-02-98	8:22p	f00a2211.elem_tot.txt
F00A22-4	TXT	27,531	12-02-98	8:22p	f00a2211.elem_m_a.txt
F00A22-5	TXT	29,076	12-02-98	8:22p	f00a2211.elem_aqu.txt
F00A22-6	TXT	28,786	12-02-98	8:41p	f00a2221.elem_min.txt
F00A22-7	TXT	28,794	12-02-98	8:41p	f00a2221.elem_m_a.txt
F00A22-8	TXT	30,411	12-02-98	8:41p	f00a2221.elem_aqu.txt
F00B21-1	TXT	8,591	12-02-98	9:18p	f00b2122.elem_tot.txt
F00A22-9	TXT	40,153	12-02-98	9:15p	f00a2222.elem_min.txt
F00A2-10	TXT	40,166	12-02-98	9:15p	f00a2222.elem_tot.txt
F00A2-11	TXT	40,161	12-02-98	9:15p	f00a2222.elem_m_a.txt
F00A2-12	TXT	42,426	12-02-98	9:15p	f00a2222.elem_aqu.txt
F00B21-2	TXT	8,578	12-02-98	9:18p	f00b2122.elem_min.txt
F00B21-3	TXT	8,586	12-02-98	9:18p	f00b2122.elem_m_a.txt
F00B21-4	TXT	9,051	12-02-98	9:18p	f00b2122.elem_aqu.txt
F00G11-1	TXT	15,748	12-02-98	9:43p	F00g1103.elem_tot.txt
F00C21-1	TXT	17,840	12-02-98	9:33p	f00c2122.elem_min.txt
F00C21-2	TXT	17,853	12-02-98	9:33p	f00c2122.elem_tot.txt
F00C21-3	TXT	17,848	12-02-98	9:33p	f00c2122.elem_m_a.txt
F00C21-4	TXT	18,841	12-02-98	9:33p	f00c2122.elem_aqu.txt
F00G11-2	TXT	15,735	12-02-98	9:43p	F00g1103.elem_min.txt
F00G11-3	TXT	15,743	12-02-98	9:43p	F00g1103.elem_m_a.txt
F00G11-4	TXT	16,616	12-02-98	9:43p	F00g1103.elem_aqu.txt
F00G22-1	TXT	31,325	12-02-98	10:31p	F00g2203.elem_tot.txt

F00G11-5	TXT	32,575	12-02-98	10:09p	F00g1104.elem_min.txt
F00G11-6	TXT	32,588	12-02-98	10:09p	F00g1104.elem_tot.txt
F00G11-7	TXT	32,583	12-02-98	10:09p	F00g1104.elem_m_a.txt
F00G11-8	TXT	34,416	12-02-98	10:09p	F00g1104.elem_aqu.txt
F00G22-2	TXT	31,312	12-02-98	10:31p	F00g2203.elem_min.txt
F00G22-3	TXT	31,320	12-02-98	10:31p	F00g2203.elem_m_a.txt
F00G22-4	TXT	33,081	12-02-98	10:31p	F00g2203.elem_aqu.txt
F01A11-1	TXT	108,368	12-03-98	12:27a	f01a1113.elem_tot.txt
F01_22-1	TXT	26,681	12-02-98	10:54p	F01_2204.elem_min.txt
F01_22-2	TXT	26,694	12-02-98	10:54p	F01_2204.elem_tot.txt
F01_22-3	TXT	26,689	12-02-98	10:54p	F01_2204.elem_m_a.txt
F01_22-4	TXT	28,186	12-02-98	10:54p	F01_2204.elem_aqu.txt
F01A11-2	TXT	108,355	12-03-98	12:27a	f01a1113.elem_min.txt
F01A11-3	TXT	108,363	12-03-98	12:27a	f01a1113.elem_m_a.txt
F01A11-4	TXT	114,516	12-03-98	12:27a	f01a1113.elem_aqu.txt
F02_20-1	TXT	32,167	12-03-98	1:48a	F02_2022.elem_tot.txt
F01B11-1	TXT	42,679	12-03-98	1:11a	f01b1113.elem_min.txt
F01B11-2	TXT	42,692	12-03-98	1:11a	f01b1113.elem_tot.txt
F01B11-3	TXT	42,687	12-03-98	1:11a	f01b1113.elem_m_a.txt
F01B11-4	TXT	45,096	12-03-98	1:11a	f01b1113.elem_aqu.txt
F02_20-2	TXT	32,154	12-03-98	1:48a	F02_2022.elem_min.txt
F02_20-3	TXT	32,162	12-03-98	1:48a	F02_2022.elem_m_a.txt
F02_20-4	TXT	33,971	12-03-98	1:48a	F02_2022.elem_aqu.txt
F00G22-5	TXT	26,694	12-03-98	2:36a	F00g2204.elem_tot.txt
F00G20-1	TXT	31,312	12-03-98	2:14a	f00g2022.elem_min.txt
F00G20-2	TXT	31,325	12-03-98	2:14a	f00g2022.elem_tot.txt
F00G20-3	TXT	31,320	12-03-98	2:14a	f00g2022.elem_m_a.txt
F00G20-4	TXT	33,081	12-03-98	2:14a	f00g2022.elem_aqu.txt
F00G22-6	TXT	26,681	12-03-98	2:36a	F00g2204.elem_min.txt
F00G22-7	TXT	26,689	12-03-98	2:36a	F00g2204.elem_m_a.txt
F00G22-8	TXT	28,186	12-03-98	2:36a	F00g2204.elem_aqu.txt
F00G10-1	TXT	22,401	12-03-98	7:57a	f00g1021.elem_aqu.txt
F00G10-2	TXT	21,208	12-03-98	7:57a	f00g1021.elem_min.txt
F00G10-3	TXT	21,221	12-03-98	7:57a	f00g1021.elem_tot.txt
F00G10-4	TXT	21,216	12-03-98	7:57a	f00g1021.elem_m_a.txt
F01G12-1	TXT	20,621	12-03-98	8:11a	f01g1203.elem_aqu.txt
F01G12-2	TXT	19,524	12-03-98	8:11a	f01g1203.elem_min.txt
F01G12-3	TXT	19,537	12-03-98	8:11a	f01g1203.elem_tot.txt
F01G12-4	TXT	19,532	12-03-98	8:11a	f01g1203.elem_m_a.txt
F01G22-1	TXT	19,958	12-03-98	8:38a	f01g2203.elem_tot.txt
F00G20-5	TXT	19,945	12-03-98	8:25a	f00g2021.elem_min.txt
F00G20-6	TXT	19,958	12-03-98	8:25a	f00g2021.elem_tot.txt
F00G20-7	TXT	19,953	12-03-98	8:25a	f00g2021.elem_m_a.txt
F00G20-8	TXT	21,066	12-03-98	8:25a	f00g2021.elem_aqu.txt
F01G22-2	TXT	19,945	12-03-98	8:38a	f01g2203.elem_min.txt
F01G22-3	TXT	19,953	12-03-98	8:38a	f01g2203.elem_m_a.txt
F01G22-4	TXT	21,066	12-03-98	8:38a	f01g2203.elem_aqu.txt
FS0A11-1	TXT	33,417	12-10-98	2:10p	fs0a1112.elem_min.txt
FS0A11-2	TXT	33,430	12-10-98	2:10p	fs0a1112.elem_tot.txt
FS0A11-3	TXT	33,425	12-10-98	2:10p	fs0a1112.elem_m_a.txt
FS0A11-4	TXT	35,306	12-10-98	2:10p	fs0a1112.elem_aqu.txt
FS0G22-1	TXT	28,186	12-10-98	2:33p	Fs0g2204.elem_aqu.txt
FS0G22-2	TXT	26,681	12-10-98	2:33p	Fs0g2204.elem_min.txt
FS0G22-3	TXT	26,694	12-10-98	2:33p	Fs0g2204.elem_tot.txt
FS0G22-4	TXT	26,689	12-10-98	2:33p	Fs0g2204.elem_m_a.txt
FS0G20-1	TXT	37,640	12-11-98	8:54a	fs0g2022.Elem_tot.txt
FS0G20-2	TXT	39,756	12-11-98	8:54a	fs0g2022.Elem_aqu.txt
FS0G20-3	TXT	37,635	12-11-98	8:54a	fs0g2022.Elem_m_a.txt
FS0G20-4	TXT	37,627	12-11-98	8:54a	fs0g2022.Elem_min.txt
FS2_20-1	TXT	30,483	12-14-98	7:02p	fs2_2022.Elem_tot.txt
FS2_20-2	TXT	32,191	12-14-98	7:02p	fs2_2022.Elem_aqu.txt
FS2_20-3	TXT	30,478	12-14-98	7:02p	fs2_2022.Elem_m_a.txt
FS2_20-4	TXT	30,470	12-14-98	7:02p	fs2_2022.Elem_min.txt

EQ6NEW	EXE	1,056,469	11-25-98	1:46p	EQ6NEW.EXE
EQ6NEW	FOR	1,322,545	12-11-98	10:50a	eq6new.for
EQLIBNEW	FOR	492,613	07-01-98	6:34p	eqlibnew.for
F01_22~1	6I	40,163	10-13-98	2:39p	f01_2204_alln.6i
F02_22~1	6I	40,385	10-21-98	11:51a	f02_2204_alln.6i
F02_20~1	6I	48,247	10-18-98	11:28a	f02_2022_alln.6i
F03_20~1	6I	48,419	10-21-98	5:46p	F03_2022_alln.6i
GD_CON~1	XLS	48,128	12-24-98	3:48p	Gd_Conc_needed_for_loss.xls
F02_22~1	XLS	3,399,168	10-29-98	3:43p	f02_2204_2022_alln_min.xls
F03_20~1	XLS	2,560,000	10-29-98	3:32p	F03_2022_alln_scratch.xls
NORM	XLS	1,559,552	12-28-98	4:40p	norm.xls
FFTF_F~1	XLS	3,690,496	12-29-98	4:28p	fftf_fuel_hws.xls
FFTF_DIR	TXT	12,691	12-29-98	4:13p	fftf_dir.txt
DATA1	NUC	791,200	11-25-98	4:15p	data1.nuc
DATA0N~1	R8A	2,299,784	11-25-98	4:15p	data0.nuc.R8a
RUNEQ6	EXE	392,181	08-18-95	5:46p	RUNEQ6.EXE
AUTOEXEC	BAT	527	12-29-98	10:58a	AUTOEXEC.BAT
327FFTF	DOC	5,528,064	12-29-98	4:11p	327fftf.doc
F00A1111	6O	3,360,135	12-02-98	7:15p	f00a1111.6o
FA0G1103	6O	1,558,663	12-02-98	6:58p	fa0g1103.6o
F00A1112	6O	4,026,245	12-02-98	7:40p	f00a1112.6o
F00A1211	6O	3,087,796	12-02-98	7:56p	f00a1211.6o
F00A2122	6O	1,357,593	12-02-98	8:06p	f00a2122.6o
F00A2211	6O	3,086,895	12-02-98	8:22p	f00a2211.6o
F00A2221	6O	3,264,835	12-02-98	8:41p	f00a2221.6o
F00A2222	6O	4,859,894	12-02-98	9:15p	f00a2222.6o
F00B2122	6O	937,816	12-02-98	9:18p	f00b2122.6o
F00C2122	6O	2,201,681	12-02-98	9:33p	f00c2122.6o
F00G1103	6O	1,598,494	12-02-98	9:43p	f00g1103.6o
F00G1104	6O	4,007,816	12-02-98	10:09p	f00g1104.6o
F00G2203	6O	3,499,718	12-02-98	10:31p	f00g2203.6o
F01_2204	6O	3,220,594	12-02-98	10:54p	f01_2204.6o
F01A1113	6O	14,802,880	12-03-98	12:27a	f01a1113.6o
F01B1113	6O	6,236,188	12-03-98	1:11a	f01b1113.6o
F02_2022	6O	3,951,444	12-03-98	1:48a	f02_2022.6o
F00G2022	6O	3,764,427	12-03-98	2:14a	f00g2022.6o
F00G2204	6O	3,178,251	12-03-98	2:36a	f00g2204.6o
F00G1021	6O	2,414,537	12-03-98	7:57a	f00g1021.6o
F01G1203	6O	2,173,140	12-03-98	8:11a	f01g1203.6o
F00G2021	6O	2,363,817	12-03-98	8:25a	f00g2021.6o
F01G2203	6O	2,143,075	12-03-98	8:38a	f01g2203.6o
FS0A1112	6O	4,045,878	12-10-98	2:10p	fs0a1112.6o
FS0G2204	6O	3,225,282	12-10-98	2:33p	fs0g2204.6o
FS!A1112	6O	4,012,117	12-10-98	3:31p	fs!a1112.6o
FS0G2022	6O	4,746,779	12-11-98	8:54a	fs0g2022.6o
FS0A2222	6O	4,908,027	12-11-98	9:51a	fs0a2222.6o
FS2_2022	6O	3,835,410	12-14-98	7:02p	fs2_2022.6o
FS1_2204	6O	3,346,009	12-14-98	6:20p	fs1_2204.6o
197 file(s)		137,562,226 bytes			
2 dir(s)		512,622,592 bytes free			